



POLITECNICO DI TORINO
Repository ISTITUZIONALE

STATIC AND DYNAMIC ANALYSIS OF HIGH-RISE BUILDINGS

Original

STATIC AND DYNAMIC ANALYSIS OF HIGH-RISE BUILDINGS / Cammarano, Sandro. - (2014).

Availability:

This version is available at: 11583/2565549 since:

Publisher:

Politecnico di Torino

Published

DOI:10.6092/polito/porto/2565549

Terms of use:

Altro tipo di accesso

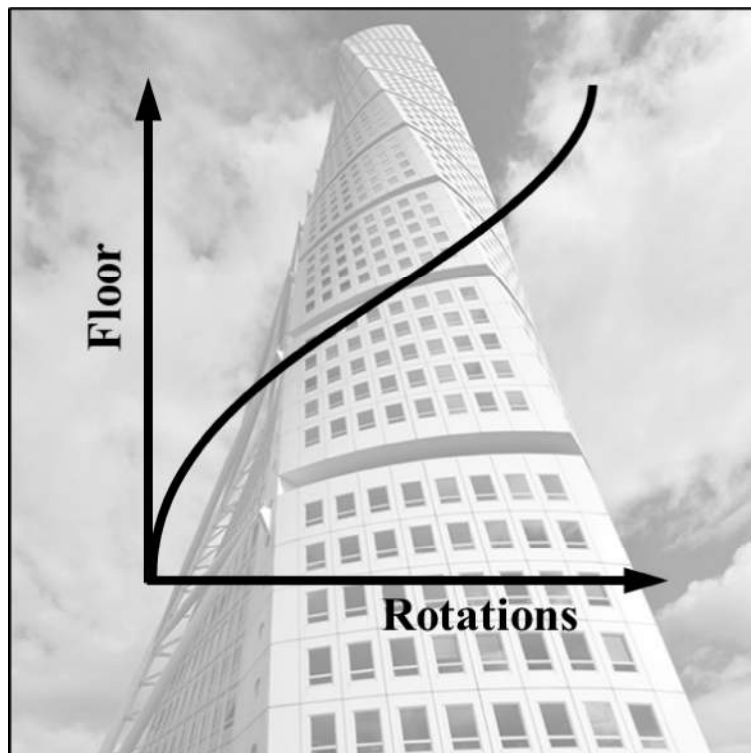
This article is made available under terms and conditions as specified in the corresponding bibliographic description in the repository

Publisher copyright

(Article begins on next page)

Sandro Cammarano

Static and Dynamic Analysis of High-Rise Buildings



Dottorato di Ricerca in Ingegneria delle Strutture
Politecnico di Torino

Sandro Cammarano

**Static and Dynamic Analysis of
High-Rise Buildings**

Tesi per il conseguimento del titolo di Dottore di Ricerca
XXVI Ciclo (2011 - 2012 - 2013)



Dottorato di Ricerca in Ingegneria delle Strutture
Politecnico di Torino

Dicembre 2013

Dottorato di Ricerca in Ingegneria delle Strutture
Politecnico di Torino, Corso Duca degli Abruzzi 24, 10129 Torino, Italy

Tutori: Prof. Alberto Carpinteri, Prof. Giuseppe Lacidogna

Coordinatore: Prof. Alberto Carpinteri

alla mia famiglia,
che mi ha dato tutto.

Acknowledgements

The more sincere acknowledgements are directed to my supervisors, prof. Alberto Carpinteri and prof. Giuseppe Lacedogna, for their endless willingness and their capability of support during all phases of my research.

A thought is also addressed to my colleagues from whom I received more than I gave.

Summary

This thesis is focused on the structural behaviour of high-rise buildings subjected to transversal loads expressed in terms of shears and torsional moments. As horizontal reinforcement, the resistant skeleton of the construction can be composed by different vertical bracings, such as shear walls, braced frames and thin-walled open section profiles, having constant or variable geometrical properties along the height. In this way, most of the traditional structural schemes can be modelled, from moment resisting frames up to outrigger and tubular systems. In particular, an entire chapter is addressed to the case of thin-walled open section shear walls which are defined by a coupled flexural-torsional behaviour, as described by Vlasov's theory of the sectorial areas.

From the analytical point of view, the three-dimensional formulation proposed by Al. Carpinteri and An. Carpinteri (1985) is considered and extended in order to perform dynamic analyses and encompass innovative structural solutions which can twist and taper from the bottom to the top of the building.

Such approach is based on the hypothesis of in-plane infinitely rigid floors which assure the connection between the vertical bracings and, consequently, reduce the number of degrees of freedom being only three for each level. By means of it, relevant design information such as the floor displacements, the external load distribution between the structural components, the internal actions, the free vibrations as well as the mode shapes can be quickly obtained.

The clearness and the conciseness of the matrix formulation allow to devise a simple computer program which, starting from basic information as the building geometry, the number and type of vertical stiffening, the material properties and the intensity of the external forces, provides essential results for preliminary designs.

Sommario

Questa tesi analizza il comportamento strutturale di edifici di notevole altezza sottoposti ad azioni trasversali, quali azioni taglianti e momenti torcenti. Il corrispondente rinforzo strutturale può essere rappresentato da diversi sistemi di controventamento, come le pareti di taglio, i telai controventati ed i profili a sezione sottile aperta, aventi proprietà geometriche costanti o variabili lungo l'altezza dell'edificio. In questo modo, può essere presa in considerazione la maggior parte degli schemi tradizionali impiegati in questo ambito: dai telai momento-resistenti fino agli schemi a trave-cappello e quelli tubolari. In particolare, viene dedicato un intero capitolo al caso delle travi a sezione sottile aperta, caratterizzate da un comportamento misto che associa le deformazioni flessionali a quelle torsionali, così come descritto dalla teoria delle aree settoriali o teoria di Vlasov.

Dal punto di vista analitico, viene ripresa ed ampliata la formulazione tridimensionale proposta da Al. Carpinteri e An. Carpinteri (1985) per poter svolgere analisi dinamiche ed includere soluzioni strutturali innovative che ruotano e si rastremano dalla base fino alla sommità della costruzione.

Tale metodo è basato sull'ipotesi di piani infinitamente rigidi che assicurano il mutuo collegamento fra i rinforzi verticali e riducono il numero di gradi di libertà ai soli spostamenti di piano. Inoltre, dalla sua applicazione, possono essere ricavate informazioni progettuali di grande interesse, come la deformata, la ripartizione del carico esterno fra le singole componenti del sistema resistente, le azioni interne, le frequenze proprie e le deformate modali.

La chiarezza e la concisione della formulazione matriciale facilitano l'ideazione di un semplice programma di calcolo che, a partire da informazioni basilari quali la geometria della costruzione, il numero ed il tipo di controventi, le proprietà del materiale e l'intensità delle azioni, fornisce risultati indispensabili per progettazioni preliminari.

Contents

Acknowledgments	V
Summary	VII
Sommario	IX
1 Horizontal Stiffening in the Design of Tall Buildings	1
1.1 Introduction	1
1.2 Structural Behaviour of Frames and Shear Walls	3
1.3 Outrigger Systems and Tube Systems	6
1.4 Innovative Structural Solutions	17
2 The Load Distribution Matrix between Vertical Bracings	25
2.1 Introduction	25
2.2 A Synthetic Three-Dimensional Approach	28
2.3 Stiffness Matrix of Frames and Braced Frames	35
2.4 Numerical Example	40
3 Thin-Walled Open Section Profiles as Vertical Stiffening	45
3.1 Introduction	45
3.2 Vlasov's Theory of Sectorial Areas	47
3.2.1 Definition of the Principal Sectorial Origin	58
3.2.2 Definition of the Principal Sectorial Pole	61
3.2.3 Numerical Example	64
3.2.4 Differential Equilibrium Equations in Principal Directions	69
3.3 Experimental Investigation on Warping Deformation	71
3.3.1 Stiffness Matrix for Thin-Walled Open Section Beams	72
3.3.2 Experimental Investigation	76
	XI

3.4	Capurso's Approach for Tall Building Design	82
3.4.1	Distribution of the External Actions between Vertical Bracings in Tall Buildings	86
3.5	The Stiffening Effect due to Lintel Beams	88
3.5.1	Numerical Example	95
4	Conceptual Design of Unconventionally Shaped Structures	99
4.1	Introduction	99
4.2	Stiffness Matrix for Bracings with Variable Cross-Section	102
4.2.1	Tapered and Twisted Bracings (Warping Negligible)	103
4.2.2	Tapered Bracings (Warping prevalent)	112
4.3	Numerical Examples	116
5	Dynamic Analysis: Evaluation of Free Vibrations and Mode Shapes	127
5.1	Introduction	127
5.2	Coupling and Uncoupling Behaviour	129
5.2.1	Analytical Procedure	130
5.2.2	Numerical Examples	137
5.3	Three-Dimensional Formulation for the Dynamics of Tall Buildings	143
5.3.1	Semi-Analytical Approach	144
5.3.2	Numerical Examples	148
6	Conclusions	155
	References	157

Chapter 1

Horizontal Stiffening in the Design of Tall Buildings

1.1 Introduction

Tall buildings have always been the symbol of supremacy of the nations engaged in their construction. Since its first appearance, this architectural typology has met approval in the public eye. Especially from a scientific point of view, it is become an appealing challenge for the designers focused on the interpretation of its structural behaviour.

Originally, high-rise structures were an American prerogative; nowadays they represent a worldwide architectural phenomenon, even for those countries regarded as less advanced, which however are demonstrating a fast industrial growth. As a matter of fact, most of the last super-tall buildings are located far from the United States: China, Korea, India and Malaysia, characterised by a considerable economic capability and technological progress, represent an evident proof of this current trend. Nevertheless, even if the geographical location of the last constructions is changed, the human attempt of overcoming the limits already achieved is still the main reason which keeps alive the interest in this field. Thereby, further goals in terms of achievable heights and unconventional shapes are expected in the next future.



Figure 1.1 – Monadnock Building in Chicago (1981, USA).

Historically, the appearance of tall buildings was due to the Industrial Revolution, at the end of the nineteenth century. In the construction field the technical evolution permitted to have available advanced materials and equipment which were indispensable for the realization of tall structures. From this point of view, the invention of the lift facilitated the evolution of these buildings as well as, in this period, a decisive transition was the use of those materials considered, until then, far from the scope of the constructors, being absent their corresponding production technology. In particular, the presence of steel in the structural skeleton involved a series of benefits, such as an increased construction speed, the availability of various shapes, the possible reuse, the high ratio between resistance and weight and a reduce degree of uncertainty about the material properties, which contributed to change the conceptual design of the constructions.

Initially the early reason of growing in height was commercial, having to compensate for the lack of space and natural light in a urban densely populated land [111].

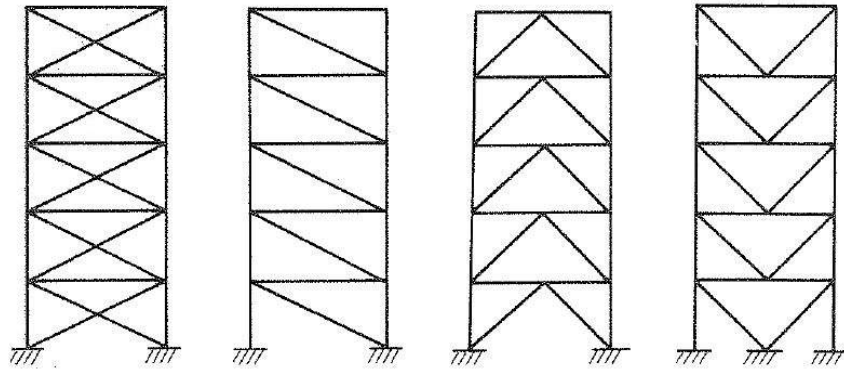


Figure 1.2– Braced frame structures.

However the higher the building, the more sensitive it became to lateral actions coming from wind and earthquakes. Without lateral stiffeners, the dimensions of the structural elements increased so that they couldn't be longer a satisfactory solution from an architectural point of view. In addition, it constituted a limit on the evolution in height of these revolutionary constructions. The 17-storey (64m) Monadnock Building in Chicago, being an impressive structure in which the resistant mechanism relies on heavy masonry walls, is even now the symbol of this issue [112].

For this purpose, the conventional load-bearing systems were substituted by new technologies which reduced the dimensions of the structural members and guaranteed the global stability of the building. The first result was a steel frame structure, which exploited the resistant properties of the material to reach an adequate stiffness, without compromising the architectural demands. This typology was followed by other systems designed to absorb and distribute the load according to their own stiffness. At this stage moment resisting frames, braced frames, shear walls and interactive frame - shear wall combinations appeared [34, 58].

1.2 Structural Behaviour of Frames and Shear Walls

The moment resisting frames are constituted by beams and columns devised to absorb the loads coming from the slab. The latter is usually outlined as an horizontal rigid diaphragm which transfers vertical and lateral loads to the

structural skeleton. In the absence of specific bracings, all the horizontal stiffness is based on the flexural and shear resistance of the network of beams and columns, being the joints designed as perfectly rigid.

The choice of this typology is due to the fact that the horizontal forces are not predominant if compared to the vertical ones. Otherwise, this entails an excessive increase of the dimensions of the structural component. In addition, pure rigid frames become not efficient for building higher than about thirty storeys, because the corresponding shear deformation determines too large drifts. To avoid these effects, further bracings, such as diagonal members between consecutive floors, are added to the previous scheme. In this way the flexural moment acting in the beams and columns decreases and the shear is absorbed as axial load by the diagonal elements so that the global behaviour becomes similar to that of a cantilever system. This is the case of braced frames in which the diagonal reinforcements contribute to the horizontal resistance by means of their axial stiffness (Fig. 1.2).

These steel configurations symbolise the turning point in the height race which started in the early twentieth century. The first structure showing a steel skeleton was the Park Row Building in New York, which reached 30 storeys in 1899, but the most popular among all was the Empire State Building, with its 102 storeys above ground in 1931.

Even though the heights of the buildings were already outstanding, due to the lack of innovative technologies and advanced analysis techniques, such reinforced solutions were realised through an excessive use of structural materials determining anyway over-designed constructions. Later on, a different approach was undertaken: the vertical behaviour was supposed to be separated from the horizontal one and specific structural elements able to absorb the entire horizontal load were devised: this was the case of the shear walls. The latter are cantilevers developing from the ground to the top of the building and, usually, characterised by thin-walled open sections which also allow to house stairwells or lift shafts. These structures are also known as core walls and can be specifically designed with particular cross sections or coupled with other walls to reproduce a resultant system with a final stiffness exceeding the sum of the individual components.

The previous schemes can be adopted together to increase the global horizontal stiffness of the building and to reduce the lateral sway, which represents one of the most restrictive conditions coming from the legislation for this type of construction. Thus shear wall – frame interaction system became a very popular scheme, which captured the attention of the scientific community in 1970s.

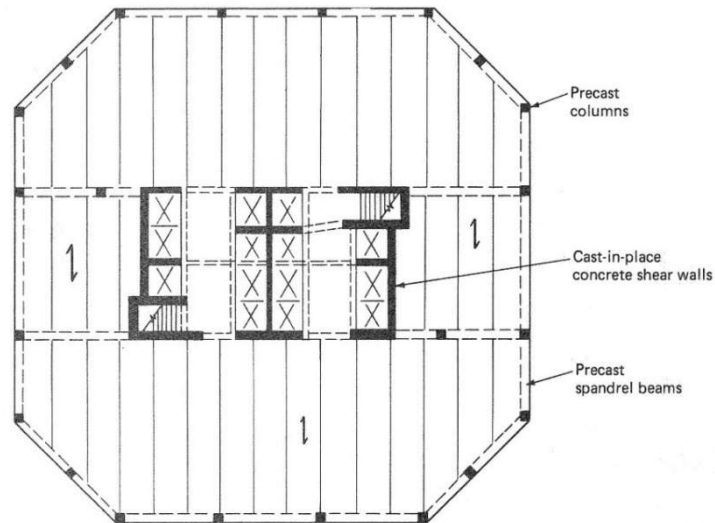


Figure 1.3 – Floor plan showing the location of some shear walls.

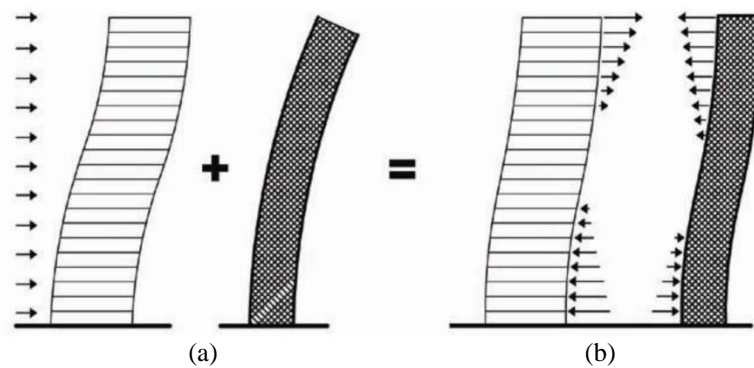


Figure 1.4 – Model of an interactive frame - shear wall combination: natural deformations of the components (a) and effect of their combination (b).

The effectiveness of this solution is due to the different deformation which characterises the frame with respect to the shear wall. In presence of horizontal actions, the former is mainly subjected to shear deformations, whereas the latter to flexural ones. In this way, in the bottom part of the building, the shear wall sustains the frame, whereas, in the top part, the frame restrains the shear wall, thus

reducing the global deformation of the resistant system (Fig. 1.4). This sophisticated configuration can be applied for building up to 70 storeys in height.

From a structural point of view, in order to design each component of the scheme, it is necessary to identify the amount of external load which is carried by each single element. To this purpose, taking into account the model of Fig. 1.4, a simplified approach hypothesizes that the connections between the members are defined by rigid trusses, so that the congruence of the horizontal displacements at each floor is satisfied. If F represents the external load vector and X the redundant unknowns defining the forces transmitted through the trusses, due to compatibility conditions the following expression can be written:

$$\mathbf{C}_1(F - X) = \mathbf{C}_2X \quad (1.1)$$

where \mathbf{C}_1 and \mathbf{C}_2 are the compliance matrices of the shear wall and frame respectively.

Defining \mathbf{C} as the sum of the matrices \mathbf{C}_1 and \mathbf{C}_2 , the numerical solution of Eqn (1.1) is

$$X = \mathbf{C}^{-1}\mathbf{C}_1F \quad (1.2)$$

which permits to evaluate the internal load distribution (Fig. 1.4b) and, thereby, to develop a preliminary design of the components of the horizontal resistant system.

1.3 Outrigger Systems and Tube Systems

Later, designers supposed that the building could be treated in a holistic manner and, therefore, analysed as a three-dimensional body rather than as a series of planar systems. This outlook gave rise to various other models which increased the lateral resistance without an excessive use of structural materials. As a consequence, the traditional analyses were gradually replaced by global approaches.

The structure was considered as a vertical cantilever or a system of cantilevers on the ground, having all the required lateral stiffness allocated to the perimeter of the building. This shrewdness aimed to increase the structural depth of lateral load-resisting elements and, thereby, their resistant contribution.

According to these outlooks and depending on the height of the construction, several solutions, such as outrigger, framed-tube, bundled-tube and tube-in-tube systems were realised (Fig. 1.5, 1.6).

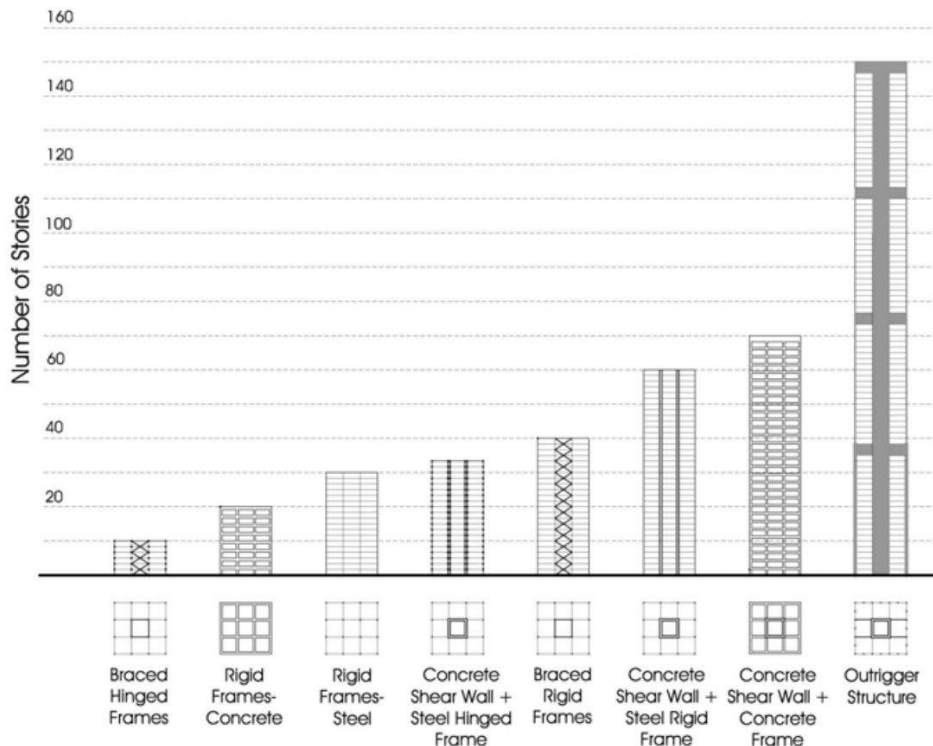


Figure 1.5 – Typologies of horizontal stiffeners.

Originally outrigger systems were employed in the sailing ship in order to increase the stability and the strength of the masts subjected to wind forces. From this point of view, a tall building could be considered analogous to the mast of a ship in presence of further elements similar in behaviour to the spreaders and stays. Thus, the engineers understood that it was possible to couple the internal core of the building with the exterior columns and realise the same scheme adopted to strengthen the ships (Fig. 1.7).

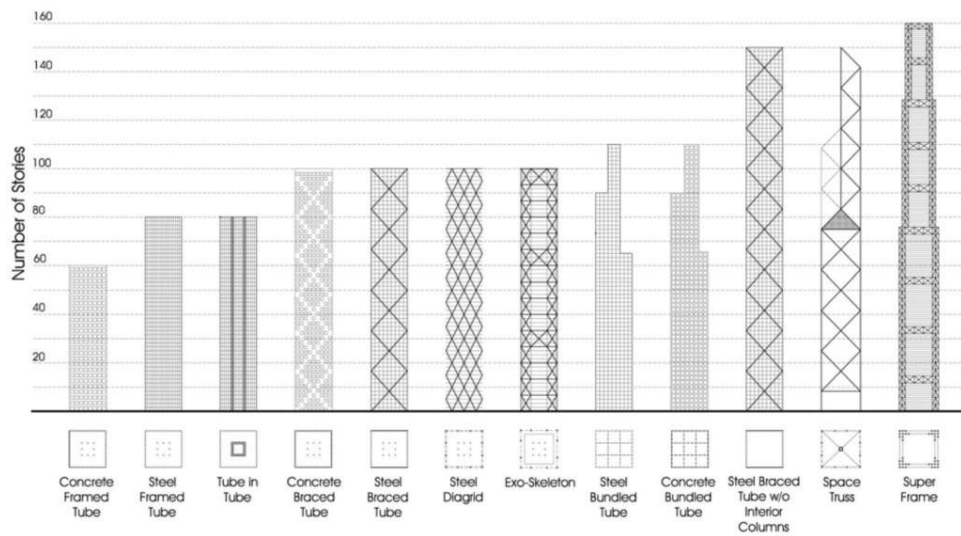


Figure 1.6 – Typologies of tube and innovative systems.

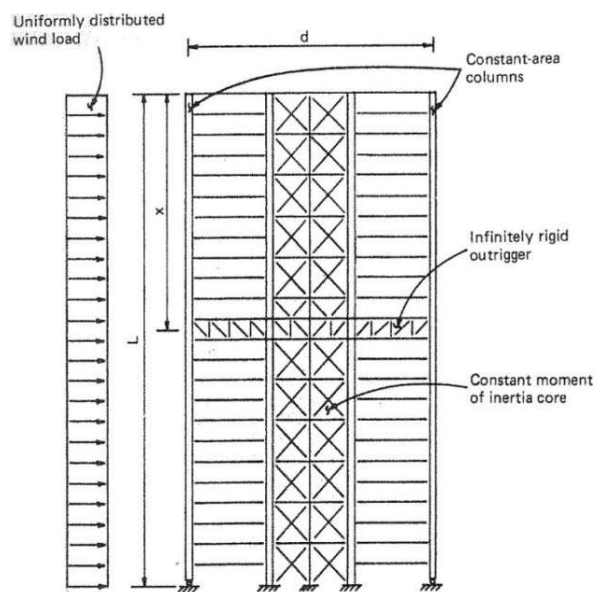


Figure 1.7 – Scheme of the outrigger system.

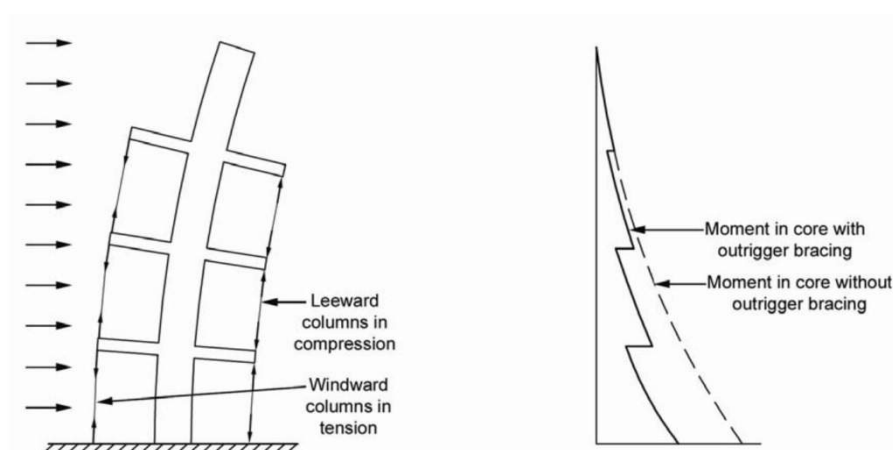


Figure 1.8 – Structural behaviour of an outrigger system; comparison in terms of moment diagram between systems with or without outrigger bracings.

It is evident that they are primarily conceived to reduce the global deformation of the building, caused by the flexural behaviour of the resistant core. This is achieved by reducing the overturning moment of the cantilever scheme and by transferring the reduced moment to the outer members through extremely rigid horizontal beams connected to the core at specific levels. When horizontal loading acts on the structure, the rotation of the core is reduced by the axial force that arises in the external columns, in particular tensile force in the windward columns and compressive force in the leeward ones (Fig. 1.8).

Roughly speaking, the resistant system can be idealised as a moment resisting spring which tends to induce a reversal of curvature in the bending behaviour of the cantilever scheme. In addition, including deep spandrel girders, which work as belts surrounding the entire building, it is possible to mobilise also the other peripheral columns to assist in restraining the outriggers, providing an improvement up to 25-30 per cent in stiffness. In order to have the outrigger and belt girder adequately stiff in flexure and shear, they often present a vertical extension which covers at least one or two storeys. Consequently, because of the obstruction caused by them, the corresponding levels are inevitably reduced to technical levels (Fig. 1.9).

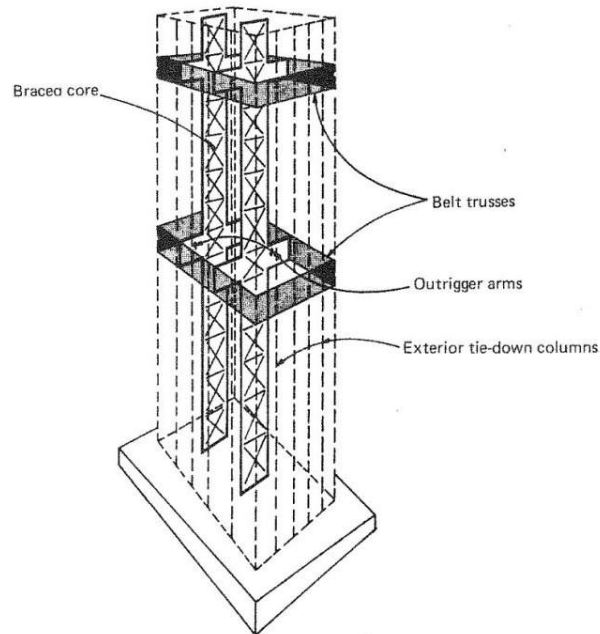


Figure 1.9 – Scheme of belt trusses working in connection with the outrigger system.

This structural typology can be easily inserted in the resistant skeleton of the building without excessively altering the original architectural shape according to two main schemes: in the first one, the core is located between the column lines with the outriggers extending on both sides (Fig. 1.8); in the second, the core is on one side of the building connected to the columns of the other side by means of horizontal cantilevers.

This solution can be employed with a single outrigger, usually located at the top of the building to maximise the restraining effect, or with some outriggers, disposed at different levels of the building. The choice depends on the needs of reducing the pure flexural behaviour of the original structure.

Many super tall buildings have been realised following this structural typology: among all, Place Victoria Office Tower (Montreal, 1965) and First Wisconsin Centre (Milwaukee, 1973, Fig. 1.10) can be mentioned.



Figure 1.10 – The U.S. Bank Centre in Milwaukee (1973, USA): example of a tall building restrained by two outrigger systems.

From the design point of view, an approximate method for a preliminary analysis can be adopted to evaluate of the optimum location of an outrigger and, thus, achieve the minimum total lateral sway of a tall building of height H .

The approach is based on some assumptions and some compatibility conditions: the material is linear elastic, the external columns are only subjected to axial forces, the outriggers are rigidly connected to the core and the latter is perfectly constrained to the ground; the rotations of the core have to match with those related to the corresponding outriggers placed at the same levels.

For the purpose, the deflection of the inner core, considered as a simple cantilever subjected first to the horizontal external actions q and, then, to the restraining effect due to the outrigger, is computed. The latter can be considered as the effect of a moment-resisting spring, whose stiffness depends on its vertical location.

The compatibility equation related to the rotation at the level ($z = H - x$) is:

$$\vartheta_q - \vartheta_{s(x)} = \vartheta_x \quad (1.3)$$

in which ϑ_q is the rotation of the cantilever at $z = (H - x)$ due to the external actions, whereas $\vartheta_{s(x)}$ is the rotation at the same level, due to the rotational spring,

with the negative sign because it acts in the opposite direction; finally ϑ_x is the rotation of the global system at $z = (H - x)$.

Eqn (1.3) can be written in the following explicit form:

$$\frac{q}{6EI} (H^3 - x^3) - \frac{M_x}{EI} (H - x) = \frac{M_x}{K_x} \quad (1.4)$$

being

- q , the distributed external action;
- EI , the flexural rigidity of the inner core;
- H , the height of the building;
- x , the unknown vertical position of the outrigger, from the top;
- M_x , the resisting moment due to the rotational spring;
- K_x , the spring stiffness obtained by means of the axial rigidity EA of the extreme columns as $EAd^2/[2(H-x)]$
- d , the relative distance between the external columns.

Once the moment M_x is acquired from Eqn (1.4), the top drift of the building can be computed taking into account the effects of the external action and the moment M_x by means of the Superposition Principle. Since the first contribution is constant, the procedure which aims to minimise the lateral sway of the building is turned into the attempt of maximising the negative top deflection caused only by the rotational spring. The latter is then differentiated with respect to x and equated to zero to define the best location of the outrigger.

$$y_x = \frac{M_x}{2EI} (H^2 - x^2) \quad (1.5)$$

$$\frac{d(y_x)}{dx} = 0 \quad (1.6)$$

The extension of the solution in the case of two or more outriggers can be obtained following the same methodology. Taranath [111] provides a summary graph, related to a 46-storey building, for the case of two contemporary outriggers systems. In Fig. 1.11 some design curves are reported, in order to identify the top displacement of a building in which the outrigger systems are arranged. The information that can be acquired are given in a non-dimensional form, so that they can be extended to consider different types of internal resistant core. In the y axis there is the number of the level to which the outrigger is associated, whereas in x axis the ratio between the top drifts related to the global resistant scheme and the one free from outrigger systems.

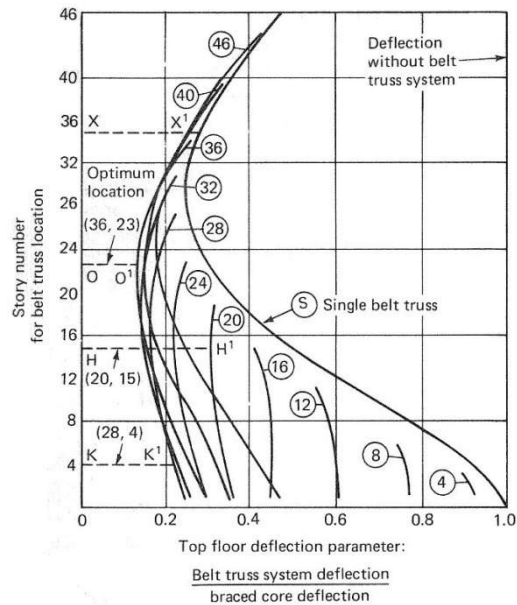


Figure 1.11 – Curves for the evaluation of the best location of two outrigger systems.

The continuous curve represents the case of only one outrigger, whose location varies along the height. If the latter is zero, the value of top drift coincides with the one related to the case of pure cantilever. In addition, it is evident that the optimum position of the single reinforcement is about 60 per cent of the entire height. On the contrary, the other curves represent the cases of two outriggers: once the upper one is fixed (defined by the circled number), the corresponding curve defines the value of the top drift as the lower is moved in the storeys immediately below. In this way, it becomes possible to identify the best configuration of two outrigger systems in order to have the minimum lateral sway of the building. For instance, if the upper reinforcement is posed at the 36th level and the lower at the 23rd level, the building shows only 17 per cent of the top displacement if compared to the case of pure cantilever behaviour. This result proves the effectiveness of this kind of structural solution, if employed in a high-rise building.

The idea of entrusting the horizontal resistance to the components constituting the perimeter of the building induced the engineers to a breakthrough in the design of the structural skeleton. If the stiffening is located along the perimeter of the

building, the corresponding lever arm increases to such an extent that the structure becomes much stiffer than the previous cases, thereby allowing to reach unimaginable heights. In this way the structure tends to behave as an equivalent huge hollow tube cantilevering out of the ground. This solution, known as framed tube, directly derives from the frame concept. Indeed, it is characterised by closely spaced columns and deep spandrel beams rigidly connected together and smeared on the perimeter of the construction. The final result is a single three-dimensional tube element, which represents the most economical and yet safe and serviceable system for the design of buildings with over 50-60 storeys [33, 37, 65].

The earliest application of the tubular notion is related to the designer Fazlur Khan that conceived the 43-storey DeWitt-Chestnut Apartment Building (Chicago) in 1965.

At present most of the super-tall buildings are built according to the tubular concept: the 100-storey John Hancock Building (Chicago, 1969), the 110-storey Sears Towers (Chicago, 1973) and the 110-storey World Trade Centre Towers (New York, 1973, destroyed by a terrorist attack in 2001) are glaring proof of this construction typology.

From the structural point of view, the building can be assimilated to a cantilever whose bending behaviour is associated with the axial forces absorbed by the columns of the tube's windward and leeward faces. If the mesh of columns and spandrel beams is adequately dense, the latter can be treated as a continuous wall element. In this way the building can be easily reduced to a vertical hollow beam, whose stiffness depends on the geometrical inertia of the global cross section. Columns arranged in facades transverse to the wind direction operate as compression and tension flanges of the box beam, whereas the rest as webs.

The distribution of the stresses is supposed to follow the assumption of plane sections, as proposed in the Euler-Bernoulli hypothesis. This construction typology allows to create diversified shapes manipulating the plan form without altering the structural efficiency. Nevertheless, due to architectural reasons, a highly dense mesh of beams and columns is in contrast with the need of natural light in the inner spaces. On the other hand, the increase of the openings causes the structure to behave as a thin-walled beam, in which the shear stresses and shear deformations are decisively much larger than in a solid beam. The corresponding effect is the distortion of the cross section, which entails the annulment of the hypothesis of plane sections. As a consequence, the classical theory of bending is no longer applicable and the intensity of the actions in the columns are no longer proportional to the distance from the neutral axis of the section. A careful analysis of the problem shows a non-linear trend of the stresses, which are lower in centre

of the flanges, but higher near the corners. This phenomenon is known as shear lag and plays a decisive role in the design of tubular schemes. Just for this reason the frame tube system is considered inefficient over 60 storeys. A further evolution of the tubular concept overcomes this problem. Braced tubes are devised by means of the addition of external diagonal elements which contribute to stiff the whole structure. Thanks to this solution, the exterior columns can be widely spaced as well as the sizes of spandrel beams and columns can be smaller, permitting to adopt larger window openings. In this case the shear stresses, which represent the main cause of the shear lag of frame tubes, are absorbed by the huge diagonals which almost annul the shear deformation through their axial stiffness, allowing a pure flexural behaviour of the building. In this way the engineers are allowed to reconsider the Euler-Bernoulli hypothesis of plane sections, being the trend of the stresses almost linear. One of the most famous braced tubes is the 100-storeys John Hancock Center in Chicago, in which the diagonals are clearly shown in the facades and placed at 45° angles to each other, forming enormous X braces on each side.

Another structural configuration which implements the tubular scheme is represented by the bundled tube. This solution was adopted to improve the horizontal resistance of super-tall buildings and to renew the architectural shapes of these constructions. A cellular or bundled tube building consists of two or more independent tubes, which operate together to the structural stability of the entire building. Since the bundled tube is derived by the connection of individual tubes, it is possible to model a variety of architectural configurations by simply terminating the tubes at different levels. This solution gives the idea that the structure is climbing towards the sky, causing at the same time the astonishment of the viewers. This expedient also allows to design super tall structures without an excessive increase of the base area, which would be necessary in presence of frame tube scheme.

It is obvious that, in the design of each tube, the shear lag has to be taken into account, even if, in a global analysis, its effect seems to be somewhat reduced. Furthermore other advantages are provided by this configuration. In presence of tubes of different heights, there is firstly a remarkable reduction of the masses from the ground to the top which influences the dynamic behaviour, being the arisen inertia forces decisively smaller as the highest floors are considered; secondly, the lateral sway due to the wind is also reduced, in virtue of less exposed surface areas. This configuration is greatly appreciated and, to this day, one of the most esteemed is Sears Tower, an outstanding 110-storey building, which was the world's tallest building from 1973 to 1998.

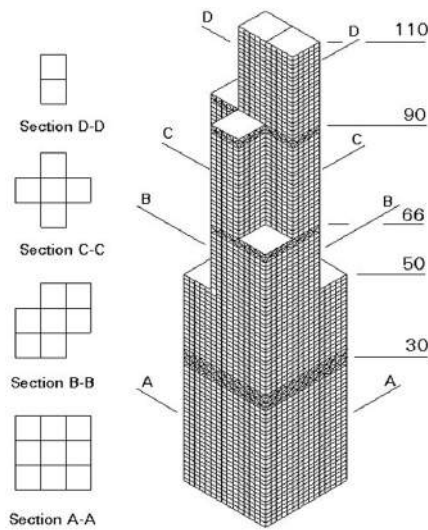


Figure 1.12 – Sear Tower in Chicago (1973, USA).

Its resistant system is composed by nine square tubes each having a different height. Four main cross sections define its external profile: the first shows all the tubes connected each other; the second loses two corner tubes, as the third case, in which other two corner tubes disappear. Finally only two tubular elements reach the total height of the building (Fig. 1.12).

The structural efficiency of bundled tubes can be further improved. The braced tube scheme can be proposed for each single tube, especially in the presence of different shapes, such as rectangular, triangular or hexagonal. This choice forces the structures to behave as an integral body with respect to the external actions and, therefore, loss of structural integrity disappears.

Finally, with the aim of increasing the global stiffness of the building, the external tube system can be connected to an internal core, which participates to resist part of the lateral load. This is the case of tube-in-tube systems, where the core itself can be made up of a solid tube, a braced tube or a framed tube and can be considered as an internal protection against unexpected impacts due to human errors or terrorist attacks. Therefore, it is evident that the tubular concept offers several opportunities to the designers, being a flexible solution able to satisfy most of the innovative architectural shapes and guarantee both stiffness and stability. It is not by chance that the current tallest building in the world is Burj Khalifa, a bundled tube structure of 830 meters, built in Dubai (Saudi Arabia) in 2010.

1.4 Innovative Structural Solutions

Only recently, next to economics, municipal regulations and politics, aesthetics has got a leading role in the planning and design of high-rise buildings. Changes in the structural form are supported by the emerging architectural trends in design and the developments in structural analysis techniques, made possible by the advent of high-speed digital computers.

One of the most known results of this tendency is the diagrid system, which confirms the breakthrough in the idea of tall building. This term is derived by the union of the words *diagonal* and *grid*. The first is associated to the effectiveness of diagonal elements with respect to the horizontal stiffening of frames as well as tubular schemes. In effect, such configurations allow to reduce the global shear deformation of the structure exploiting primarily the axial forces arisen in the diagonal members, which are much less troubling from the design point of view.

The term *grid* refers to the base idea of the tubular schemes, that is the ability to smear most of the horizontal resistance on the external perimeter of the building. The result is a mesh, completely surrounding the building, constituted by only diagonal elements arranged in a triangulated pattern and able to absorb the total horizontal action.

However, if compared to conventional braced configurations, the outstanding originality introduced by diagrid systems is the absence of vertical elements. This means that the mesh is designed to carry, at the same time, gravity loads and lateral actions. Furthermore, even if the structural importance of diagonal bracings has always been acknowledged, most of times they have been hidden within the structure in order to avoid interfering with the building aesthetics. On the contrary, diagrid structures have shown the architectural potentialities of the diagonals, which have become an innovative feature of tall buildings. It suffices to say that their triangulated configuration uniformly arranged on the entire façade enables to model groundbreaking shapes, which contribute to characterise the hosting communities. An example is the 30 St Mary Axe (London, 2004), a 41-storey building defined by a curved form which earns it the name of “the Gherkin”. Such construction demonstrates that current architecture has forsaken prismatic forms, to embrace curved ones.

In the early phases of the design process, two main information are needed to model an elementary scheme for a diagrid structure: the optimum angle of the diagonals and a preliminary assessment of the area constituting the structural grid.

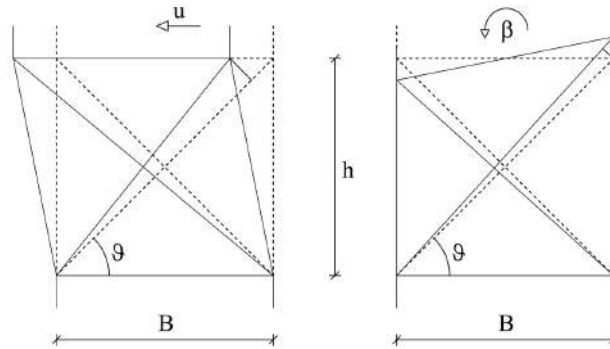


Figure 1.13 – Axial deformation of diagonal bracings due to horizontal displacement and rotation of the braced frame.

In the first case, the optimum angle can be acquired comparing the requirements of the shear strength with the ones related to the bending strength. In the latter case, the value which allows to carry gravity loads and offers the adequate bending stiffness is obviously 90 degrees. This solution is insufficient for the shear resistance, as shown by frames without diagonal bracings. In order to find the best angle for the shear deformation, a simple scheme of a braced frame, reported in Fig. 1.13, facilitates the evaluation. Due to the horizontal displacement u caused by a force F , the diagonals are subjected to axial deformations and, therefore, internal actions F_d arise equilibrating the external force.

$$2F_d \cos \vartheta = F \quad (1.7)$$

In a linear elastic domain, the force F_d is related to the axial deformation ε_d by means of the cross section A and Young's modulus E . In addition, ε_d is function of the horizontal displacement u and the geometrical characteristics of the model. By substituting these information in the previous equilibrium equation, a relationship between the external action F and the corresponding horizontal displacement u is obtained.

$$F_d = EA\varepsilon_d \quad (1.8)$$

$$\varepsilon_d = \frac{u \cos \vartheta}{(h/\sin \vartheta)} = \frac{u \cos \vartheta \sin \vartheta}{h} \quad (1.9)$$

$$F = \frac{1}{h} (\sin 2\vartheta \cos \vartheta EA)u = k_h u \quad (1.10)$$

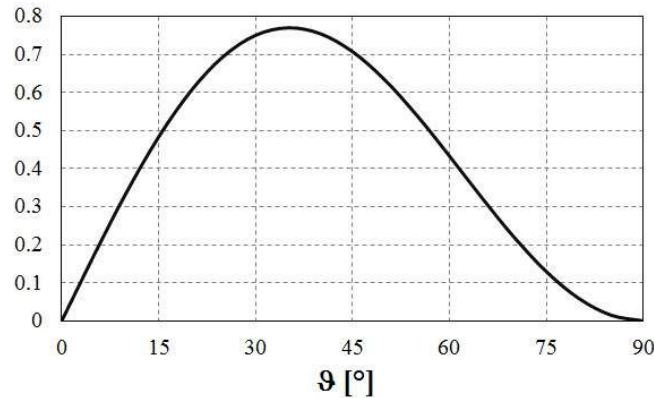


Figure 1.14 – Optimum value of the angle of inclination of the diagonal elements.

The optimum value of ϑ can be deduced plotting the function k_h , which represents the horizontal stiffening of the model. As it can be seen from Fig. 1.14, the optimum ϑ corresponds to about 35° . Since diagrid structures have to resist to both shear and bending actions, it is expected that the angle of the diagonal constituting the external mesh will fall between 90° and 35° . Furthermore, it will be dependent on the geometrical properties of the building: for short buildings having low aspect ratio (height/width), the shear behaviour is dominant and ϑ will move downwards, whereas, for tall buildings with high aspect ratio, the behaviour will be purely flexural and the angle will be close to 90° .

These findings can be confirmed by an example regarding a building with an aspect ratio of 6.7, being the height equal to 240 m and the width to 36 m. In this case two main scheme are modelled: one is constituted by an external mesh together with four corner columns; the other shows only the mesh without any vertical components. In each scheme the inclination of the diagonals is modified according to seven configurations, as shown in Fig. 1.15. A static analysis is performed considering the same horizontal actions for all the cases. The results in terms of top displacements are carried out in Fig. 1.16 and 1.17. In the first model, where the corner columns are employed, the analysis demonstrates that the lateral stiffness is not too sensitive to angle in the region of 63° . Therefore, the inclinations between 53° and 69° can be equally taken into account. In the second model, since no vertical elements are present, the diagonals have to carry, at the same time, both gravity and horizontal loads. The corresponding effect is the upward shift of the optimum value of ϑ , with an average value of about 70° .

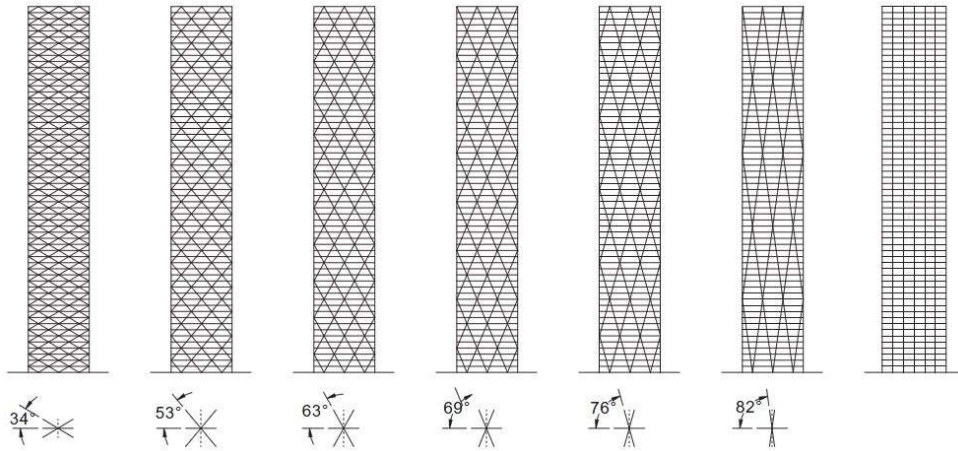


Figure 1.15 – Different schemes of diagrid structures in terms of angle of inclination of the diagonal bracings.

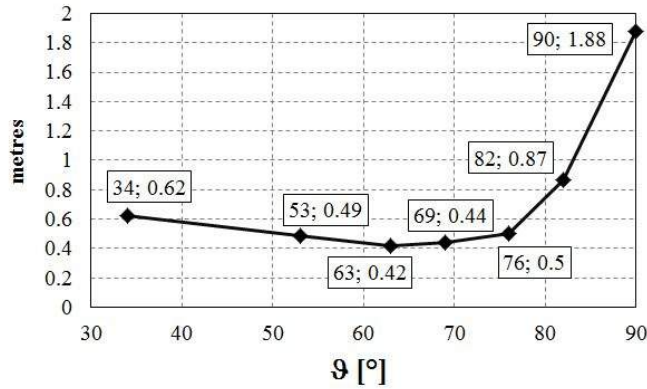


Figure 1.16 – Top displacement of a tall building stiffened by an external mesh constituted by vertical and diagonal elements: effect of the inclination of the diagonals on the results.

Another important point of a preliminary design is the evaluation of the amount of area in the diagonals of the mesh. For this purpose the building can be divided into modules which define single diagrid patterns. Depending on the direction of the load, the faces, in which the structural elements are considered subjected to only axial forces, act as webs or flanges.

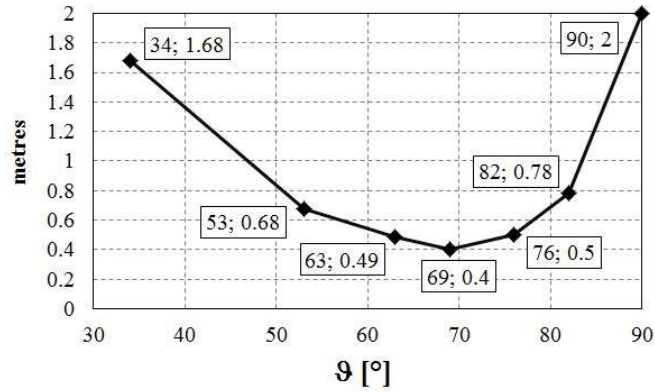


Figure 1.17 – Top displacement of a tall building stiffened by an external mesh constituted by diagonal elements: effect of the inclination of the diagonals on the results.

With respect to Fig. 1.18, a relation between the external actions and the corresponding displacements can be acquired. Taking into account the scheme of Fig. 1.13, the following relations can be written:

$$V = k_T u \quad (1.11)$$

$$M = k_M \beta \quad (1.12)$$

where

$$k_T = 2 \left(\frac{A_{dw} E}{L_d} \cos^2 \vartheta \right) N_w \quad (1.13)$$

$$k_M = \left(\frac{A_{df} E}{2L_d} B^2 \sin^2 \vartheta \right) N_f \quad (1.14)$$

The terms N_w and N_f represent the number of diagonals belonging to the webs and flanges respectively. Once the external load is defined as well as the maximum displacements are derived from the limits imposed by legislation, the approximate value of area of the diagonals can be obtained:

$$A_{dw} = \frac{VL_d}{2N_w E \cos^2 \vartheta} \quad (1.15)$$

$$A_{fw} = \frac{2ML_d}{N_f E B^2 \sin^2 \vartheta} \quad (1.16)$$

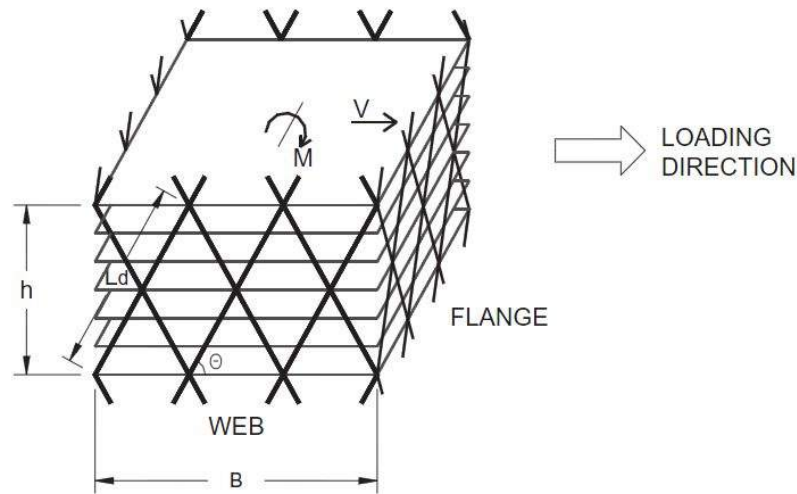


Figure 1.18 – Scheme of a diagrid structure for a preliminary design of the diagonals.

The expressions (1.15) and (1.16) have to be applied to both the principal directions of load, in order to evaluate the upper bound value related to the areas. These information can be employed in the phases of the conceptual design, to identify the preliminary geometrical characteristics of the structure according to the architectural requirements.

Nowadays other lateral load resisting systems, such as space trusses, which are modified braced tube with diagonals connecting the exterior to the interior, superframes, in which mega-columns are realised as components of braced frames, and exoskeleton structures, which have the horizontal resistance placed outside the building line, are gaining ground.

Nevertheless, it is evident that developments regarding the design of high-rise and irregular buildings are described by a continuously evolving process. The interference coming from the new architectural trends is leading the building design towards solutions which have to optimise the structural skeleton with respect to the exterior shapes, such as aerodynamic, twisted, tapered, tilted or even free ones.

As a matter of fact, all over the world, some bizarre shapes have already been commissioned and, in some cases, just built: for instance, the HSB Turning Torso, a twisted skyscraper of 54 storeys in Malmo (Sweden), and the 66-storey London Bridge Tower, also known as Shard of Glass, a pyramidal shaped building now the

tallest structure in Europe, are very appreciated. In addition, many futuristic projects have already been proposed: among all the Millennium Tower by Sir Norman Foster, which is a 170-storey tower reaching 840 meters of height, and the Kingdom Tower, which should be over 1 km high, can be remembered.

For the future, it is expected that the already achieved limits will feed the pursuit of new heights and unconventional shapes and, therefore, it will probably determine improvements in technology of structural systems and materials.

Even if the increase of the complexity of the forms is balanced by powerful computers and several multi-function Finite Element (FE) software, the choice of an appropriate model able to thoroughly identify the key parameters governing the response of the structure as well as the force flow acting within the stiffening members remains crucial. On the one hand, FE programs can evaluate the construction in its entirety, reaching high degree of accuracy. They can model any detail, giving the idea that nothing gets lost.

Nevertheless this skill can hide some drawbacks [61, 103]. During the design stage, it's very difficult to assess the resistant contributions coming from different stiffeners as well as handle an enormous amount of data. In effect, especially during the phase of evolution of the concept, the former could cause time-consuming misunderstandings; the latter could be easily a source for errors. Moreover, the great number of input and output data does not support a clear explanation of the structural mechanism and does not allow the designers to identify the distribution of the external forces among the stiffening members.

On the other hand, based on some carefully chosen hypotheses, simplified procedures could represent a valid alternative in the early stage of conceptual design being characterised by some advantages, such as a faster data preparation and a more transparent method of analysis, which can make the process less liable to unexpected errors. In addition, unlike FE simulations, the limited degree of accuracy is balanced by the capability to provide a comprehensive picture of the structural behaviour and to gain knowledge of the key parameters governing the response of the building.

In any case, being reciprocally complementary instruments, both approaches can lend support to the engineer's judgment. While, in the early stages, approximate methods evaluate the basic characteristics of the project, in the final ones, FE models can conduct a more thorough computation.

Chapter 2

The load Distribution Matrix between Vertical Bracings

2.1 Introduction

In most buildings the horizontal resistant system consists of different elements which can vary one to another according to their specific stiffness properties. The use of in-parallel members is a structural solution which immediately appeared as a simple way of increasing the horizontal stiffening of high-rise structures. From the design point of view, many researches were developed to identify the distribution of the external forces among the internal bracings.

The earliest models, dating back to 1960's and 1970's, were provided for the preliminary design of tall buildings, in particular to offer approximate and quick approaches that were at engineers' disposal. In some cases, design curves were proposed in order to address the structural solutions towards the best ones for the specific loading case. At that time the comparison between analytical methods and those relying on digital computers started to appear. Nevertheless, the drawbacks of the analytical approaches were related to the fact that they could be applied to restricted cases, defined by simple structural combinations. As a matter of fact, in most cases planar configurations were studied and only one degree of freedom per storey was considered.

The formulations conceived in this field were based on the following fundamental hypotheses:

- the structural material is homogeneous, isotropic and obeys Hooke's law;
- the floor slabs are rigid in their own plane but their out-of-plane rigidity is neglected;
- only static and conservative loads are taken into account in the analysis;
- for transversal analysis, the axial deformation of the structural elements due to gravity loads is considered negligible.

The earliest methods took into account the case of shear-wall versus frame interaction. Related to this scheme, the approaches by Khan and Sbarounis [64], Coull and Irwin [34], Heidebrecht and Stafford Smith [58, 59], Haris [56] and Mortelmans *et al.* [84] can be mentioned.

The papers by Khan and Sbarounis represent the first effort to this study. Coull and Irwin proposed a simple coefficient method for the assessment of the load distribution in three-dimensional structures stiffened by shear walls; Heidebrecht and Stafford Smith devised an approximate method of analysis of open section shear walls subjected to torsional actions as well as a simple hand method for the static and dynamic analysis of uniform and non-uniform structure consisting in frames coupled with shear walls, both defined by planar loading and deformation; Haris focused his attention on the matrix approach for the determination of the load distribution matrix related to in-parallel planar frames. Furthermore his paper was one of the first which included the torsional behaviour in the analysis. Finally Mortelmans, also followed the way traced by Haris and proposed an approximate method for the combined bending and twisting of high-rise buildings under wind loading. He reduced the problem to the solution of a linear system of four equations with four unknowns, from which the bending and twisting moments in any element of the structure could be acquired, regardless the number of floors but with an high degree of accuracy.

Other approaches followed, most of which were based on the continuum medium technique. This method permitted to take into account the elements which connect the vertical bracings at the floor levels. The base idea was to replace the effective connection by continuously shear forces, which produced a stiffening effect on the behaviour of the global system. Rosman [95, 96] was the pioneer of this approach. In effect he was the first to analyse shear walls with openings which could be treated as distinct walls characterised by a global stiffening due to rigid connecting beams. After him, Beck [9] extended the formulation taking into consideration the axial deformation of the walls and offered simplified formulas for the determination of the redundant unknowns arising in the connecting elements.

The continuum medium technique was followed by other works: among all, the papers by Schwaighofer [98], Coull and Choudhury [31], Qadeer and Stafford Smith [90] can be pointed out. Later, Stamato and Mancini [102], Gluck and Krauss [54] used the same technique to analyse three-dimensional problems concerning frames and walls.

The evolution of the construction typologies due to the search for greater heights as well as the development of innovative architectural shapes, involved the conception of different formulations. The first results were represented by Khan [65], Coull and Bose [37], who dealt with tubular structures. The same research was further extended to other structural issues, as the case of Hoenderkamp and Snijder [60], who focused on the structural effects of flexible connections, while Lee *et al.* [71] proposed an analytical method for the design of outrigger systems.

In some cases, the approaches were derived from different research areas, however proving to be adequate for the analysis of tall constructions. Developed for framed-tube systems, the stringer-shear panel method by Connor and Pougare [30] was derived from aeronautics. Modelling the resistant skeleton as a stringer-shear panel assembly in which the stringers were supposed to carry only axial loads without bending stiffness and the panels were defined by shear rigidity without axial or bending strength, the building could be reduced to stringers on any side and shear panels in between.

In another case, a core tube could be analysed as an equivalent rod, in which the effects of the bending and shear deformation as well as shear lag and torsion were taken into account. Closed-form solutions were acquired for the deflection, shear lag and torsional angle, by means of the elastic theory by Takabatake and Matsuoka [107, 108].

Other methods, starting from aerospace engineering, imagined to subdivide the structure into substructures and to operate as the case of Finite Element (FE) approach, in which the substructures were considered as super-elements. The first focused on this methodology were Leung [72], Leung and Wong [73], Wong and Lau [125], followed, more recently, by Kim and Lee [66] and Steenbergen and Blaauwendraad [103].

A further formulation was proposed by Pekau *et al.* [86, 87], by means of their approach, called Finite Storey Method (FSM). The global behaviour of the construction could be reduced to the nodal displacements obtained from the analysis of two-storey substructures. The main advantage was a reduced number of nodes so that the computational time of the method proved to be very short; in addition, both frames and shear walls, in a single scheme or composed to represent tube-in-tube configurations, could be considered.

As it can be seen, many formulations can be employed for the static analysis of a tall building; however, most of them are characterised by a deep lack of generality, which impedes to analyse different structural typologies and, above all, tends to reduce a three-dimensional examination to a planar problem. In this way, it is evident that they become inappropriate, especially in the case of very complex shapes, which cannot be grossly simplified.

2.2 A Synthetic Three-Dimensional Approach

In line with the mentioned formulations, a more general semi-analytical approach is here described. It is a three-dimensional method, directly derived from the papers by Carpinteri *et al.* [24, 25], in which only three degrees of freedom per storey are taken into account. This choice allows to study, at the same time, the bending and the torsional behaviour of the structure.

The approach proves to be general, since it is possible to consider any type of vertical bracings, from simple frames to free-shaped tube systems. Furthermore, it is defined by the following benefits: firstly, the load distribution matrix, which defines the amount of external force absorbed by each structural element according to its own stiffness and its position in the building plan, can be evaluated; secondly, an easy identification of the structural parameters on which the horizontal behaviour of the building depends can be performed; finally, the formulation proves to be extremely clear and concise, limiting in this way the risk of unexpected errors and guaranteeing, in presence of very complex structures, very short times of modelling and analysis, if compared to FE programs.

Starting from the previously mentioned hypotheses, a N-storey building is considered having M vertical bracings, each defined by an arbitrary position in the floor plan. The right-handed system XYZ defines the global coordinate system of the problem. Since the slabs, which interconnect the bracings each other, are considered infinitely rigid in their plane, the degrees of freedom of the problem can be represented by the transversal displacements of the floors: in particular, two translations ξ and η directed according to the X and Y direction and the transversal rotation ϑ , for each storey. In the same way, the external load applied to the building is expressed by the 3N-vector f , in which 2N shears p_x , p_y and N torsional moments m are included (Fig. 2.1).

$$f = \begin{Bmatrix} p \\ m \end{Bmatrix} = \begin{Bmatrix} p_x \\ p_y \\ m \end{Bmatrix} \quad (2.1)$$

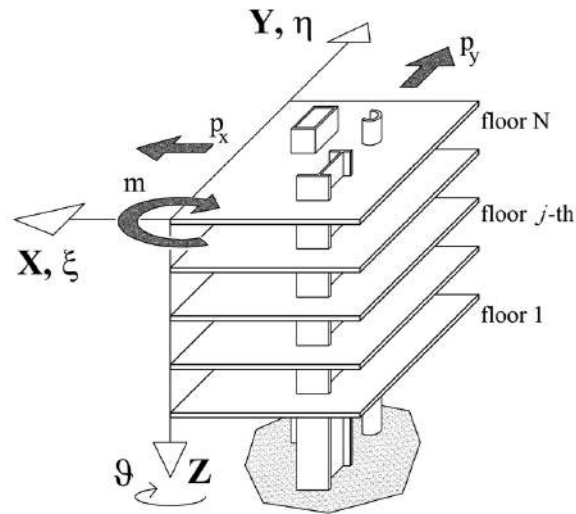


Figure 2.1 – Scheme of a tall building stiffened by M vertical bracings and subjected to transversal actions.

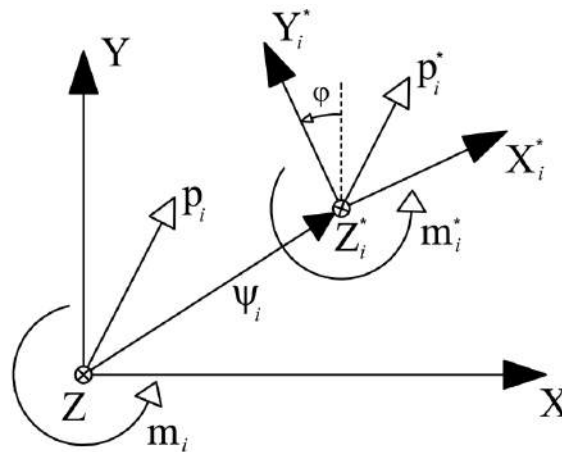


Figure 2.2 – Global and local coordinate systems. The Z -axis completes the right-handed global system XYZ and Z_i^* completes the right-handed local system $X_i^* Y_i^* Z_i^*$.

For the i -th bracing the right-handed system $X_i^* Y_i^* Z_i^*$ represents its local coordinate system.

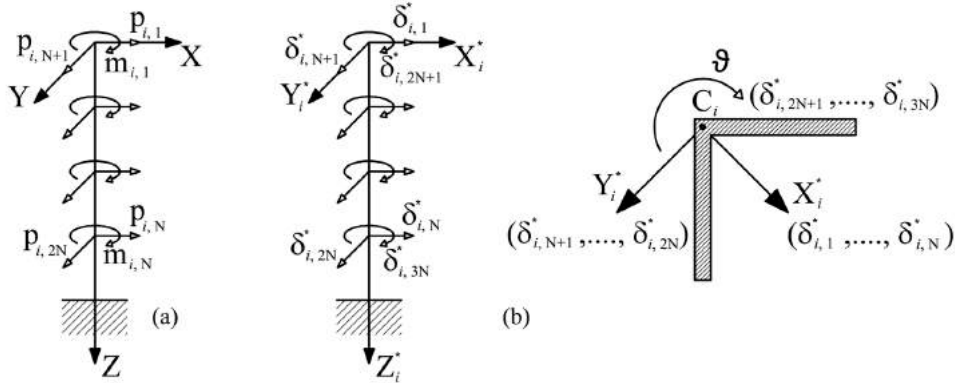


Figure 2.3 – Internal loadings f_i transmitted to the i -th bracing in the global coordinate system (a); degrees of freedom of the i -th bracing in the local coordinate system $X_i^*Y_i^*Z_i^*$, axonometry and top view (b). Note that the highest floor is indicated with 1 and the lowest with N.

The $3N$ -load vector f_i^* and the $3N$ -displacement vector δ_i^* describe the amount of external load absorbed by the i -th element and its transversal displacements respectively, both in the local coordinate system (Fig. 2.2).

The loading vector f_i^* can be reduced to f_i , which refers to the global coordinate system XYZ , by means of the following expressions:

$$p_i^* = N_i p_i \quad (2.2)$$

$$m_i^* = m_i - \psi_i \wedge p_i \cdot u_z \quad (2.3)$$

$$f_i = \begin{Bmatrix} p_i \\ m_i \end{Bmatrix} \quad (2.4)$$

where the superscript $*$ indicates that the coordinate system is the local one.

The term N_i represents the orthogonal matrix from the system XY to the system $X_i^*Y_i^*$; ψ_i is the coordinate vector of the origin of the local system in the global one; u_z is, instead, the unit vector associated to the Z direction.

The orthogonal matrix N_i can be represented by means of the angle φ between the Y axis and the Y_i^* axis (Fig. 2.2):

$$N_i = \begin{bmatrix} \cos \varphi & \sin \varphi \\ -\sin \varphi & \cos \varphi \end{bmatrix} \quad (2.5)$$

in which each term is a diagonal $N \times N$ sub-matrix.

$$\mathbf{cos} \varphi = \begin{bmatrix} \cos \varphi & 0 & 0 \\ 0 & \dots & 0 \\ 0 & 0 & \cos \varphi \end{bmatrix} \quad (2.6)$$

Eqns (2.2) and (2.3) can be re-written in the following matrix form

$$\mathbf{f}_i^* = \mathbf{A}_i \mathbf{f}_i \quad (2.7)$$

The matrix \mathbf{A}_i gathers the information regarding the reciprocal rotation between the local and global coordinate systems and the location of the i -th bracing in the global system XY :

$$\mathbf{A}_i = \begin{bmatrix} \mathbf{N}_i & \mathbf{0} \\ -\mathbf{u}_z \wedge \psi_i & \mathbf{I} \end{bmatrix} \quad (2.8)$$

where \mathbf{I} is the identity matrix and $\mathbf{0}$ the null matrix. The component $-\mathbf{u}_z \wedge \psi_i$, valid for each floor, is a relation obtained from Eqn (2.3) exploiting the fact that the scalar triple product is invariant under any cyclic permutation of its terms. For the sake of simplicity, in order to take into account the N floors of the structure, this vector product can be written as a final $2N \times N$ matrix \mathbf{C}_i composed by two diagonal sub-matrices containing the coordinates (x_i, y_i) of the origin of the local system $X_i^* Y_i^*$.

$$-\mathbf{u}_z \wedge \psi_i = - \begin{vmatrix} \bar{i} & \bar{j} & \bar{k} \\ 0 & 0 & 1 \\ x_i & y_i & 0 \end{vmatrix} = -[-y_i \quad x_i] = -\mathbf{C}_i^T \quad (2.9)$$

Thus the final expression for the matrix \mathbf{A}_i is:

$$\mathbf{A}_i = \begin{bmatrix} \mathbf{N}_i & \mathbf{0} \\ -\mathbf{C}_i^T & \mathbf{I} \end{bmatrix} \quad (2.10)$$

In the same way, the vector δ_i^* , constituted by $2N$ translations ξ_i^* , η_i^* and N rotations ϑ_i^* , can be connected with the same one, referred to the global coordinate system δ_i , by means of the synthetic $N \times N$ matrix \mathbf{B}_i :

$$\delta_i^* = \mathbf{B}_i \delta_i \quad (2.11)$$

Since the following relationships are valid for the displacements:

$$\begin{Bmatrix} \xi_i^* \\ \eta_i^* \end{Bmatrix} = \mathbf{N}_i \begin{Bmatrix} \xi_i \\ \eta_i \end{Bmatrix} \quad (2.12)$$

$$\vartheta_i^* = \vartheta_i \quad (2.13)$$

the matrix \mathbf{B}_i is similar to the matrix \mathbf{A}_i , in which the term \mathbf{C}_i^T is reduced to a null matrix.

$$\mathbf{B}_i = \begin{bmatrix} \mathbf{N}_i & \mathbf{0} \\ \mathbf{0} & \mathbf{I} \end{bmatrix} \quad (2.14)$$

A relation between f_i^* and δ_i^* is well-known by means of the condensed stiffness matrix \mathbf{k}_i^* , referred to the local coordinate system:

$$f_i^* = \mathbf{k}_i^* \delta_i^* \quad (2.15)$$

Substituting Eqns (2.7) and (2.11) into Eqn (2.15), the load vector f_i turns out to be connected with the displacement vector δ_i through a product of matrices, which identifies the stiffness matrix \mathbf{k}_i of the i -th bracing in the global coordinate system XY.

$$f_i = (\mathbf{A}_i^{-1} \mathbf{k}_i^* \mathbf{B}_i) \delta_i = \mathbf{k}_i \delta_i \quad (2.16)$$

Exploiting the presence of in-plane rigid slabs, the transversal displacements of each element can be computed considering only the three generalised floor displacements ξ , η and ϑ . This is performed through the matrix \mathbf{T}_i , which takes into account the location of the bracing in the floor plan by means of the coordinates $(x_i; y_i)$.

If we consider the equation which describes the rigid displacements of a point P with respect to another point O, the following vector expression is derived:

$$d_P = d_O + \vartheta \bar{\mathbf{k}} \wedge (P - O) \quad (2.17)$$

which, in expanded form, becomes

$$\begin{Bmatrix} u_P \\ v_P \end{Bmatrix} = \begin{Bmatrix} u_O \\ v_O \end{Bmatrix} + \begin{bmatrix} 0 & -\vartheta \\ \vartheta & 0 \end{bmatrix} \begin{Bmatrix} x_P - x_O \\ y_P - y_O \end{Bmatrix} \quad (2.18)$$

If the point P represents the origin of the local coordinate system, whereas O the origin of the global one, Eqn (2.17) can be re-written as

$$d_i = d + \vartheta \bar{\mathbf{k}} \wedge \psi_i \quad (2.19)$$

The translation in X direction of Eqn (2.19) is computed by means of the unit vector u_x :

$$u_i = u + \vartheta \bar{\mathbf{k}} \wedge \psi_i \cdot u_x \quad (2.20)$$

Exploiting the properties of the scalar triple product, Eqn (2.20) becomes

$$u_i = u + \psi_i \wedge u_x \cdot \vartheta \bar{k} \quad (2.21)$$

In the same way, the translation in Y direction is

$$v_i = v + \psi_i \wedge u_y \cdot \vartheta \bar{k} \quad (2.22)$$

As in the case of Eqn (2.9), it is possible to define a final matrix containing the vector products of Eqns (2.21) and (2.22), which assumes the same form of the aforementioned matrix \mathbf{C}_i .

$$d_i = d + \begin{bmatrix} \psi_i \wedge u_x \\ \psi_i \wedge u_y \end{bmatrix} \vartheta \bar{k} \quad (2.23)$$

The expansion of Eqn (2.23) to consider N floors gives rise to

$$\begin{bmatrix} \psi_i \wedge u_x \\ \psi_i \wedge u_y \end{bmatrix} = \begin{bmatrix} -y_i \\ x_i \end{bmatrix} = \mathbf{C}_i \quad (2.24)$$

and, therefore, the $3N \times 3N$ matrix \mathbf{T}_i is easily acquired.

$$\delta_i = \begin{bmatrix} \mathbf{I} & \mathbf{C}_i \\ \mathbf{0} & \mathbf{I} \end{bmatrix} \delta = \mathbf{T}_i \delta \quad (2.25)$$

The substitution of Eqn (2.25) in (2.16) allows to identify the stiffness matrix of the i -th bracing, referred to the global coordinate system XYZ and to the generalised floor displacements ξ , η and ϑ :

$$f_i = (\mathbf{A}_i^{-1} \mathbf{k}_i^* \mathbf{B}_i \mathbf{T}_i) \delta = \bar{\mathbf{k}}_i \delta \quad (2.26)$$

For the global equilibrium, the external load f applied to the structure is equal to the sum of the M vectors f_i . In this way a relationship between the external load and the floor displacements is obtained and the global stiffness matrix of the structure is computed. By means of this matrix, once the external load is defined, the displacements of the structure are acquired, from which information regarding each single bracing can be deduced.

$$f = \sum_{i=1}^M f_i = \sum_{i=1}^M (\mathbf{A}_i^{-1} \mathbf{k}_i^* \mathbf{B}_i \mathbf{T}_i) \delta = \sum_{i=1}^M \bar{\mathbf{k}}_i \delta = \mathbf{K} \delta \quad (2.27)$$

and, therefore,

$$\delta = \mathbf{K}^{-1} f \quad (2.28)$$

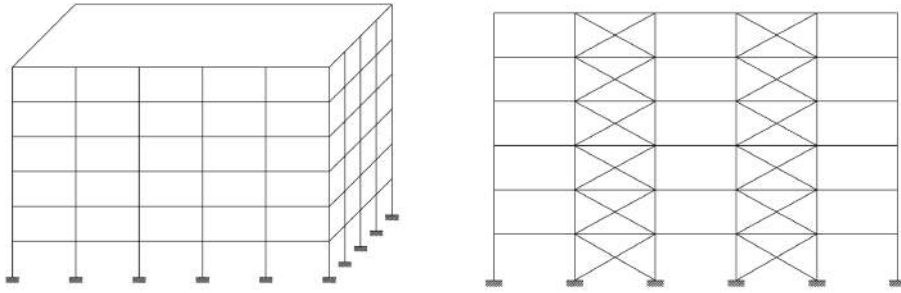


Figure 2.4 – Horizontal stiffening in tall buildings: a 3D frame and a planar braced frame.

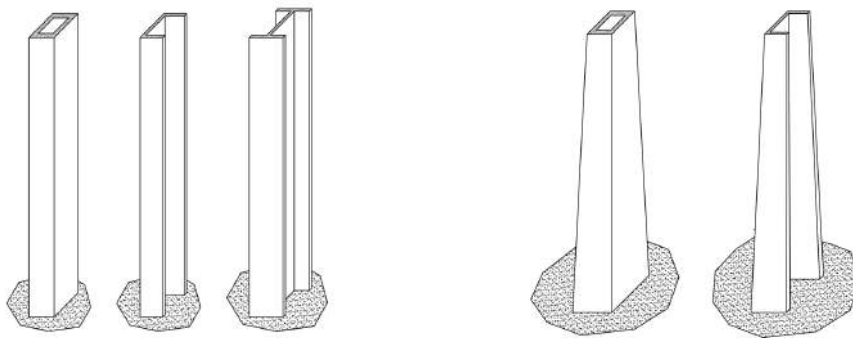


Figure 2.5 – Horizontal stiffening in tall buildings: shear walls with constant section and tapering profiles.

Recalling Eqn (2.26) and comparing it with Eqn (2.28), an equation connecting the vector f with f_i allows to define the amount of the external load absorbed by the i -th vertical stiffening:

$$\delta = \mathbf{K}^{-1}f = \bar{\mathbf{k}}_i^{-1}f_i \quad (2.29)$$

$$f_i = \bar{\mathbf{k}}_i \mathbf{K}^{-1}f = (\mathbf{A}_i^{-1} \mathbf{k}_i^* \mathbf{B}_i \mathbf{T}_i) \mathbf{K}^{-1}f = \mathbf{R}_i f \quad (2.30)$$

The load distribution matrix \mathbf{R}_i , obtained from Eqn (2.30), demonstrates that each bracing is subjected to a load which is directly proportional to the external load f and to its own stiffness matrix \mathbf{k}_i^* , but inversely proportional to the global stiffness matrix \mathbf{K} , as the case of in-parallel bracings in a plane problem. Once the generalised displacement vector δ is known, recalling Eqns (2.11), (2.15) and (2.25), the displacements and the corresponding forces related to the i -th bracing,

in its local coordinate system, can be computed. Consequently, since the loads applied to each element are clearly identified, a preliminary design can be easily performed.

$$\delta_i^* = \mathbf{B}_i \mathbf{T}_i \mathbf{K}^{-1} \mathbf{f} \quad (2.31)$$

$$\mathbf{f}_i^* = \mathbf{k}_i^* \mathbf{B}_i \mathbf{T}_i \mathbf{K}^{-1} \mathbf{f} \quad (2.32)$$

Eqn (2.32) solves the problem of the external loading distribution between the resistant elements employed to stiffen a three-dimensional tall building. Such formulation proves to be general and can be adopted with any kind of structural elements, provided that their own condensed stiffness matrix \mathbf{k}_i^* is known. Therefore most of the common horizontal stiffeners, such as frames, braced frames, shear walls and tube-systems can be easily implemented in this static formulation (Fig. 2.4, 2.5).

2.3 Stiffness Matrix of Frames and Braced Frames

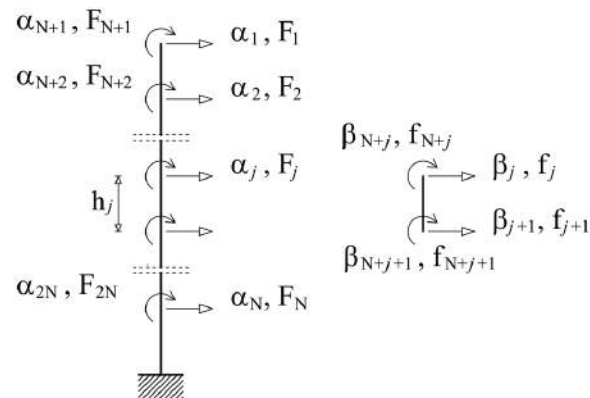


Figure 2.6 – Scheme for the computation of the stiffness matrix of a cantilever beam.

Particular attention is focused on the computation of the stiffness matrix of a frame structure. Before deeply analysing this topic, the procedure which allows to define the condensed stiffness matrix of a vertical cantilever is proposed, according to the method proposed by Pozzati [88].

Let us consider a shear wall subjected to concentrated horizontal forces F_i (Fig. 2.6).

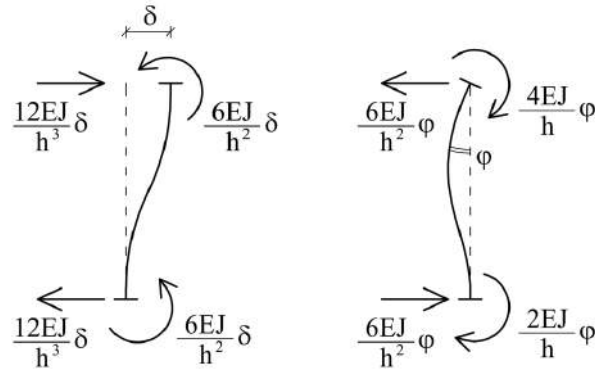


Figure 2.7 – Components of the stiffness matrix of a beam.

Each inter-floor segment, whose dimension is constant and equal to h , is defined by the corresponding stiffness matrix \mathbf{k}_j , which refers to the horizontal displacements $(\alpha_1, \dots, \alpha_N)$ and rotations $(\alpha_{N+1}, \dots, \alpha_{2N})$ (Fig. 2.7).

$$\mathbf{k}_j = \frac{EJ_j}{h^3} \begin{bmatrix} 12 & -12 & -6h & -6h \\ -12 & 12 & 6h & 6h \\ -6h & 6h & 4h^2 & 2h^2 \\ -6h & 6h & 2h^2 & 4h^2 \end{bmatrix} \quad (2.33)$$

The global stiffness matrix of shear wall can be obtained expanding and adding the contributions of all the segments. Therefore, in the case of a 3-storey shear wall having constant geometrical dimensions, the global stiffness matrix is:

$$\mathbf{K} = \frac{EJ}{h^3} \begin{bmatrix} 12 & -12 & 0 & -6h & -6h & 0 \\ -12 & 24 & -12 & 6h & 0 & -6h \\ 0 & -12 & 24 & 0 & 6h & 0 \\ -6h & 6h & 0 & 4h^2 & 2h^2 & 0 \\ -6h & 0 & 6h & 2h^2 & 8h^2 & 2h^2 \\ 0 & -6h & 0 & 0 & 2h^2 & 8h^2 \end{bmatrix} \quad (2.34)$$

The latter can be written highlighting some terms:

$$\mathbf{F} = \mathbf{K}\delta \rightarrow \begin{Bmatrix} F_d \\ 0 \end{Bmatrix} = \begin{bmatrix} \mathbf{k}_{dd} & \mathbf{k}_{dr} \\ \mathbf{k}_{rd} & \mathbf{k}_{rr} \end{bmatrix} \begin{Bmatrix} \delta_d \\ \delta_r \end{Bmatrix} \quad (2.35)$$

in which δ_d and δ_r stand for horizontal displacements and rotations respectively.

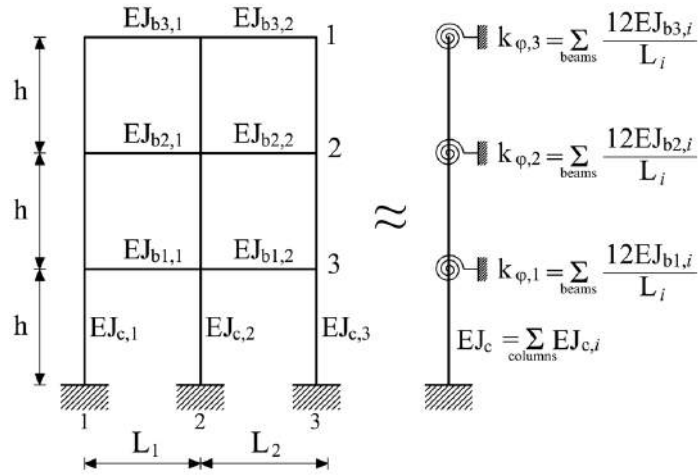


Figure 2.8 – Equivalence between a frame with rigid connections and a shear wall.

From Eqn (2.35) the condensed stiffness matrix \mathbf{K}^* of the shear wall can be obtained and the relationship between actions and horizontal displacements can be acquired:

$$\mathbf{K}^* = \mathbf{k}_{dd} - \mathbf{k}_{dr} \mathbf{k}_{rr}^{-1} \mathbf{k}_{rd} \tag{2.36}$$

$$\mathbf{F}_d = \mathbf{K}^* \delta_d = (\mathbf{k}_{dd} - \mathbf{k}_{dr} \mathbf{k}_{rr}^{-1} \mathbf{k}_{rd}) \delta_d \tag{2.37}$$

In the case of a frame with rigid connections, the previous formulation can be used if we consider that the rotations of the nodes belonging to the same floor are equal each other. This assumption can be considered true in presence of infinitely rigid floors, when the frame shows a perfectly shear type behaviour; otherwise, it describes only an approximate behaviour. Following this hypothesis, the rotational resistance due to each bay is given by $6EJ_b/L$ for each node, being J_b and L the second moment of inertia and the length of the horizontal beam respectively. The contributions of all the bays can be added together and considered as the effect of a rotational spring applied to the corresponding floor.

Therefore, recalling Eqn (2.35), its effect can be directly included in the main diagonal of the sub-matrix \mathbf{k}_r . On the other hand, excluding the bays, the frame can be easily treated as a shear wall in which the resistance of each segment is equal to the sum of the resistances of the corresponding columns.

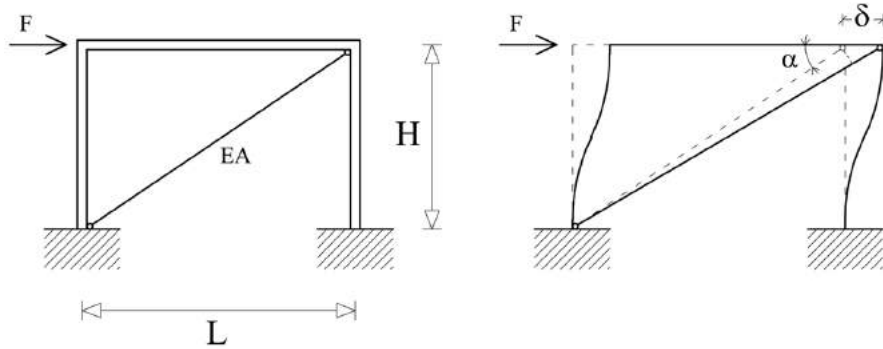


Figure 2.9 – Scheme of a braced frame with a single diagonal element.

In the case of a 3-storey frame with a constant floor height (Fig. 2.8), the corresponding stiffness matrix can be defined by two components: the first one is related to the columns, whereas the second to the bays:

$$\mathbf{K} = \mathbf{k}_c + \mathbf{k}_b \quad (2.38)$$

The matrix \mathbf{k}_c can be written taking into account Eqn (2.34):

$$\mathbf{k}_c = \frac{(\sum E J_{c,i})}{h^3} \begin{bmatrix} 12 & -12 & 0 & -6h & -6h & 0 \\ -12 & 24 & -12 & 6h & 0 & -6h \\ 0 & -12 & 24 & 0 & 6h & 0 \\ -6h & 6h & 0 & 4h^2 & 2h^2 & 0 \\ -6h & 0 & 6h & 2h^2 & 8h^2 & 2h^2 \\ 0 & -6h & 0 & 0 & 2h^2 & 8h^2 \end{bmatrix} \quad (2.39)$$

On the contrary, the matrix \mathbf{k}_b is a null matrix with the exception of the component \mathbf{k}_{rr} which is given by:

$$\mathbf{k}_b = \begin{bmatrix} \mathbf{0} & \mathbf{0} \\ \mathbf{0} & \mathbf{k}_{rr} \end{bmatrix} \rightarrow \mathbf{k}_{rr} = \begin{bmatrix} k_{\varphi 3} & 0 & 0 \\ 0 & k_{\varphi 2} & 0 \\ 0 & 0 & k_{\varphi 1} \end{bmatrix} \quad (2.40)$$

Finally, exploiting Eqn (2.36), the condensed stiffness matrix of the frame is obtained.

The same formulation can be extended in order to encompass braced frames by considering the effects of the resistant diagonals.

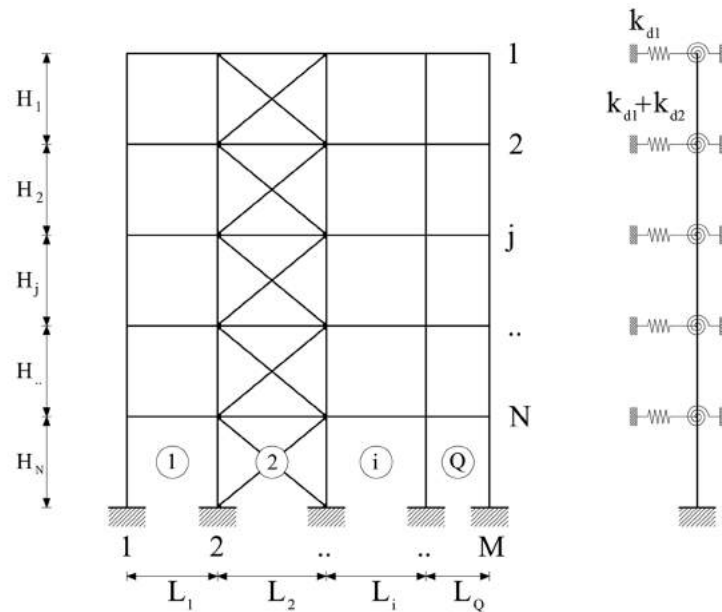


Figure 2.10 – Model of a braced frame equivalent to a shear wall.

Defining EA as the axial rigidity of the diagonal elements, only bracings in tension are assumed to be engaged in the analysis. The simplified scheme of Fig. 2.9, showing the deformed configuration of a braced frame stiffened by a single diagonal element, helps to identify a further resistant contribution.

Due to the displacement δ of the frame, the diagonal bracing is subjected to an axial deformation, which is a function of the angle α . As a result, an axial force arises in the element:

$$N_d = \left(\frac{EA}{\sqrt{L^2 + H^2}} \cos \alpha \right) \delta \quad (2.41)$$

The horizontal component of this force constitutes the resistant contribution of the diagonal bracing with regard to the lateral displacement of the frame.

$$F = \left[\frac{EA}{\sqrt{L^2 + H^2}} (\cos \alpha)^2 \right] \delta = k_d \delta \quad (2.42)$$

Therefore, the structural scheme proposed by Pozzati (Fig. 2.8) can be modified, adding to each floor a fictitious horizontal spring whose stiffness is the sum of the terms k_d related to the diagonals connected to the floor (Fig. 2.10).

This resistant contribution can be directly added to the coefficients of the main diagonal of the sub-matrix \mathbf{k}_{dd} previously described in Eqn (2.35).

In the case of diagonals which refer to Q non-consecutive floors, it is better to define a reduced $Q \times Q$ stiffness matrix, which only represents the contribution of the diagonal bracings. The latter, adequately expanded to N -dimension, can be added to the $N \times N$ stiffness matrix of the corresponding simple frame and, then, included in the general formulation [27].

2.4 Numerical Example

The capability of the analytical method is highlighted by the execution of a numerical example on a high-rise building, loaded by transversal static actions.

A 40-storey building, whose horizontal resistance is provided by three open section shear walls reaching an height of 200 meters, is considered. Their dimensions and geometrical properties are shown respectively in Fig. 2.11 and in Table 2.1.

Table 2.1 – Geometrical properties of the shear walls.

Element N.	1	2	3
I_x [m ⁴]	483.45	19.22	71.18
I_y [m ⁴]	80.76	176.40	469.99
I_{ω} [m ⁶]	3611.67	487.50	1997.06
J_t [m ⁴]	0.54	0.31	1.29
x_s [m]	-15.21	0.00	16.45
y_s [m]	3.43	-13.79	6.97
α [°]	-32.45	0.00	-8.69

The structural material is concrete, whose mechanical properties are an elastic modulus and Poisson's ratio equal to 30000 MPa and 0.18 respectively.

The loading is defined by concentrated transversal actions applied to the floors, according to the global coordinate system XYZ (Fig. 2.11).

In particular, along the X direction a resultant force of 99 kN for each floor is considered, whereas in Y direction it becomes equal to 104 kN. In this specific case a clockwise torsional moment of 183.5 kNm is taken into account.

This structural scheme is modelled through both the present method and a computer program implementing the Finite Element method.

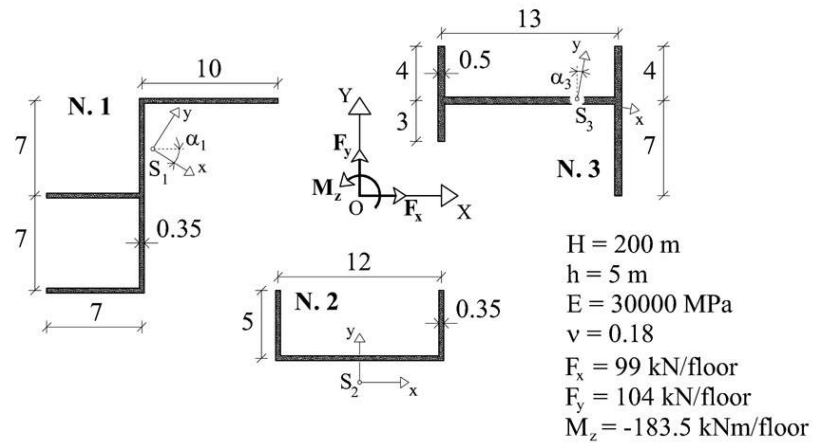


Figure 2.11 – Internal core system of a tall building constituted by thin-walled open section shear walls (measures in metres).

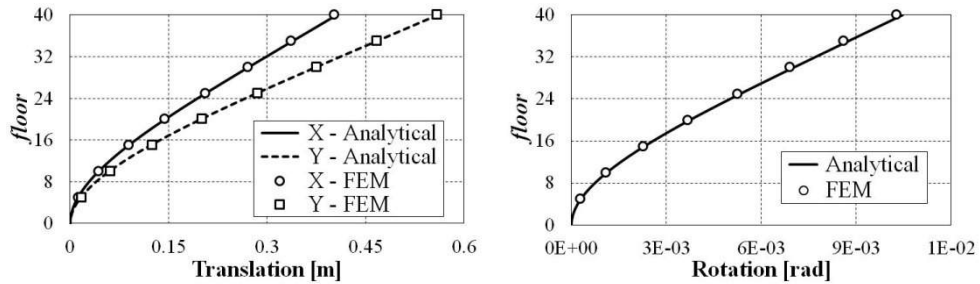


Figure 2.12 – Comparison between the analytical and FE method in terms of displacements of the building.

The results with which the comparison is performed are expressed in terms of displacements, in particular translations and rotations of the floors according to the global coordinate system XYZ. The corresponding curves are reported in Fig. 2.12. It is self-evident the outstanding convergence of the aforementioned methods, which confirms the usability of the analytical method at least in the first phases of the design process.

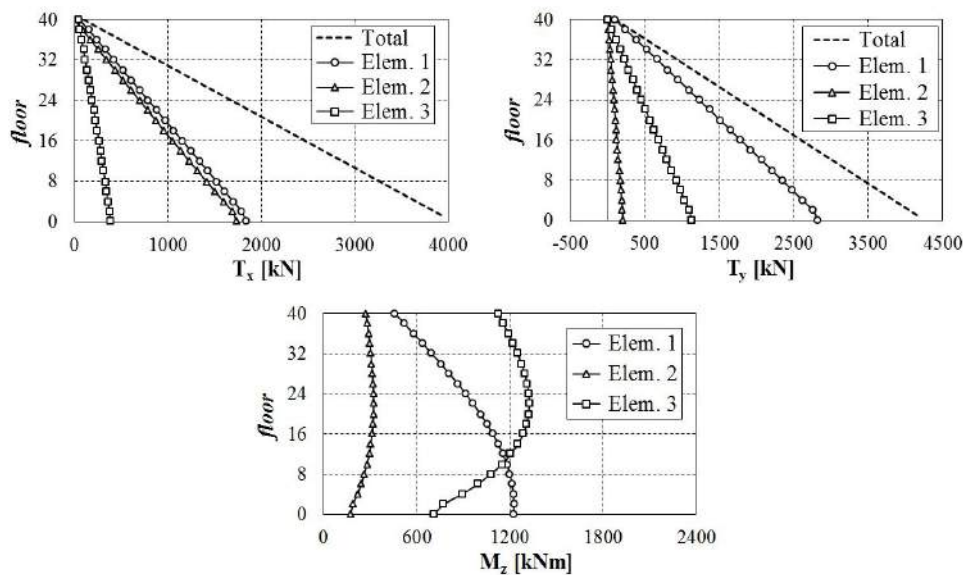


Figure 2.13 – Load distribution between the components of the core system in terms of shears in X and Y direction and torque.

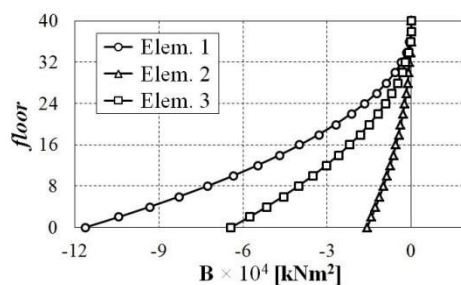


Figure 2.14 – Bimoment action in the shear walls constituting the core system.

Unlike FE simulations, the load distribution between the stiffening elements can be easily computed. In this way, it is possible to identify the percentage of action absorbed by each bracing and, consequently, to evaluate the intensity of the arisen internal forces, such as shears and torsional moment (Fig. 2.13).

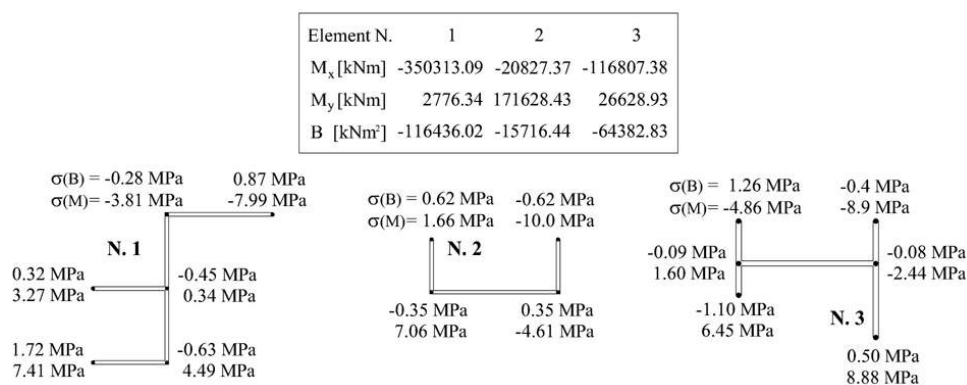


Figure 2.15 – Comparison of the stress state due to bending and warping of the walls.

In the case of thin-walled open section shear walls, which follow the Vlasov's theory of the sectorial areas, the analytical method also allows to define the trend of the bimoment action, which is known as the cause of the warping deformation of this type of sections when subjected to torsional loads.

The main effect of this uncommon internal action is the development of an additional state of stresses defined by normal and tangential components. Their intensity can be, in some cases, comparable to the one derived by pure flexural behaviour. Therefore, since the latter can affect the structural behaviour of the entire building, the evaluation of the bimoment action during the design process has to be performed. In Fig. 2.14 the curves of bimoment related to each shear wall are shown, whereas in Fig. 2.15 information regarding the additional stress state in terms of normal components are reported. In the latter figure, a comparison with the stress state caused by the pure bending behaviour is highlighted and it can be seen that, in some cases, the bimoment action determines an increase in tension of about 20-30 per cent [17].

Chapter 3

Thin-Walled Open Section Profiles as Vertical Stiffening

3.1 Introduction

In the design of tall buildings the horizontal actions become predominant if compared to the vertical ones. In effect, due to gravity loading, the geometrical dimensions of the resistant members increase from the top to the bottom proportionally to the height of the structure. If we consider a regular construction, each floor is similar to the others and, therefore, the corresponding vertical actions can be considered constant for each level. On the contrary, when horizontal forces are considered, in the absence of specific resistant systems, the actions developed in the structural skeleton increase as the third power of the total height, implying an unreasonable growth of the structural dimensions. For this reason, over specific heights, it is compulsory to analyse the vertical behaviour separately from the horizontal one.

As described in Chapter 1, most of the resistant solutions, appeared since the 70', employed vertical elements arranged as cantilevers constrained at the base and designed to absorb the total horizontal force coming from earthquakes and wind. These members, commonly known as shear walls, can be freely located in the plan of the structure and used with or without other vertical bracings to obtain an adequate stability without an excessive supply of structural material. Besides,

just for these reasons, it became very popular for those constructions whose maximum height was lower than seventy floors.

These bracings can be constituted by steel braced frames or concrete walls, both with different sectional shapes. In the case of not excessive heights, they can be represented by a simple plane element whose resistance is proportional to the maximum dimension of the section. For greater heights, they are designed to behave as three-dimensional elements, having an appropriate bending resistance in two principal directions as well as a good torsional stiffness, giving rise to thin-walled hollow or open section walls.

The sectional shape, the number of vertical bracings and their location in the floor plan are chosen in order to absorb almost the total twisting action applied to the structure and, at the same time, to house the stairwells or the lift shafts, which are indispensable in a tall structure.

Unlike hollow sections, in presence of torsional actions, thin-walled open sections elements reveal a particular behaviour, which is far from the common one. In effect, once the torsional deformations take place, the section twists around its shear centre but, at the same time, does not remain plane, since it undergoes different longitudinal extension causing the out-of-plane distortion or warping of the section. As a consequence, a further longitudinal stress state, absent in the theory of pure torsion, develops in the thickness of the section. Therefore, in the analysis of this type of structures, Saint Venant's theory and Euler-Bernoulli's hypothesis of plane sections prove to be inadequate to describe their structural behaviour.

Due to their wide versatility, thin-walled open section beams draw engineers' attention. Originally their application was united to the development of aeroplane structures, since these elements perfectly met the requirements of weight-saving, however offering an adequate stiffness.

Only later their purpose was extended to cover structural functions in the building and bridge design. The analytical approach related to these profiles started about a century ago, but most of the developments in this area were accomplished in more recent times, about fifty years ago, by means of the methods proposed by S.P. Timoshenko [114] and V.Z. Vlasov [119]. Both of them focused the attention on the identification of an exhaustive theory which, even if approximate, was able to describe the structural behaviour of thin-walled open section profiles. Actually, Vlasov was the one who led a meticulous study on this topic, whose goals were even recognised by Timoshenko himself. Such thorough work was then synthesised in his book *Thin-walled elastic beams*, which remains a milestone in the scientific literature.

3.2 Vlasov's Theory of Sectorial Areas

V.Z. Vlasov devoted an entire lifetime of scientific activity to the theory of thin-walled structures. The author started his research by devising an approximate formulation for the analysis of shell structures. It was based on a variational approach which allowed to reduce the partial differential equations describing the problem to a system of ordinary equations, which were type familiar to those employed in the common theory of structures. Such method was adopted for the analysis of shells and hipped systems of open and closed sections. However, the flexibility of his method permitted to extend the dissertation to consider thin-walled open section elements and to obtain a comprehensive treatise on the problem of their flexural-torsional instability and vibrations.

Hereinafter a complete summary of the method is proposed, from which the analytical approach for the evaluation of the structural behaviour of thin-walled open section shear walls used to stiffen horizontally a tall building has been derived.

Thin-walled open section profiles can be considered as long prismatic shells, in which their three main dimensions are all of different order of magnitude: the thickness δ is small if compared with any characteristic dimension d of the cross section as well as the cross sectional dimensions are small if compared with the length l of the shell; the following proportions define this typology:

$$\frac{\delta}{d} \leq 0.1 \qquad \frac{d}{l} \leq 0.1 \qquad (3.1)$$

In the theory the author refers to the *middle surface*, as the surface lying midway through the plates constituting the beam, the *generators*, as the lines parallel to the beam axis and lying on the middle surface, and the *profile line*, as the intersection of the middle surface with a plane normal to the generators. In this way, an orthogonal coordinate system can be derived, since each point of the cross section can be found by means of two coordinates: z is the one along the generator and s along the profile line.

Two main geometrical hypotheses are at the base of Vlasov's theory:

- the section is considered rigid and, therefore, its shape is undeformable;
- the shear deformations of the middle surface, that are due to the change of the right angle between the generators and the profile line, are assumed to vanish.

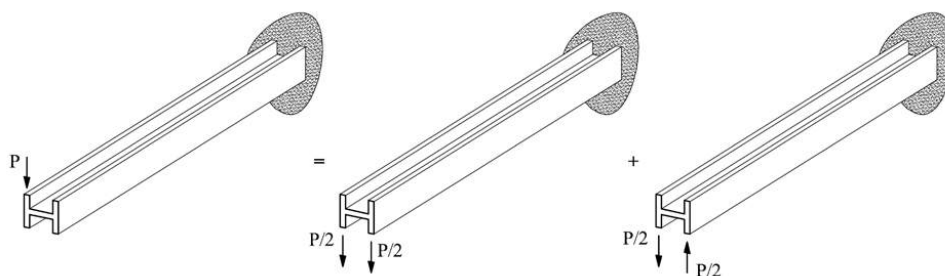


Figure 3.1 – Cantilever I-beam subjected to a concentrated load on one of its flanges.

Let us consider the case of a cantilever I-beam subjected to a concentrated load on one of its flanges (Fig. 3.1). Exploiting the Superposition Principle, this load can be reduced to the sum of two different loading cases: one is purely flexural and can be studied by the law of plane sections; the other is defined as flexural torsion, since the extreme flanges are forced to bend in opposite directions in their own plane as a result of the torsion induced by the specific loading case. This means that the section does not remain plane and normal stresses appear in addition to the tangential ones. These additional stresses give rise to a generalized longitudinal force, called bimoment action, which is directly connected with the warping of the section and consists of two bending moments, each acting on one flange, having the same magnitude but opposite sign.

In the case of solid beams, this self-equilibrated action has a local character and its effect rapidly falls off with increasing distance from the point of application of the load. On the contrary, in the case of thin-walled open section beams, the warping stresses fall off slowly as much as the walls are thin. The intensity of this stress state cannot be neglected for these profiles and the application of Saint Venant's theory could lead to gross errors in the design process. As a matter of fact, this particular behaviour demonstrates that the torsion can take place not only under the action of transversal torsional loads, but even under the action of longitudinal forces if these cause the development of the bimoment action.

For an adequate analysis of these profiles, the need of a theory, able to take into account the out-of-plane distortion of the sections, is evident.

Let's consider a free shaped thin-walled open section beam, located in a generic coordinate system, in which the Z axis is parallel to the longitudinal axis, or centroidal axis, of the beam (Fig. 3.2). Defined a specific cross section at $z = \text{const.}$, X and Y axes complete the right-handed coordinate system XYZ . Each

point of the profile line can be determined by using the coordinates (x, y) or the sectional coordinate s .

With the aim of defining the equations which govern the structural behaviour of thin-walled profiles, it is assumed that the beam is subjected to some deformations. As a result of these, each point of the section is characterised by a new position in the general coordinate system XYZ.

According to the first geometrical hypothesis, the beam is deformed, but the shape of the section remains unchanged. Therefore, it behaves as a perfectly rigid body, whose position can be evaluated by means of only three independent variables corresponding to three transversal displacements: two translations of a chosen point A connected to the profile, which are ξ in X direction and η in Y direction, and the rotation ϑ of the section.

The transversal displacements ξ_M and η_M of any point $M(x; y)$ belonging to the cross section can be determined through the well-known expressions:

$$\xi_M = \xi - (y - y_A)\vartheta \quad \eta_M = \eta + (x - x_A)\vartheta \quad (3.2)$$

in which $(x_A; y_A)$ are the coordinates of the point A in the XYZ system.

The full displacement of M can be described by a vector, whose components are: the longitudinal displacement u , defined positive if it increases as the coordinate z ; the transversal tangential displacement v , directed long the tangent t to the profile line and considered positive if it increases as the sectional coordinate s ; and, finally, the transversal normal displacement w , whose positive direction n is defined by the fact that u , v and w must represent a right-handed coordinate system (Fig. 3.2).

If α is the angle between the positive direction of the X axis and the positive direction of the tangential axis t , the transversal displacements v and w , related to the generic point $M(z, s)$, can be computed by means of the projections of ξ_M and η_M on the tangent t or the normal n :

$$v(z, s) = \xi_M \cos \alpha + \eta_M \sin \alpha \quad (3.3)$$

$$w(z, s) = \eta_M \cos \alpha - \xi_M \sin \alpha \quad (3.4)$$

By substituting Eqns (3.2) in Eqn (3.3) and (3.4), the following expressions are obtained:

$$v(z, s) = \xi \cos \alpha + \eta \sin \alpha + \vartheta[(x - x_A) \sin \alpha - (y - y_A) \cos \alpha] \quad (3.5)$$

$$w(z, s) = -\xi \sin \alpha + \eta \cos \alpha + \vartheta[(x - x_A) \cos \alpha + (y - y_A) \sin \alpha] \quad (3.6)$$

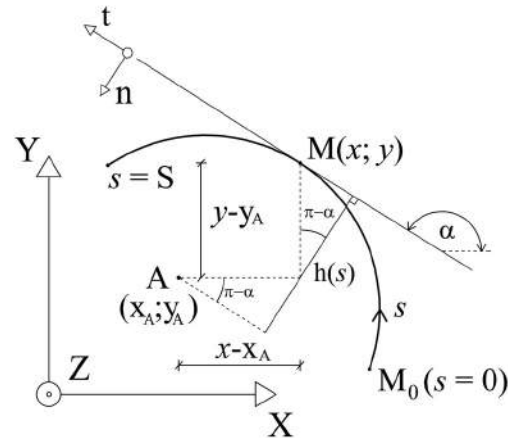


Figure 3.2 – Thin-walled open section in a right-handed coordinate system.

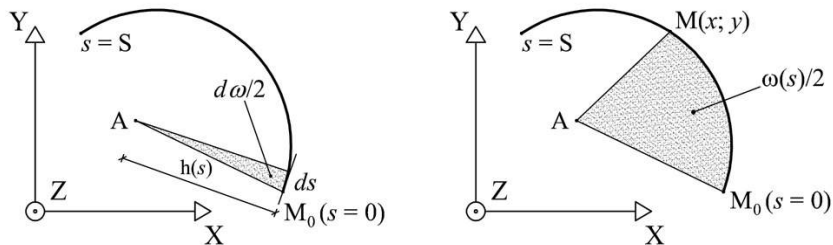


Figure 3.3 – Computation of the sectorial coordinate ω .

Starting from Eqns (3.5) and (3.6), the lengths of the perpendiculars $h(s)$ and $d(s)$ from the point A to the tangent and normal respectively of the profile line at M can be highlighted:

$$h(s) = (x - x_A) \sin \alpha - (y - y_A) \cos \alpha \quad (3.7)$$

$$d(s) = (x - x_A) \cos \alpha + (y - y_A) \sin \alpha \quad (3.8)$$

The longitudinal displacement component u can be acquired by exploiting the second hypothesis of Vlasov's theory, according to which the shear deformations of the middle surface are considered negligible in the analysis. Therefore, if γ is

the shear strain representing the variation of the angle between the lines $s = \text{const.}$ and $z = \text{const.}$:

$$\gamma = \frac{\partial u}{\partial s} + \frac{\partial v}{\partial z} = 0 \quad (3.9)$$

Since the expression of v is known, the analytical expression of u is derived by integration.

$$u(z, s) = \zeta(z) - \int_0^s \frac{\partial v}{\partial z} ds \quad (3.10)$$

$$\frac{\partial v}{\partial z} ds = \xi'(z) \cos \alpha(s) ds + \eta'(z) \sin \alpha(s) ds + \vartheta'(z) h(s) ds \quad (3.11)$$

Taking into account the following relationships:

$$\cos \alpha ds = dx$$

$$\sin \alpha ds = dy$$

$$h ds = d\omega \quad (3.12)$$

the equation of u is clearly obtained:

$$u(z, s) = \zeta(z) - \xi'(z)x(s) - \eta'(z)y(s) - \vartheta'(z)\omega(s) \quad (3.13)$$

The term $\zeta(z)$ is an arbitrary function, depending only on z , which describes a uniform longitudinal displacement of the entire section; $d\omega$ is twice the area of the elementary triangle whose base is the infinitesimal length ds and whose height is the distance h , defined by (3.7). Therefore, $\omega(s)$ is twice the area enclosed between the arc M_0 - M and the construction lines which connect the point A with the points M_0 ($s = 0$) and $M(s)$. This term is defined as sectorial area or sectorial coordinate, whereas A is the sectorial pole and M_0 the sectorial origin (Fig. 3.3).

Observing Eqn (3.13), it can be seen that the longitudinal component u is composed by four terms. The first three are well-known, since they are related to Saint Venant's theory and arise as result of extension and bending in the XZ and YZ planes. This means that, due to these terms, the sections deforms but remains plane.

The component, which describes the warping of the section, is totally expressed by the fourth term and, in particular, ϑ' can be considered as an amplitude, whereas ω as the shape of the warped section at $z = \text{const.}$

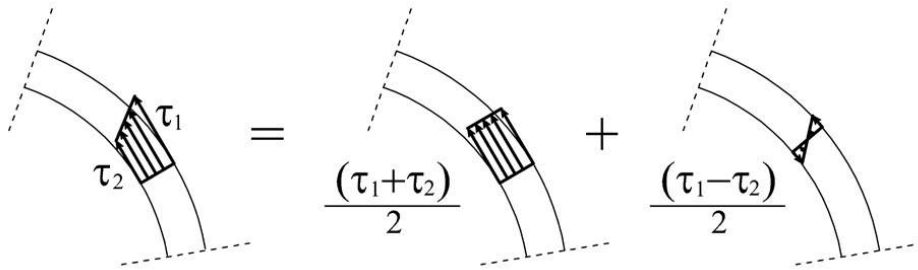


Figure 3.4 – Components of the tangential stress state.

Once the displacement field is acquired, by differentiating u with respect to the variable z , it is possible to obtain the expression of the longitudinal deformation ε :

$$\varepsilon = \frac{\partial u}{\partial z} = \varepsilon(z, s) = \zeta'(z) - \xi''(z)x(s) - \eta''(z)y(s) - \vartheta''(z)\omega(s) \quad (3.14)$$

From Eqn (3.14) it is clear that the hypothesis of uniform torsion, according to which the angle of twist per unit length should be constant, fails.

Eqn (3.14) does not fully determine the strain ε , since the functions ζ , ξ , η and ϑ are unknown. To overcome this problem, it is necessary to use the static conditions, or conditions of equilibrium for an elastic body which undergoes a definite deformation. In this case, in effect, internal forces arise in the beam and, in particular, the author considers only two types of stresses: normal stresses, acting in the direction of the generators, and tangential stresses, in the direction of the tangent to the profile line; on the contrary, the tangential stresses acting perpendicularly to the profile are assumed to vanish.

The normal stresses are supposed to be constant over the thickness of the beam, whereas the tangential stresses vary according to a linear law. The latter can be considered as the sum of two components: the first is given by the constant average value of the stresses, the second takes into account the difference between the linear and the constant distribution of the stresses (Fig. 3.4). In addition, the former are function of the variables z and s , the latter is only dependent on z .

Therefore, according to these hypotheses, the second component can be referred to the torsional moments considered in the theory of the pure torsion, that is, to a resultant torque M_z given by the product of the derivative of the angle of rotation and the torsional rigidity GJ_t .

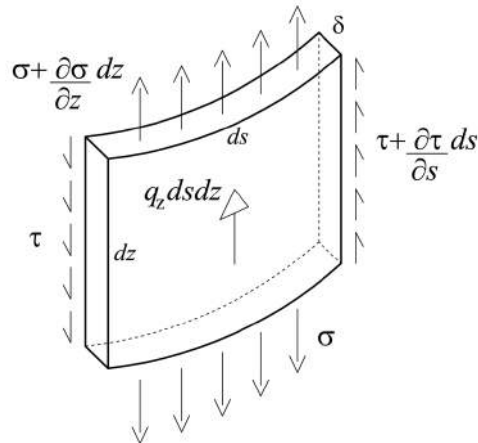


Figure 3.5 – Longitudinal equilibrium of an infinitesimal strip of beam.

Taking into account the Hooke's law, the stress field is directly derived from the strain field. If we consider two perpendicular directions, that are longitudinal and transversal, the relative extensions of the beam can be computed by means of the corresponding normal stresses:

$$\varepsilon = \frac{1}{E}(\sigma - \nu\sigma_1) \quad (3.15)$$

$$\varepsilon_1 = \frac{1}{E}(\sigma_1 - \nu\sigma) \quad (3.16)$$

in which the subscript 1 indicates the transversal direction and the term ν is Poisson's ratio.

In accordance with the second geometrical hypothesis, the deformation ε_1 of the contour is null and, consequently, the strain ε can be highlighted.

$$\sigma_1 = \nu\sigma \quad (3.17)$$

$$\varepsilon = \frac{1-\nu^2}{E}\sigma \cong \frac{\sigma}{E} \quad (3.18)$$

Substituting Eqn (3.14) in Eqn (3.18) the general law for the distribution of the normal stresses is:

$$\sigma(z, s) = E(\zeta' - \xi''x - \eta''y - \vartheta''\omega) \quad (3.19)$$

This expression demonstrates that normal stresses can appear not only in presence of uniform extension and bending of the beam, represented by the first three terms, but also as a result of the torsion of the cross section. In the theory of pure torsion, this specific contribution is usually assumed to vanish.

The equation which describes the tangential stresses characterised by a constant average distribution can be obtained considering the longitudinal equilibrium of an elementary part of beam whose dimensions are the length dz , the width ds and the thickness δ (Fig. 3.5).

$$(d\sigma)\delta ds + (d\tau)\delta dz + q_z ds dz = 0 \quad (3.20)$$

being q_z a longitudinal distributed external force.

Dividing Eqn (3.20) by $ds dz$ and integrating with respect to the variable s , the expression of the tangential stresses is found.

$$\frac{(\partial\sigma)\delta}{\partial z} + \frac{(\partial\tau)\delta}{\partial s} + q_z = 0 \quad (3.21)$$

$$\tau(z, s) = \frac{1}{\delta} \left[T_0(z) - \int_0^s q_z ds - \int_0^s \frac{\partial\sigma}{\partial z} \delta ds \right] \quad (3.22)$$

The term T_0 is an arbitrary function of z and can be computed setting $s = 0$. In this case, in effect, we obtain:

$$T_0(z) = \tau(z, 0)\delta \quad (3.23)$$

which means that T_0 is the shear force per unit length of beam acting on the longitudinal section $s = 0$.

The substitution of Eqn (3.19) in (3.22) gives rise to:

$$\begin{aligned} \tau(z, s) = \frac{1}{\delta} \left[T_0(z) - \int_0^s q_z ds - E(\zeta'' \int_0^s dA - \xi''' \int_0^s x dA - \eta''' \int_0^s y dA + \right. \\ \left. - \vartheta''' \int_0^s \omega dA) \right] \quad (3.24) \end{aligned}$$

The latter can be re-written in a synthetic form if the following expressions are used, among which, in addition to the well-known static moments, the sectorial static moment S_ω appears:

$$\begin{aligned} \int_0^s dA &= A(s) & \int_0^s x dA &= S_y(s) \\ \int_0^s y dA &= S_x(s) & \int_0^s \omega dA &= S_\omega(s) \end{aligned} \quad (3.25)$$

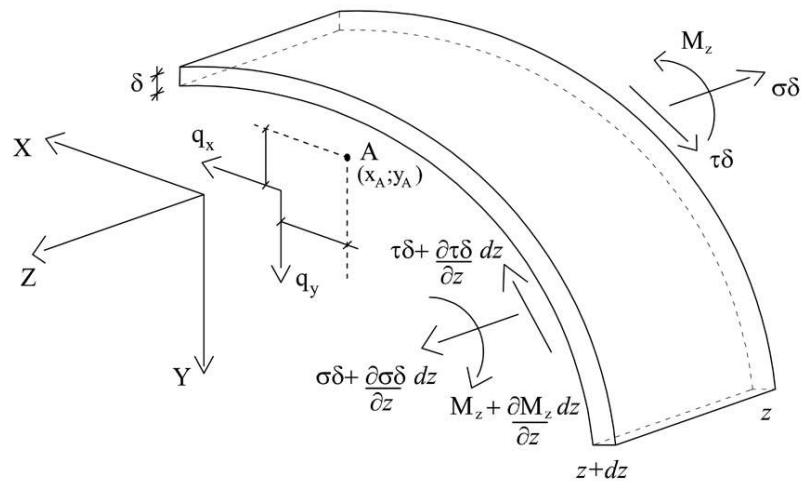


Figure 3.6 - Equilibrium of a strip of beam subjected to transversal loads.

Moreover, in the hypothesis that the distributed force q_z and the shear force per unit length T_0 are null, Eqn (3.24) becomes:

$$\tau(z, s) = \frac{E}{\delta} [\zeta'' A(s) - \xi''' S_y(s) - \eta''' S_x(s) - \vartheta''' S_\omega(s)] \quad (3.26)$$

A careful examination of this expression reveals that the first term is due to the external action represented by longitudinal shear forces applied to the lateral edges of the beam; the second and third are related to the well-known formulation proposed by Jourawsky for the computation of the tangential stresses in presence of bending, whereas the last term describes a constant distribution of tangential stresses over the thickness as effect of the non-uniform torsion.

As it can be seen, both the equations describing the normal and the tangential stresses are expressed in terms of the unknowns ζ , ξ , η and ϑ . Such displacements are computed applying the equilibrium conditions. To this aim, a strip of beam, included between the cross sections at $z = \text{const.}$ and $z+dz = \text{const.}$, is considered (Fig. 3.6).

The actions applied to the strip are:

- the normal and tangential stresses and the torsional moment M_z related to the section at $z = \text{const.}$;

- the same just mentioned, increased by a certain value proportional to the differential dz , related to the section at $z+dz = \text{const.}$;
- the distributed transversal loads q_x and q_y , acting along the X and Y direction respectively.

If S represents the whole curve of the profile line, the equilibrium equations are defined as

$$\begin{aligned}
 \sum_Z = 0 &\rightarrow \int_S \frac{\partial \sigma}{\partial z} \delta dz ds = 0 \\
 \sum_X = 0 &\rightarrow \int_S \frac{\partial \tau}{\partial z} \cos \alpha \delta dz ds + q_x dz = 0 \\
 \sum_Y = 0 &\rightarrow \int_S \frac{\partial \tau}{\partial z} \sin \alpha \delta dz ds + q_y dz = 0 \\
 \sum_{M_A} = 0 &\rightarrow \int_S \frac{\partial \tau}{\partial z} \delta dz [(x - x_A) \sin \alpha - (y - y_A) \cos \alpha] ds + \\
 &+ m dz + \frac{\partial M_z}{\partial z} dz = 0
 \end{aligned} \tag{3.27}$$

The last equation, which describes the null resultant moment with respect to an arbitrary point A(x_A ; y_A), is composed by the following contributions: the first represents the effect of the shear stresses defined by a constant distribution over the thickness of the section; the second is function of the external distributed actions; the third depends on the torsional moments which are proportional to the torsional rigidity GJ_t .

Exploiting the expressions (3.12) and integrating by parts the last three equations, Eqns (3.27) become:

$$\begin{aligned}
 \int_S \frac{\partial \sigma}{\partial z} dA &= 0 \\
 \frac{\partial \tau}{\partial z} x \delta \Big|_0^S - \int_S x \frac{\partial}{\partial s} \left[\frac{\partial \tau}{\partial z} \delta \right] ds + q_x &= 0 \\
 \frac{\partial \tau}{\partial z} y \delta \Big|_0^S - \int_S y \frac{\partial}{\partial s} \left[\frac{\partial \tau}{\partial z} \delta \right] ds + q_y &= 0 \\
 \frac{\partial \tau}{\partial z} \omega \delta \Big|_0^S - \int_S \omega \frac{\partial}{\partial s} \left[\frac{\partial \tau}{\partial z} \delta \right] ds + m + \frac{\partial M_z}{\partial z} &= 0
 \end{aligned} \tag{3.28}$$

For the equilibrium, since no external forces are applied to the lateral edges of the beam, the first terms of the Eqns (3.28b, c, d) are equal to zero.

If the partial derivatives with respect to z and s are interchanged and the Eqns (3.19) and (3.21) are considered, the following expressions can be derived:

$$\frac{\partial \sigma}{\partial z} dA = E(\zeta'' - \xi'''x - \eta'''y - \vartheta''' \omega) dA \quad (3.29)$$

$$\frac{\partial}{\partial z} \left[\frac{\partial \tau}{\partial s} \delta \right] ds = \frac{\partial}{\partial z} \left[-\frac{\partial \sigma}{\partial z} \delta \right] ds = -E(\zeta''' - \xi^{IV}x - \eta^{IV}y - \vartheta^{IV} \omega) dA \quad (3.30)$$

$$\frac{\partial M_z}{\partial z} = GJ_t \vartheta'' \quad (3.31)$$

Consequently, if the substitution of the previous equations in the system (3.28) is performed, the final system of the equilibrium equations is obtained.

$$\begin{aligned} E(\zeta'' A - \xi''' S_y - \eta''' S_x - \vartheta''' S_\omega) &= 0 \\ -E(\zeta''' S_y - \xi^{IV} I_y - \eta^{IV} I_{xy} - \vartheta^{IV} I_{\omega y}) &= q_x \\ -E(\zeta''' S_x - \xi^{IV} I_{xy} - \eta^{IV} I_x - \vartheta^{IV} I_{\omega x}) &= q_y \\ -E(\zeta''' S_\omega - \xi^{IV} I_{\omega y} - \eta^{IV} I_{\omega x} - \vartheta^{IV} I_\omega) - GJ_t \vartheta'' &= m \end{aligned} \quad (3.32)$$

where the sectorial characteristics of the section are defined as

$$\begin{aligned} \int_S \omega dA &= S_\omega & \int_S \omega^2 dA &= I_\omega \\ \int_S \omega x dA &= I_{\omega y} & \int_S \omega y dA &= I_{\omega x} \end{aligned} \quad (3.33)$$

In addition to the sectorial static moment, the sectorial moment of inertia I_ω and the sectorial products of inertia $I_{\omega y}$ and $I_{\omega x}$ appear.

The system (3.32) of differential equilibrium equations is synthetic and allows to compute the four unknowns of the analytical problem. Nevertheless it proves to be complicated and especially complex to be solved. Observing the coefficients of the unknowns, it is evident that the system is dependent on the arbitrary functions $x(s)$, $y(s)$ and $\omega(s)$. In the described procedure, generic information regarding the coordinate system XYZ, the sectorial pole and the sectorial origin have been indicated. Therefore, with the aim of simplifying the system (3.32), it is possible to choose a reference system which causes the vanishing of the following integrals:

$$S_y = \int_S x dA = 0 \quad S_x = \int_S y dA = 0$$

$$I_{xy} = \int_S xy dA = 0 \quad (3.34)$$

$$S_\omega = \int_S \omega dA = 0 \quad I_{\omega y} = \int_S \omega x dA = 0$$

$$I_{\omega x} = \int_S \omega y dA = 0 \quad (3.35)$$

The conditions (3.34) can be immediately fulfilled if the coordinate system XYZ is modified so that its axes become the central axes of the section. As regard the conditions (3.35), the choice of a particular sectorial pole and a particular sectorial origin, which determines the annullment of the integrals, is not straightforward.

3.2.1 Definition of the Principal Sectorial Origin

If we consider the thin-walled open section of Fig. 3.7, we can define the sectorial coordinate ω taking into account the sectorial pole and the sectorial origin, on which the numerical value of ω depends:

$$\omega = \omega_B(s_1; s) \quad (3.36)$$

being the point B the sectorial pole and s_1 its sectorial origin on the section.

If a point s_0 of the section is considered, the expression (3.36) can be re-written as the sum of two contributions of area:

$$\omega_B(s_1; s) = \omega_B(s_1; s_0) + \omega_B(s_0; s) \quad (3.37)$$

in which the first term of the sum is numerically defined, being s_1 and s_0 known, whereas the second one depends on the variable s .

The following hypotheses can be established:

- the origin s_0 is such that the corresponding diagram of the sectorial coordinate $\omega_B(s_0; s)$ is defined by a sectorial static moment $S_\omega(s_0)$ equal to zero;
- the origin s_1 is such that the corresponding diagram of the sectorial coordinate $\omega_B(s_1; s)$ is defined by a sectorial moment $S_\omega(s_1)$ different from zero.

Taking into account Eqn (3.37), the expression of the sectorial static moment related to the origin s_0 is

$$S_\omega(s_0) = \int_A \omega_B(s_0; s) dA = \int_A \omega_B(s_1; s) dA - \int_A \omega_B(s_1; s_0) dA = 0 \quad (3.38)$$

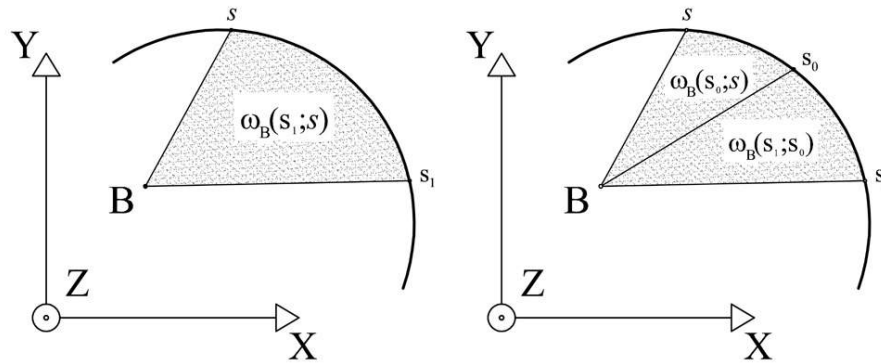


Figure 3.7 – Identification of the principal sectorial origin with respect to the pole B.

Since the term $\omega_B(s_1; s_0)$ is a constant unknown, it can be directly computed from Eqn (3.38).

$$\omega_B(s_1; s_0) = \int_A \omega_B(s_1; s) dA / A = S_{\omega}(s_1) / A \quad (3.39)$$

Therefore, the following assumption can be expressed: once a generic sectorial pole B and a generic sectorial origin s_1 are defined for the computation of the sectorial characteristics of the section, Eqn (3.39) substituted in Eqn (3.37) allows to find the diagram of the sectorial coordinate ω_B whose sectorial origin s_0 is principal and, thereby, the corresponding sectorial static moment is null. This specific diagram is called the principal diagram referred to pole B.

From a graphic point of view, we can operate in this way: once the diagram of a generic sectorial coordinate is drawn, in order to find the diagram to which a null sectorial static moment corresponds, it is necessary to deduct from the original diagram the constant value given by the ratio between the sectorial static moment related to the original diagram and the total area of the section. Once the diagram has been modified, it is easy to recognise the point of the section which represents the principal sectorial origin, related to the arbitrarily chosen sectorial pole. In Fig. 3.8 an example of this simple process is shown.

Moreover, if we apply Eqns (3.37) and (3.39) in the definition of the other sectorial characteristics (Eqns 3.35), we find out simple equations that permit the calculation of the sectorial moment of inertia and the sectorial products of inertia related to the principal sectorial origin starting from those related to the generic sectorial origin.

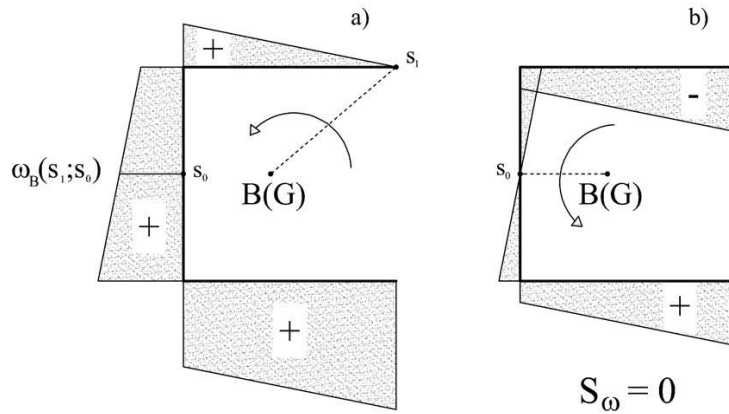


Figure 3.8 – Computation of the principal sectorial diagram for a U-shaped section: generic diagram $\omega_B(s_1)$ (a) and principal diagram $\omega_B(s_0)$ (b).

As regard the sectorial moment of inertia, exploiting Eqn (3.39) we obtain:

$$I_\omega(s_0) = \int_A \omega_B^2(s_0; s) dA \quad (3.40)$$

$$I_\omega(s_0) = \int_A \omega_B^2(s_1; s) dA + \int_A \omega_B^2(s_1; s_0) dA + \\ - 2 \int_A \omega_B(s_1; s_0) \omega_B(s_1; s) dA \quad (3.41)$$

$$I_\omega(s_0) = I_\omega(s_1) - \omega_B^2(s_1; s_0) A \quad (3.42)$$

In the same way, as regard the sectorial products of inertia,

$$I_{\omega x}(s_0) = \int_A \omega_B(s_0; s) y dA = \int_A \omega_B(s_1; s) y dA + \\ - \omega_B(s_1; s_0) \int_A y dA \quad (3.43)$$

$$I_{\omega y}(s_0) = \int_A \omega_B(s_0; s) x dA = \int_A \omega_B(s_1; s) x dA + \\ - \omega_B(s_1; s_0) \int_A x dA \quad (3.44)$$

$$I_{\omega x}(s_0) = I_{\omega x}(s_1) - \omega_B(s_1; s_0) y_G A \quad (3.45)$$

$$I_{\omega y}(s_0) = I_{\omega y}(s_1) - \omega_B(s_1; s_0) x_G A \quad (3.46)$$

where the following relations have been used:

$$\int_A y dA = y_G A$$

$$\int_A x dA = x_G A$$

The expressions (3.42), (3.45) and (3.46) are valid for any arbitrarily chosen sectorial pole.

Finally, observing the relations (3.45) and (3.46), it can be seen that, in the hypothesis of a centroidal coordinate system, the sectorial products of inertia are independent from the sectorial origin.

3.2.2 Definition of the Principal Sectorial Pole

Considering the section of Fig. 3.9, the sectorial coordinate ω having the point A as the sectorial pole can be computed by means of Eqns (3.7) and (3.12):

$$d\omega_A = \left[(x - x_A) \frac{dy}{ds} - (y - y_A) \frac{dx}{ds} \right] ds = (x - x_A) dy - (y - y_A) dx \quad (3.47)$$

The same expression referred to another point B becomes:

$$d\omega_B = (x - x_B) dy - (y - y_B) dx \quad (3.48)$$

Developing the subtraction between the previous differential expressions and integrating, we obtain a relation between ω_A and ω_B :

$$\omega_A = \omega_B + (y_A - y_B)x - (x_A - x_B)y + C \quad (3.49)$$

The integration constant C depends on the sectorial origin of the two sectorial coordinates. Assuming, therefore, the generic point s_0 , whose coordinates are $(x_0; y_0)$, as the origin of both ω_A and ω_B , the numerical value of C is easily determined:

$$C = (x_A - x_B)y_0 - (y_A - y_B)x_0 \quad (3.50)$$

Thereby, Eqn (3.49) becomes:

$$\omega_A = \omega_B + (y_A - y_B)(x - x_0) - (x_A - x_B)(y - y_0) \quad (3.51)$$

or, in a synthetic form,

$$\omega_A = \omega_B + \alpha_y x - \alpha_x y + \alpha \quad (3.52)$$

being

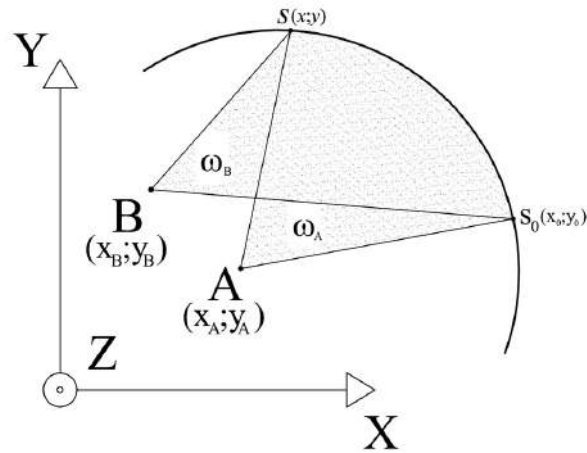


Figure 3.9 – Sectorial calculus with respect to two different sectorial poles A and B.

$$\alpha_y = (y_A - y_B)$$

$$\alpha_x = (x_A - x_B)$$

$$\alpha = (x_A - x_B)y_0 - (y_A - y_B)x_0$$

Now, the expression (3.52) can be used to define the sectorial moment of inertia and the sectorial products of inertia related to the sectorial pole A.

$$I_{\omega A} = \int_A \omega_A^2 dA = \int_A (\omega_B + \alpha_y x - \alpha_x y + \alpha)^2 dA$$

$$I_{\omega y A} = \int_A \omega_A x dA = \int_A (\omega_B + \alpha_y x - \alpha_x y + \alpha) x dA$$

$$I_{\omega x A} = \int_A \omega_A y dA = \int_A (\omega_B + \alpha_y x - \alpha_x y + \alpha) y dA \quad (3.53)$$

If we define the principal sectorial pole as the pole which determines the annulment of the sectorial products of inertia, through the last two equations of the system (3.53) it is possible to calculate its geometrical coordinates. For the sake of simplicity, a central coordinate system is established for the calculation:

$$I_{\omega y A} = I_{\omega y B} + \alpha_y I_y - \alpha_x I_{xy} + \alpha S_y$$

$$I_{\omega x A} = I_{\omega x B} + \alpha_y I_{xy} - \alpha_x I_x + \alpha S_x$$

which, according to the particular coordinate system and the hypothesis on the point A, are reduced to

$$I_{\omega y A} = I_{\omega y B} + \alpha_y I_y = 0 \quad (3.54)$$

$$I_{\omega x A} = I_{\omega x B} - \alpha_x I_x = 0 \quad (3.55)$$

The geometrical coordinates of the principal pole A can be directly computed, since they are the only unknowns of the problem. In addition, it must be noticed that Eqns (3.54) and (3.55) are valid for any generic sectorial pole B and do not depend on the position of the sectorial origin on the section.

If the arbitrary pole B is posed in the centroid of the section, the computation of the coordinates of A is further simplified:

$$y_A = -I_{\omega y B} / I_y \quad (3.56)$$

$$x_A = I_{\omega x B} / I_x \quad (3.57)$$

As it can be seen, the principal sectorial pole is a special point, whose position depends only on the geometrical dimensions of the cross section, in contrast to the principal sectorial origin, which depends on the arbitrary sectorial pole.

If an axis of symmetry exists, the principal pole lies on this axis; moreover, the intersection point between this axis and the profile line of the section unequivocally defines the corresponding principal sectorial origin.

For a beam of constant section, the principal sectorial pole coincides with the shear centre of the section. This means that, through Eqns (3.56) and (3.57), the coordinates of the shear centre of a thin-walled open section can be easily acquired.

Starting from these findings, the following corollaries can be expressed:

- in a centroidal coordinate system, the principal sectorial diagram whose reference pole is the shear centre C (x_c ; y_c) can be directly computed knowing the principal sectorial diagram whose reference pole is the centroid G of the section:

$$\omega_C = \omega_G + y_c x - x_c y \quad (3.58)$$

- in a central coordinate system, the sectorial characteristics related to the principal sectorial diagram whose reference pole is the shear centre C (x_c ; y_c) are related to those derived from the principal sectorial diagram whose reference pole is the centroid G of the section:

$$\begin{aligned}
I_{\omega_C} &= I_{\omega_G} + y_c^2 I_y + x_c^2 I_x + 2y_c I_{\omega_{yG}} - 2x_c I_{\omega_{xG}} \\
I_{\omega_{yC}} &= I_{\omega_{yG}} + y_c I_y = 0 \\
I_{\omega_{xC}} &= I_{\omega_{xG}} - x_c I_x = 0
\end{aligned} \tag{3.59}$$

- in a generic coordinate system, the positions of the principal sectorial pole and its corresponding principal sectorial origin can be obtained solving the following system of three equations, in which B is a generic sectorial pole and the terms α , α_x and α_y are the unknowns of the problem:

$$\begin{aligned}
S_{\omega_A} &= \int_A \omega_A dA = \int_A (\omega_B + \alpha_y x - \alpha_x y + \alpha) dA = 0 \\
I_{\omega_{yA}} &= \int_A \omega_A x dA = \int_A (\omega_B + \alpha_y x - \alpha_x y + \alpha) x dA = 0 \\
I_{\omega_{xA}} &= \int_A \omega_A y dA = \int_A (\omega_B + \alpha_y x - \alpha_x y + \alpha) y dA = 0
\end{aligned}$$

Once the unknowns are computed, exploiting Eqn (3.52) the principal diagram ω_A can be constructed, from which the position of the principal sectorial origin can be deduced. In addition, this procedure demonstrates that the sectorial products of inertia whose reference pole is the shear centre are null only if the corresponding sectorial origin is the principal one for that pole. On the contrary, if the coordinate system is centroidal, regardless the sectorial origin, the sectorial products of inertia whose reference pole is the shear centre are always null, as demonstrated by Eqns (3.54) and (3.55).

3.2.3 Numerical Example

In this section a numerical example regarding the computation of the sectorial properties of a thin-walled open section is proposed and described in depth. To this aim, let us consider the section shown in Fig. 3.10, which represents a typical shape for shear walls constituting the horizontal resistant skeleton of a tall building.

The computation starts with the hypothesis that the geometrical properties of the section are known and referred to the central axes of the section. For clearness, the numerical details are reported in Table 3.1.

The first step of the procedure is the choice of an arbitrary sectorial pole and an arbitrary sectorial origin. Since the coordinate system is central, for the sake of simplicity, the centroid is considered as sectorial pole and the free end of the section as sectorial origin.

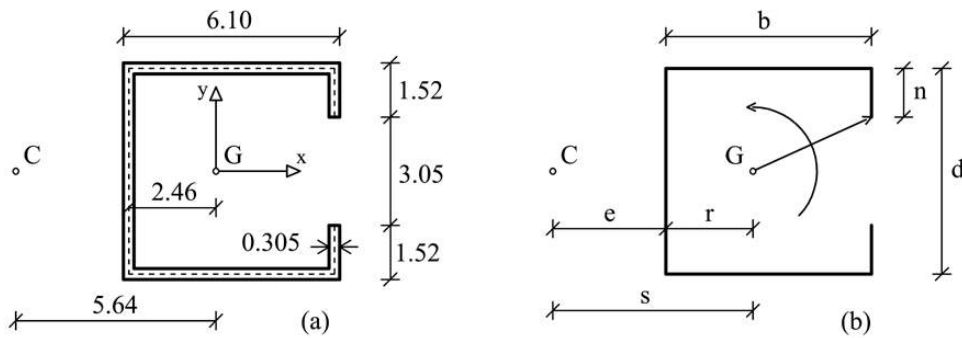


Figure 3.10 – Thin-walled open section in a central coordinate system (a); scheme for the sectorial calculus: the dimensions are referred to the profile line of the section (b).

Table 3.1 – Geometrical properties of the thin-walled open section beam.

A [m ²]	I _x [m ⁴]	I _y [m ⁴]	J _t [m ⁴]
6.14	38.8	30.5	0.189

Now, chosen the positive sense of the ray which connects the pole to the points of the section, the diagram of the coordinate $\underline{\omega}_G$ can be easily computed according to Eqn (3.47). Then the sectorial static moment can be defined and, consequently, exploiting Eqns (3.37) and (3.39) the principal diagram related to the pole G, that is ω_G , is obtained. In Fig. 3.11 these passages are shown for clearness.

$$S_{\underline{\omega}_G} = \int_A \underline{\omega}_G dA = 174.9 \text{ m}^4$$

$$\underline{\omega}_G(s_1; s_0) = S_{\underline{\omega}_G} / A = 28.48 \text{ m}^2$$

$$\omega_G = \underline{\omega}_G - \underline{\omega}_G(s_1; s_0)$$

The next step is the evaluation of other sectorial properties, such as the sectorial moment of inertia I_{ω} , the sectorial products of inertia $I_{\omega y}$ and $I_{\omega x}$ according to the relations (3.33).

$$I_{\omega_G} = \int_A \omega_G^2 dA = 1538.8 \text{ m}^6$$

$$I_{\omega y_G} = \int_A \omega_G x dA = 0 \text{ m}^5 \quad I_{\omega x_G} = \int_A \omega_G y dA = -219 \text{ m}^5$$

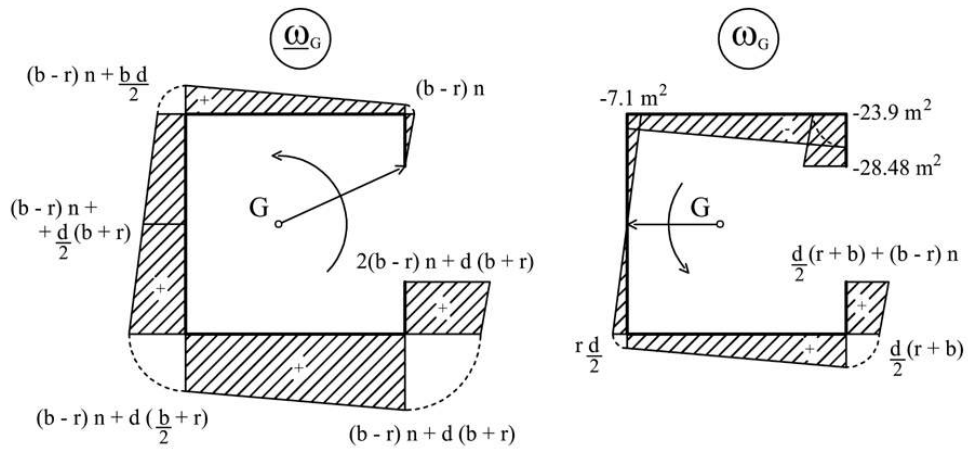


Figure 3.11 – Generic sectorial diagram ω_G and principal sectorial diagram ω_G , both referred to the centroid supposed to be the sectorial pole.

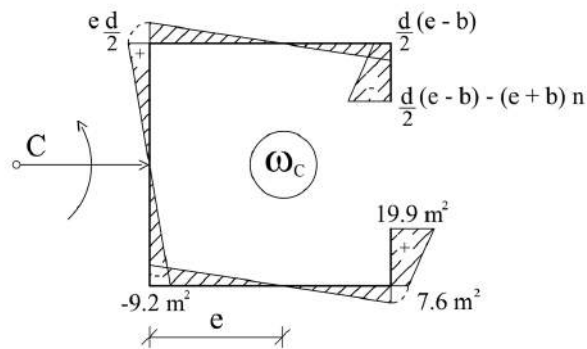


Figure 3.12 – Principal sectorial diagram referred to the shear centre supposed to be the sectorial pole.

The term $I_{\omega y}$ is null since the diagram of the variables ω_G and x are such that their product is null over the entire cross-section; whereas the term $I_{\omega x}$ is different from zero and, in particular, equal to -219 m^5 . As a consequence, the coordinates of the shear centre of the section are acquired through Eqns (3.56) and (3.57):

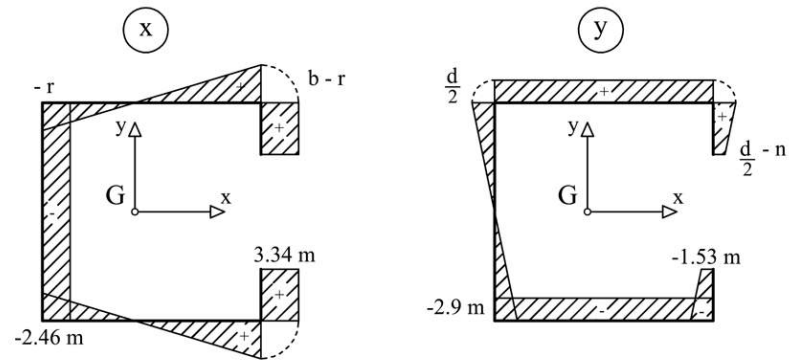


Figure 3.13 – Diagrams of the variables x and y .

$$y_C = -I_{\omega y_G} / I_y = -\frac{0}{30.5} = 0 \text{ m}$$

$$x_C = I_{\omega x_G} / I_x = -\frac{219}{38.8} = -5.64 \text{ m}$$

Once the location of the shear centre is known, the corresponding sectorial characteristics can be defined.

The principal diagram of the coordinate ω_C is computed through the application of Eqn (3.58), in which the principal diagram ω_G is used. In Fig. 3.12 the result of this equation over the entire cross-section is shown.

Finally, exploiting the system (3.59), the sectorial properties related to the shear centre and to the principal sectorial origin are:

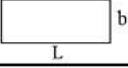
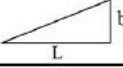
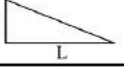
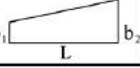

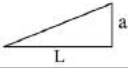
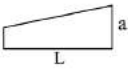
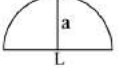
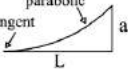
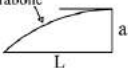
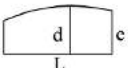
$$\begin{aligned} I_{\omega_C} &= I_{\omega_G} + y_C^2 I_y + x_C^2 I_x + 2y_C I_{\omega y_G} - 2x_C I_{\omega x_G} \\ &= 1538.8 + 5.64^2 (38.8) - 2(-5.64)(-219) = 302.7 \text{ m}^6 \end{aligned}$$

$$I_{\omega y_C} = I_{\omega y_G} + y_C I_y = 0 + 0(30.5) = 0 \text{ m}^5$$

$$I_{\omega x_C} = I_{\omega x_G} - x_C I_x = -219 + 5.64(38.8) = 0 \text{ m}^5$$

Detailed information for the calculation of the sectorial properties are reported for clearness hereinafter. In particular, the procedure can be performed employing the Table 3.2 of the product integrals and referring to the diagrams of the variables x , y and ω_G indicated in Fig. 3.11 and 3.13.

Table 3.2 – Product integral table for $\int_0^L F_1(x)F_2(x)dx$.

$F_1(x) \backslash F_2(x)$				
	abL	$\frac{1}{2} abL$	$\frac{1}{2} abL$	$\frac{aL(b_1+b_2)}{2}$
	$\frac{1}{2} abL$	$\frac{1}{3} abL$	$\frac{1}{6} abL$	$\frac{aL(b_1+2b_2)}{6}$
	$\frac{bL(a_1+a_2)}{2}$	$\frac{bL(a_1+2a_2)}{6}$	$\frac{bL(2a_1+a_2)}{6}$	$\frac{L(2a_1b_1+a_1b_2+a_2b_1+2a_2b_2)}{6}$
	$\frac{2}{3} abL$	$\frac{1}{3} abL$	$\frac{1}{3} abL$	$\frac{aL(b_1+b_2)}{3}$
	$\frac{1}{3} abL$	$\frac{1}{4} abL$	$\frac{1}{12} abL$	$\frac{aL(b_1+3b_2)}{12}$
	$\frac{2}{3} abL$	$\frac{5}{12} abL$	$\frac{1}{4} abL$	$\frac{aL(3b_1+5b_2)}{12}$
	$\frac{bL(c+4d+e)}{6}$	$\frac{bL(2d+e)}{6}$	$\frac{bL(c+2d)}{6}$	$\frac{L}{6} [b_1(c+2d) + b_2(2d+e)]$

$$S_{\omega_G} = 0.305 \left[\frac{1}{2} (4.56)(1.37) + \frac{5.8}{2} (4.56 + 21.35) + \frac{5.8}{2} (21.35 + 35.6) + \frac{5.8}{2} (35.6 + 52.4) + \frac{1.37}{2} (52.4 + 57) \right] = 174.9 \text{ m}^4$$

$$I_{\omega_G} = 2(0.305) \left[\frac{5.8}{6} (2(7.1^2) + 2(23.9^2) + 2(7.1)(23.9)) + \frac{1.37}{6} (2(23.9^2) + 2(28.48^2) + 2(23.9)(28.48)) + \frac{1}{3} (7.1)^2 \left(\frac{5.8}{2} \right) \right] = 1538.8 \text{ m}^6$$

$$I_{\omega_{x_G}} = 2(0.305) \left[\frac{1.37}{6} \left(-2(23.9) \left(\frac{5.8}{2} \right) - 2(28.48)(1.5) - (23.9)(1.5) - (28.48) \left(\frac{5.8}{2} \right) \right) + \right.$$

$$\left. - \frac{1}{3} \left(\frac{5.8}{2} \right)^2 (7.1) - \left(\frac{5.8}{2} \right)^2 (7.1 + 23.9) \right] = -219 \text{ m}^5$$

3.2.4 Differential Equilibrium Equations in Principal Directions

The system of equations (3.32) can be strongly simplified operating some sharp choices: in effect, if a central coordinate system is considered, as well as the sectorial pole coincides with the shear centre of the section and the corresponding sectorial origin is principal, the conditions (3.34) and (3.35) are all immediately satisfied. This means that the system (3.32) is reduced to four independent equilibrium equations:

$$\begin{aligned}\zeta''AE &= 0 \\ EI_y\xi^{IV} &= q_x \\ EI_x\eta^{IV} &= q_y \\ EI_\omega\vartheta^{IV} - GJ_t\vartheta'' &= m\end{aligned}\quad (3.60)$$

Choosing the opportune boundary conditions, the system can be solved and the functions ζ , ξ , η and ϑ can be determined. From these, the normal and tangential stresses and, consequently, the corresponding internal actions can be found. Taking into account Eqn (3.19), the latter are given by:

$$\begin{aligned}N &= \int_A \sigma dA = EA\zeta' \\ M_y &= \int_A \sigma x dA = EI_y\xi'' \\ M_x &= -\int_A \sigma y dA = -EI_x\eta'' \\ B &= \int_A \sigma \omega dA = -EI_\omega\vartheta''\end{aligned}\quad (3.61)$$

The fourth equation describes a new static term which is defined as bimoment action and represents a generalised balanced force system composed by two bending moments, each having the same magnitude but opposite sign.

The substitution of the expressions (3.61) in (3.19) gives an equation which connects the normal stresses with the corresponding internal actions:

$$\sigma = \frac{N}{A} - \frac{M_y}{I_y}x + \frac{M_x}{I_x}y + \frac{B}{I_\omega}\omega\quad (3.62)$$

The first three contributions derive from the classical theory of strength of materials and are based on the hypothesis of plane sections; the fourth describes the normal stresses arisen in the beam due to the out-of-plane warping of the

section. As it can be seen, this term is similar to those derived from the bending: in effect, it is directly proportional to the action and to the corresponding variable function and inversely proportional to a coefficient of inertia.

Similarly the internal actions connected to the tangential stresses are:

$$\begin{aligned} T_x &= \int_A \tau \delta \cos \alpha \, ds = \int_A \tau \delta \, dx \\ T_y &= \int_A \tau \delta \sin \alpha \, ds = \int_A \tau \delta \, dy \\ M_{z\omega} &= \int_A \tau \delta h \, ds = \int_A \tau \delta \, d\omega \end{aligned} \quad (3.63)$$

Substituting Eqn (3.26) in the system (3.63) and considering, from the integration by parts, that:

$$\begin{aligned} \int_A S_x \, dx &= 0 & \int_A S_x \, d\omega &= 0 \\ \int_A S_\omega \, dx &= 0 & & \\ \int_A S_y \, dy &= 0 & \int_A S_y \, d\omega &= 0 \\ \int_A S_\omega \, dy &= 0 & & \\ \int_A S_y \, dx &= -I_y & \int_A S_x \, dy &= -I_x \\ \int_A S_\omega \, d\omega &= -I_\omega & & \end{aligned} \quad (3.64)$$

the following relationships are obtained:

$$\begin{aligned} T_x &= -EI_y \xi''' \\ T_y &= -EI_x \eta''' \\ M_{z\omega} &= -EI_\omega \vartheta''' \end{aligned} \quad (3.65)$$

As the case of normal stresses, an equation which connects the tangential stresses with the internal transversal actions can be highlighted:

$$\tau = -\frac{E}{\delta} \left[\frac{T_x}{I_y} S_y(s) + \frac{T_y}{I_x} S_x(s) + \frac{M_{z\omega}}{I_\omega} S_\omega(s) \right] \quad (3.66)$$

Again, the first two terms are the same proposed by Jourawsky in the theory of plane sections, whereas the last one, having a similar expression, is derived from the theory of the sectorial areas.

Comparing Eqns (3.65) with Eqns (3.61), it is possible to connect the longitudinal actions with the transversal ones. In this way the complete formal analogy between the well-known bending formulation and the flexural-torsional one is confirmed:

$$T_x = -M'_y \quad T_y = M'_x \quad M_{z\omega} = B' \quad (3.67)$$

Observing Eqn (3.67c) it is evident that the section is, actually, subjected to two types of torsional actions, resulting from the fact that the tangential stresses are subdivided into two different components, as shown in Fig. 3.4. Therefore, the total resistant torsional moment is finally given by the sum of two separated contributions:

$$M_Z = M_z + M_{z\omega} = GI_t \vartheta' - EI_\omega \vartheta''' \quad (3.68)$$

3.3 Experimental Investigation on Warping Deformation

The analytical formulation proposed by Vlasov, known as the theory of the sectorial areas, is rarely used when thin-walled open section beams are taken into account. Nevertheless, even though in the literature many papers, focused on the structural behaviour of these elements, have been published, to the author's best knowledge, none proposed a specific experimental technique to evaluate first-hand their particular out-of-plane distortion, when subjected to torsional actions. In order to verify the theory of the sectorial areas, in the present section an experiment regarding a thin-walled open section profile subjected to flexural and torsional loads is performed. For this purpose, a steel beam showing a U profile has been realised. With the aim of an optical device, suitable for precision measurements, the warping deformation of the section, as a consequence of the application to different levels of concentrated torsional actions, can be defined.

The evaluation of the effectiveness of the analytical formulation consists in the comparison of the results obtained experimentally with those coming from two different methods: the first implements the equation of Vlasov's theory, whereas the second relies on the Finite Element method.

First, a brief summary of the main passages of the analytical formulation which allows to define the stiffness matrix of thin-walled open section beams subjected

to transversal loads is provided below. Finally, the main phases of the experimental test are described.

3.3.1 Stiffness Matrix for Thin-Walled Open Section Beams

The warping deformation is an unusual distortion which characterises thin-walled open section beams. This phenomenon, usually neglected for most of structural elements, appears in presence of transversal loads, in particular if they cause torsional effects.

Let's consider a linear-elastic isotropic and homogeneous beam having a thin walled open section in a right-handed reference system OXYZ (Fig. 3.14). Let ξ , η and ζ be the translations of the origin O along the directions X, Y and Z respectively and ϑ the rotation of the section.

In a general loading case, the equilibrium equations of the beam are expressed by:

$$\begin{aligned} E(\zeta''A - \xi'''S_y - \eta'''S_x - \vartheta'''S_\omega) &= q_z \\ -E(\zeta'''S_y - \xi^{IV}I_y - \eta^{IV}I_{xy} - \vartheta^{IV}I_{\omega y}) &= q_x \\ -E(\zeta'''S_x - \xi^{IV}I_{xy} - \eta^{IV}I_x - \vartheta^{IV}I_{\omega x}) &= q_y \\ -E(\zeta'''S_\omega - \xi^{IV}I_{\omega y} - \eta^{IV}I_{\omega x} - \vartheta^{IV}I_\omega) - GJ_t\vartheta'' &= m \end{aligned} \quad (3.69)$$

which can be simplified applying the conditions described in Section 3.2.4.

Therefore, the system (3.69) turns into

$$\begin{aligned} EA\zeta'' &= q_z \\ EI_y\xi^{IV} &= q_x \\ EI_x\eta^{IV} &= q_y \\ EI_\omega\vartheta^{IV} - GJ_t\vartheta'' &= m \end{aligned} \quad (3.70)$$

The equations, initially coupled each other through the variables ξ , η , ζ and ϑ , are now independent. In Eqn (3.70d) the term which refers to Saint Venant's theory is, for now, disregarded. Its contribution will be added later, in the final expression which defines the stiffness matrix of the element.

If the system of external forces is only represented by transversal actions, Eqn (3.70a) can be neglected.

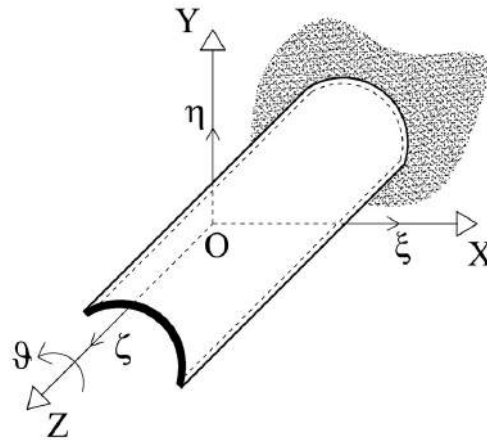


Figure 3.14 – Thin-walled open section beam in a right-handed coordinate system.

The remaining equations can be organised in a matrix form through the following vectors of the displacements δ and the actions q :

$$\delta = \begin{Bmatrix} \xi \\ \eta \\ \theta \end{Bmatrix} \quad q = \begin{Bmatrix} q_x \\ q_y \\ m \end{Bmatrix} \quad (3.71)$$

$$EI\delta^{IV} = q \quad (3.72)$$

in which \mathbf{I} is a diagonal 3×3 matrix whose diagonal coefficients are expressed by I_y , I_x and I_ω , being all the other elements equal to zero.

Since \mathbf{I} is symmetrical and positive definite until the geometry of the section is such that the corresponding sectorial moment of inertia I_ω is different from zero, it is possible to invert the expression (3.72) in order to highlight the vector of displacements δ .

If the actions are not represented by forces distributed along the beam, but concentrated in correspondence to N specific sections (Fig. 3.15a), Eqn (3.72) remains valid in each segment circumscribed by these sections and shows the following form:

$$\delta''' = -\mathbf{I}^{-1} F/E \quad (3.73)$$

where the relation between the vectors q and F is given by:

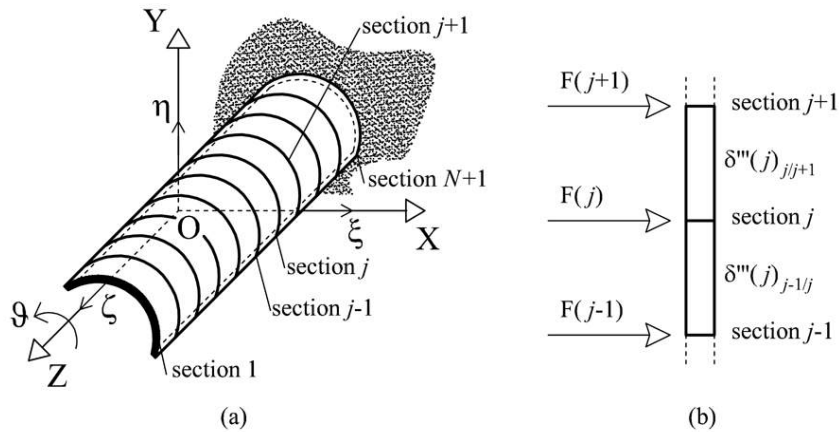


Figure 3.15 – Thin-walled open section beam subjected to concentrated transversal actions applied to specific sections (a); scheme for the continuity conditions between different sections (b).

$$q = -\frac{\partial}{\partial z} F = -\frac{\partial}{\partial z} \begin{Bmatrix} F_x \\ F_y \\ M_z \end{Bmatrix} \quad (3.74)$$

The transversal displacements ξ , η and ϑ are acquired integrating Eqn (3.73) in each domain where the expression is defined and introducing the adequate boundary conditions. Such conditions are subdivided in continuity and global conditions.

The continuity conditions for the j -th section ($j = 2, \dots, N$) are:

$$\begin{aligned} \delta(j)_{j-1/j} &= \delta(j)_{j/j+1} \\ \delta'(j)_{j-1/j} &= \delta'(j)_{j/j+1} \end{aligned} \quad (3.75)$$

$$\begin{aligned} \delta''(j)_{j-1/j} &= \delta''(j)_{j/j+1} \\ EI\delta'''(j)_{j-1/j} &= EI\delta'''(j)_{j/j+1} + F(j) \end{aligned} \quad (3.76)$$

in which the first two are kinematic, whereas the last are equilibrium conditions (Fig. 3.15b).

If the beam is constrained as a cantilever beam, the global conditions for the free edge ($j = 1$) are given by the equilibrium conditions:

$$\begin{aligned}\delta''(1) &= 0 \\ \delta'''(1) &= -\mathbf{I}^{-1} \mathbf{F}(1)/E\end{aligned}\quad (3.77)$$

whereas, for the opposite edge ($j = N+1$), two kinematic conditions are considered:

$$\begin{aligned}\delta(N+1) &= 0 \\ \delta'(N+1) &= 0\end{aligned}\quad (3.78)$$

For the sake of simplicity, the transversal displacements of the sections are reported in a single $3N$ vector $\underline{\delta}$, in which the translations along the X axis, then those along the Y axis and, finally, the rotations are posed. Similarly, a global $3N$ vector $\underline{\mathbf{F}}$ containing N shear forces F_x , N shear forces F_y and, finally, N torque moments M_z is assembled.

By means of the procedure of integration previously mentioned, it is possible to obtain a relationship between $\underline{\delta}$ and $\underline{\mathbf{F}}$ through the compliance matrix \mathbf{C} or its inverse, the stiffness matrix \mathbf{k} .

$$\underline{\delta} = \mathbf{C}\underline{\mathbf{F}} = \mathbf{k}^{-1}\underline{\mathbf{F}}\quad (3.79)$$

Finally the torsional contribution coming from Saint Venant's theory, which is proportional to the torsional inertia J_t , is added to the torsional component of the calculated stiffness matrix.

Once the external actions are known, by means of Eqn (3.79), it is possible to obtain the displacements of the corresponding sections in terms of ξ , η and ϑ . Then, differentiating the latter with respect to the coordinate z and exploiting the last component of Eqn (3.13), the axial displacements which define the warping of the section are deduced, according to the theory of the sectorial areas.

3.3.2 Experimental Investigation

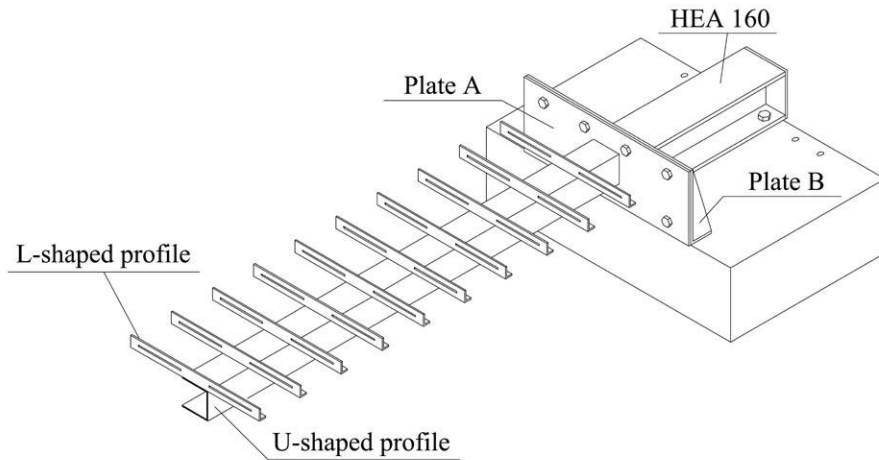


Figure 3.16 – Scheme of the test on a thin-walled U-shaped section steel beam.

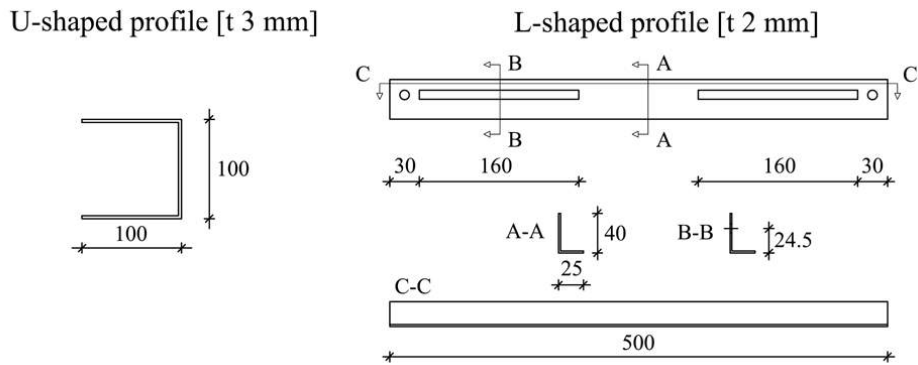


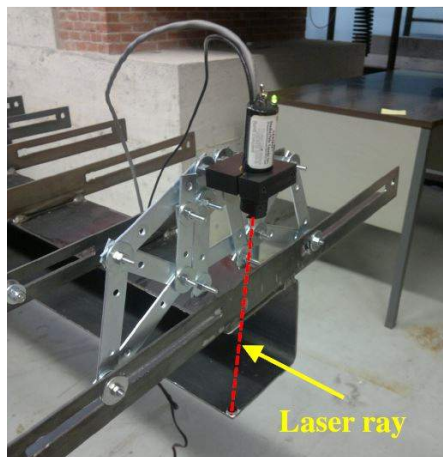
Figure 3.17 – Geometrical properties of the thin-walled steel profiles.

Specific experimental investigations for the evaluation of the effective out-of-plane deformation of thin-walled open section beams subjected to torsional actions are almost absent in the literature of the past fifty years.

Therefore, the contribution described below proves to be particularly innovative for the structural analysis of these profiles.



Figure 3.18 – Application of the external concentrated loads.



(a)



(b)

Figure 3.19 – Picture of the little steel frame, applied to the extreme L-shaped profile, to which the laser is connected (a); scheme of the reflection of the laser (b).

The evaluation of the warping deformation is performed by means of an experimental test on a 1.6 m long steel beam, constrained as an horizontal cantilever. The cross section is defined by a thin-walled U profile (Fig. 3.16).

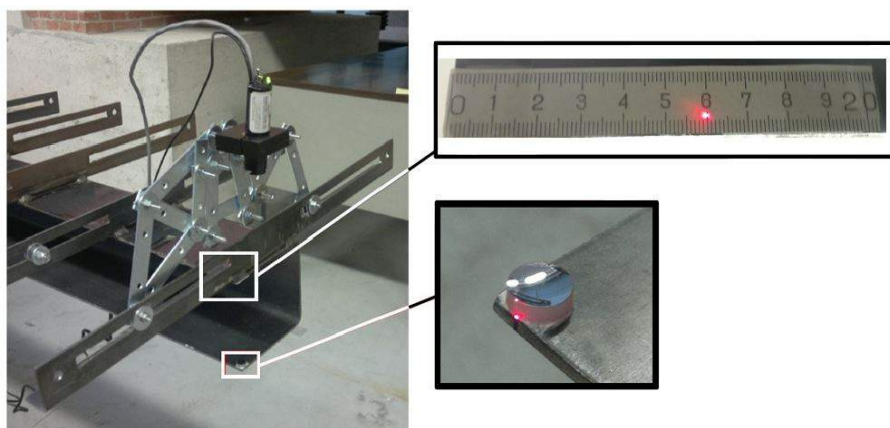


Figure 3.20 – Location of the optical device and the ruler which allows the measurement of the warping of the section.

On the upper flange, at distance of 0.16 m each other, some little beams, having L-shaped section and conveniently altered for the application of the transversal actions, are welded. The geometrical dimensions of the structural components are reported in Fig. 3.17.

The applied loads are represented by masses, each of 3.08 kg, located at 0.23 m far from the shear centre of the U-shaped section. In this way, at the same time, shear forces and anticlockwise torsional moments are produced (Fig. 3.18).

The rigid constraint of the cantilever scheme is realised at one of the edges of the beam by means of welding on a steel plate, which is in turn bolted to a fixed system (Fig. 3.16, plate A).

The system for detecting the axial displacements defining the warping of the section is constituted by three main components. The first is a little steel frame which is connected, through bolts, to the L-shaped section beam posed at the free edge of the examined U-shaped section beam. The second is a laser, rigidly connected to the steel frame, whose ray is directed to the free edge of the bottom flange of the U-shaped profile (Fig. 3.19a). The last is a spherical mirror, characterised by specific geometrical properties adequate for precision measurements, which is placed where the ray meets the bottom flange of the main beam. According to this configuration, the ray of the laser is reflected on the inner side of the upper flange of the U-shaped section beam, where a ruler is pasted (Fig. 3.19b-3.20).

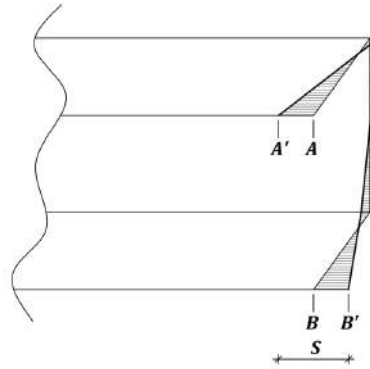


Figure 3.21 – Relative displacement s between the laser ($A \rightarrow A'$) and the mirror ($B \rightarrow B'$).

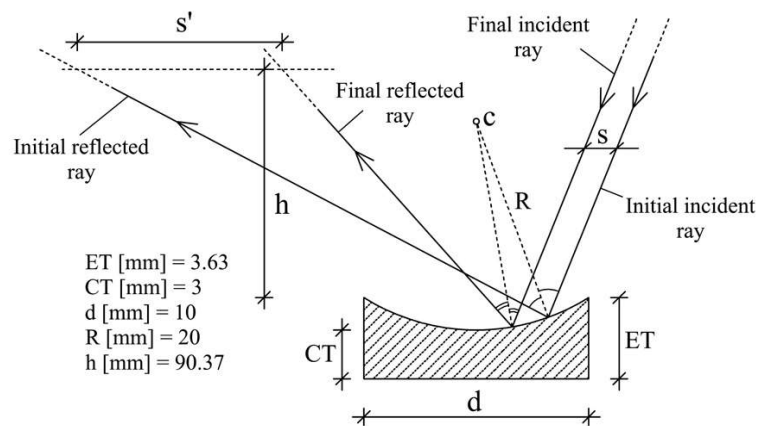


Figure 3.22 – Amplification of s due to the geometrical characteristics of the spherical mirror.

Because of the concentrated torsional moments, the section twists around its shear centre, undergoing, at the same time, a distortion out of its own plane. This deformation can be expressed by the system of axial displacements of the points constituting the section, once the pure flexural deformations are removed.

Experimentally, it may be evaluated considering the relative axial displacement of two symmetrical points of the section: the application point of the laser and the one of the mirror (Fig. 3.21).

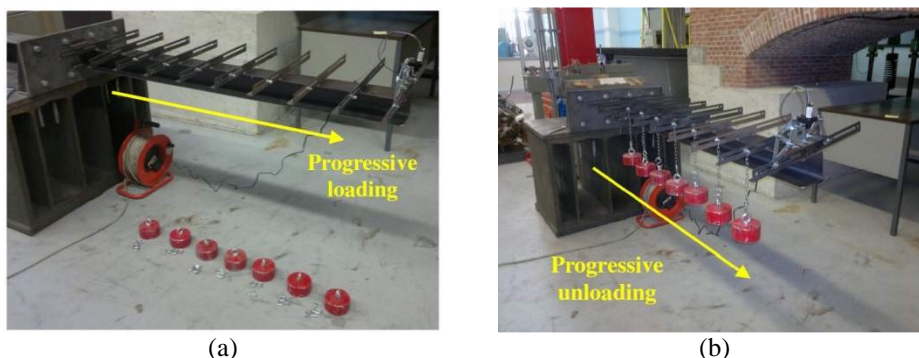


Figure 3.23 – Different loading conditions: loading (a) and unloading (b) phase.

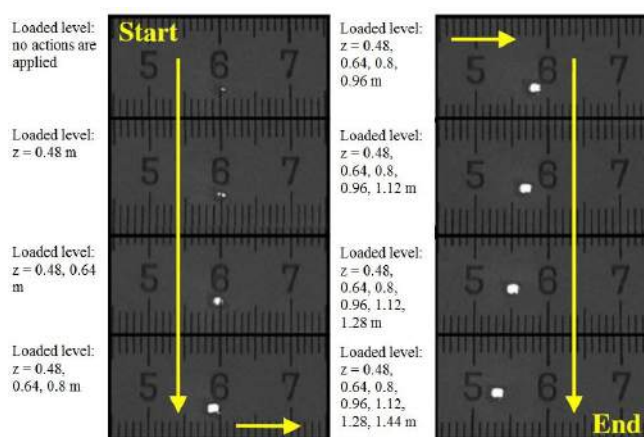


Figure 3.24 – Measurement of the displacement s' during the loading phase: the white dots represent the consecutive positions of the reflected ray on the ruler.

Exploiting the geometrical properties of the mirror, as a consequence of the displacement s of the incident ray, it is possible to detect, on the upper flange of the U-shaped section, the displacement s' related to the reflected ray. Because of the curvature of the mirror, the term s' represents an amplification of s and, therefore, its measurement becomes much easier (Fig. 3.22). In this case, the geometrical characteristics of the mirror are such that the amplification factor, that is the ratio between s' and s , is about 12.

Table 3.3 – Comparison between analytical and FE method.

TYPE OF PROCESS:		LOADING				UNLOADING			
Level N.	z [m]	Loaded level	s [mm]		Err. [%]	Loaded level	s [mm]		Err. [%]
			Analytical	FEM			Analytical	FEM	
1	0.48	1	7.61E-03	7.56E-03	0.61	1 ÷ 7	2.52E-01	2.46E-01	2.58
2	0.64	1, 2	2.13E-02	2.10E-02	1.23	2 ÷ 7	2.44E-01	2.38E-01	2.64
3	0.80	1 ÷ 3	4.29E-02	4.22E-02	1.56	3 ÷ 7	2.31E-01	2.25E-01	2.71
4	0.96	1 ÷ 4	7.44E-02	7.32E-02	1.74	4 ÷ 7	2.09E-01	2.03E-01	2.79
5	1.12	1 ÷ 5	1.18E-01	1.16E-01	1.86	5 ÷ 7	1.77E-01	1.72E-01	2.94
6	1.28	1 ÷ 6	1.76E-01	1.73E-01	2.00	6, 7	1.34E-01	1.30E-01	3.23
7	1.44	1 ÷ 7	2.52E-01	2.46E-01	2.58	7	7.54E-02	7.26E-02	3.95

$$\text{Error [\%]} = (\text{Analytical} - \text{FEM})/\text{FEM} \times 100$$

The experimental analysis was performed varying the loading condition: in a first phase the L-shaped section beams were progressively loaded from $z = 0.48$ m to $z = 1.44$ m, being $z = 0$ m the constrained edge of the beam; then, the unloading process was conducted following the same order (Fig. 3.23).

In Fig. 3.24 the experimental results, which describe the amplified displacement s' related to the loading phase, are reported. It is evident that the use of the optical device facilitates the detection of the warping displacements which are, otherwise, invisible to the naked eye.

The same structure was, finally, examined in a Finite Element (FE) program in order to verify the effectiveness of the analytical method in the individuation of the structural behaviour of thin-walled open section beams. In this case, the steel U-shaped section beam was modelled by means of thin shell elements. In Table 3.3 the numerical comparison between the analytical and the FE method is shown and a good convergence can be acknowledged, since the main difference is about 4%.

Similarly, the same correspondence can be noticed comparing the numerical results with experimental ones: in Fig. 3.25 normalised values of the axial displacement s are reported taking into account every single loading condition, during both the loading and unloading process.

Since Vlasov's theory proves to reach enough accuracy, until the material is linear elastic, the proposed analytical formulation can be easily extended to consider beams with greater dimensions, as the case of thin-walled open section bracings which are usually employed to stiffen horizontally tall buildings [19].

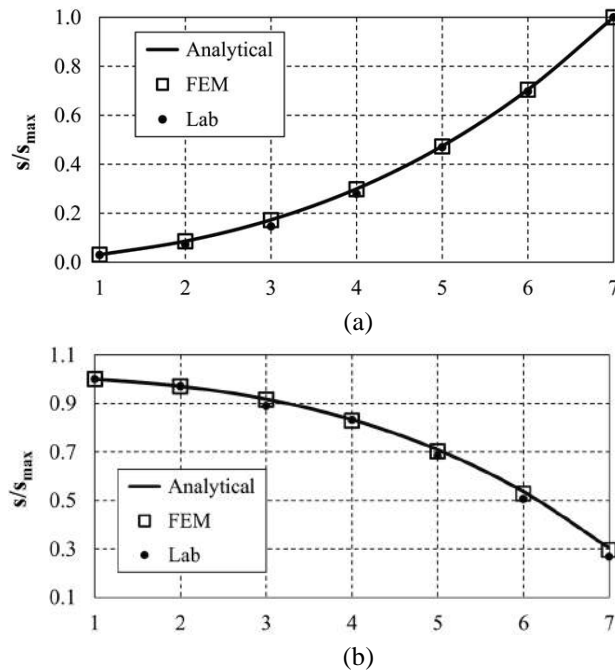


Figure 3.25 – Comparison of the results in terms of normalised values of the axial displacement s , during the loading (a) and unloading (b) process.

3.4 Capurso's Approach for Tall Building Design

In the design of tall buildings, the structural contribution for horizontal actions can be considered predominant if compared to the requirements coming from the vertical resistance. As regard medium-high building, one of the most popular solutions employed to absorb the horizontal load is the shear wall scheme.

Since these bracings often house lift shafts or stairwells, some openings are needed along the vertical profile in order to allow the accessibility of the internal spaces of the building. This means that most of times they can be treated as thin-walled open section cantilevers. Nevertheless, in these cases the following assumptions must be formulated:

- each thin plate obeys to Euler-Bernoulli hypothesis of plane sections;
- the torsional rigidity of each plate derived from Saint Venant's theory can be considered negligible;

- the stiffening effects due to rigid connecting beams, located along the cut edge, are neglected.

The third assumption is, actually, very strong and tends to underestimate the transversal stiffness of the global structure. With the increase of the building height and, therefore, the increase of the number of floors, the stiffening effect caused by the connecting beams is such that the torsional behaviour of the whole element is halfway between the cases of closed and open section, determining a completely different deformation of the structure.

The first hypothesis is in line with Vlasov's theory, since it involves that the longitudinal fibres remain orthogonal to the transversal ones and, therefore, the shearing strain γ_{zs} is null. Similarly, the second assumption asserts that, in the design of vertical bracings characterised by thin-walled open sections, the stiffness contribution related to the sectorial rigidity EI_ω is much larger than the one associated to Saint Venant's theory, which is proportional to the torsional rigidity GJ_t .

According to the previous hypotheses, the analytical formulation proposed by Vlasov can be adopted to evaluate the structural behaviour of a tall building stiffened by a single thin-walled open section cantilever [23].

In a generic coordinate system, the attention is focused on the case in which only the transversal concentrated actions T_x , T_y and M_z are considered. For the computation of the sectorial characteristics, the origin of the right-handed system XYZ coincides with the sectorial pole, whereas the sectorial origin on the profile line is generic.

Supposing to disregard the axial force in the vertical bracing, the following systems of transversal and longitudinal equilibrium equations can be written:

$$\begin{aligned} E(\zeta''S_y - \xi'''I_y - \eta'''I_{xy} - \vartheta'''I_{\omega y}) &= T_x \\ E(\zeta''S_x - \xi'''I_{xy} - \eta'''I_x - \vartheta'''I_{\omega x}) &= T_y \\ E(\zeta''S_\omega - \xi'''I_{\omega y} - \eta'''I_{\omega x} - \vartheta'''I_\omega) &= -M_{z\omega} \end{aligned} \quad (3.80)$$

$$\begin{aligned} E(\zeta'A - \xi''S_y - \eta''S_x - \vartheta''S_\omega) &= N = 0 \\ E(\zeta'S_y - \xi''I_y - \eta''I_{xy} - \vartheta''I_{\omega y}) &= M_y \\ E(\zeta'S_x - \xi''I_{xy} - \eta''I_x - \vartheta''I_{\omega x}) &= M_x \\ E(\zeta'S_\omega - \xi''I_{\omega y} - \eta''I_{\omega x} - \vartheta''I_\omega) &= B \end{aligned} \quad (3.81)$$

Eqn (3.81a) allows to highlight the term ζ' :

$$\zeta' = \xi'' \frac{S_y}{A} + \eta'' \frac{S_x}{A} + \vartheta'' \frac{S_\omega}{A} \quad (3.82)$$

In this expression the first two terms hide the geometrical coordinates of the centroid of the section, whereas the third one gives information about the diagram of the sectorial coordinate ω . In effect, considering the expression (3.39), it represents the constant value which, subtracted to the original diagram, gives rise to the principal one related to the initially chosen sectorial pole. Consequently, Eqn (3.82) becomes:

$$\zeta' = \xi'' x_G + \eta'' y_G + \vartheta'' \omega_0 \quad (3.83)$$

The substitution of Eqn (3.83) in the last three equations of the system (3.81) permits to define new expressions of the longitudinal actions.

$$\begin{aligned} -E(\xi'' J_y + \eta'' J_{xy} + \vartheta'' J_{\omega y}) &= M_y \\ -E(\xi'' J_{xy} + \eta'' J_x + \vartheta'' J_{\omega x}) &= M_x \\ -E(\xi'' J_{\omega y} + \eta'' J_{\omega x} + \vartheta'' J_\omega) &= B \end{aligned} \quad (3.84)$$

where:

$$\begin{aligned} J_y &= I_y - Ax_G^2 & J_x &= I_x - Ay_G^2 \\ J_{xy} &= I_{xy} - Ax_G y_G \end{aligned} \quad (3.85)$$

$$\begin{aligned} J_\omega &= I_\omega - A\omega_0^2 & J_{\omega y} &= I_{\omega y} - Ax_G \omega_0 \\ J_{\omega x} &= I_{\omega x} - Ay_G \omega_0 \end{aligned} \quad (3.86)$$

Eqns (3.85) represent the implementation of Huygens-Steiner theorem, which transfers the system XYZ from the generic origin to the centroid of the section; similarly, Eqns (3.86), previously shown as Eqns (3.42), (3.45) and (3.46), describe new sectorial properties, for which the principal sectorial diagram is considered.

The expressions (3.85) and (3.86) also affect the system (3.80), which turns into:

$$\begin{aligned} -E(\xi''' J_y + \eta''' J_{xy} + \vartheta''' J_{\omega y}) &= T_x \\ -E(\xi''' J_{xy} + \eta''' J_x + \vartheta''' J_{\omega x}) &= T_y \end{aligned}$$

$$-E(\xi'''J_{\omega y} + \eta'''J_{\omega x} + \vartheta'''J_{\omega}) = M_{z\omega} \quad (3.87)$$

If the matrix of inertia \mathbf{J} and the vectors δ , M and T are introduced:

$$\mathbf{J} = \begin{bmatrix} J_y & J_{xy} & J_{\omega y} \\ J_{xy} & J_x & J_{\omega x} \\ J_{\omega y} & J_{\omega x} & J_{\omega} \end{bmatrix} \quad (3.88)$$

$$\delta = \begin{Bmatrix} \xi \\ \eta \\ \vartheta \end{Bmatrix} \quad M = \begin{Bmatrix} M_y \\ M_x \\ B \end{Bmatrix} \quad T = \begin{Bmatrix} T_x \\ T_y \\ M_{z\omega} \end{Bmatrix} \quad (3.89)$$

it is possible to write the systems (3.84) and (3.87) in a synthetic form:

$$M = -E\mathbf{J}\delta'' \quad T = -E\mathbf{J}\delta''' \quad (3.90)$$

Since the matrix of inertia is symmetrical and positive definite until the geometry of the section is such that the moment I_{ω} is different from zero, it is possible to invert it and obtain a relationship between the vector δ''' and the concentrated actions T .

$$\delta''' = -\frac{1}{E}\mathbf{J}^{-1}T \quad (3.91)$$

The analytical solution which gives the transversal displacements of the section is acquired integrating the Eqn (3.91) through the boundary conditions at the base and at the top of the cantilever.

At the constrained end ($z = 0$):

$$\delta = 0 \quad \delta' = 0 \quad (3.92)$$

whereas, at the top end ($z = l$):

$$\delta'' = 0 \quad (3.93)$$

Once ξ , η and ϑ are known, exploiting Eqn (3.83), the uniform axial displacement ζ can be computed, taking into account that the corresponding boundary condition requires:

$$\zeta(z = 0) = 0 \quad (3.94)$$

from which we obtain:

$$\zeta = \xi'x_G + \eta'y_G + \vartheta'\omega_0 \quad (3.95)$$

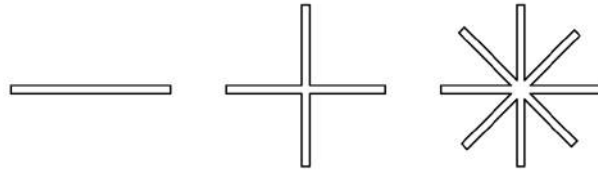


Figure 3.26 - Shear walls constituted by thin plates converging in a single point.

Finally, the displacement components u , v and w can be easily derived from Eqns (3.5), (3.6) and (3.13), whereas the internal stress state is given by Eqns (3.19) and (3.26).

This analytical formulation cannot be applied in presence of specific sections for which the matrix of inertia becomes singular. These are the cases of shear walls constituted by a single thin rectangular plate or many thin plates converging in a single point, as shown in Fig. 3.26. In the first case, in effect, one of the two moments of inertia J_x , J_y and the sectorial moment J_ω become null; in the second case, only J_ω is equal to zero. Therefore, in both cases, the matrix \mathbf{J} cannot be inverted and the equation (3.90b) cannot be solved.

3.4.1 Distribution of the External Actions between Vertical Bracings in Tall Buildings

The described formulation is extended to consider the case of N vertical cantilevers which represent the horizontal resistant skeleton of a tall building subjected to transversal actions applied to the floors according to the global coordinate system XYZ (Fig. 3.27). The vertical bracings are connected each other by means of in-plane rigid slabs, whose out-of-plane rigidity can be considered negligible.

The unknown variables of the problem are the floor displacements, identified by the translations ξ and η in X and Y direction respectively, and the torsional rotation ϑ .

If T_i indicates the vector of the transversal actions absorbed by the i -th cantilever, by virtue of Eqn (3.90b):

$$T_i = -EJ_i \delta''' \quad (3.96)$$

where the matrix \mathbf{J}_i contains the moments of inertia referred to the centroid of the section and to the principal sectorial origin; δ''' gathers the derivatives of the floor displacements ξ , η and ϑ .

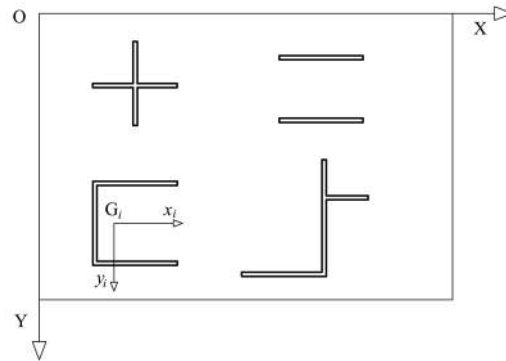


Figure 3.27 – Floor plan of a tall building stiffened by various vertical bracings.

If T is the vector of the external loads, the equilibrium condition imposes:

$$T = \sum_{i=1}^N T_i = -E(\sum_{i=1}^N J_i)\delta''' \quad (3.97)$$

Therefore, the combination of N cantilevers behaves as a single cantilever whose matrix of inertia is given by the sum of the N matrices related to the single cantilevers.

$$\sum_{i=1}^N J_i = J \quad (3.98)$$

$$\delta''' = -\frac{1}{E}J^{-1}T \quad (3.99)$$

Eqn (3.99) can be solved following the procedure previously described for the case of a single vertical bracing.

Once the floor displacements are known, by means of Eqns (3.2) the displacements of each cantilever can be deduced and information regarding the stress state can be obtained.

Finally, it is interesting to observe the relation between the vector T_i of the i -th cantilever and the global vector T :

$$T_i = J_i J^{-1}T \quad (3.100)$$

It is evident that each bracing is subjected to an amount of the external load proportional to its own inertia, but inversely proportional to the inertia of the global system, just like Chapter 2 highlights.

3.5 The Stiffening Effect due to Lintel Beams

In multi-storey buildings, open section shear walls are normally used as an economical solution which provides the required lateral stability against wind and earthquakes and the possibility of housing stairwells and lift shafts. To this aim, they are often rigidly connected, at each floor, to some structural elements, such as lintel beams or slabs. This configuration can be analysed as the case of a tubular element perforated by a series of regular openings along the height. In this scheme, the discrete horizontal components located along the longitudinal cut of the profile determine a considerable increase of its torsional stiffness and, thereby, the structural behaviour of the element can be completely different, halfway between the case of closed section beams and the case of open section beams. Therefore, in the design process the evaluation of the interchanged actions between the vertical bracings and the structural components of the floors becomes indispensable to identify the actual behaviour of the global resistant system.

Many authors dealt with this issue. In effect, the first papers started analysing coupled planar shear walls connected each other by means of rigid horizontal elements. The pioneers of these studies were H. Beck [9] and R. Rosman [90], which proposed a method, called the continuum medium technique, on which several further papers relied for similar problems. The principle of the method is to replace the effect of individual beams or slabs, which interconnect the walls at each floor, by continuously distributed shear forces, that concur to stiffen the structure. In this way, the system of shear walls can be idealised as a single shear flexural cantilever characterised by a stiffness greater than the sum of its single components. Two simple hypotheses are at the base of this method:

- the points of contra-flexure are assumed to be at mid-span of the connecting beams, as long as the cross sections of the walls are such that the difference in rigidity is quite negligible;
- the sections of the walls remain plane after the deformation, whereas it does not happen if the whole cross section of the resultant cantilever is considered;
- the connecting beams show a pure flexural behaviour, being axially absolutely rigid.

According to this approach, many papers were derived. As regard the analysis of coupled planar shear walls connected through rigid lintel beams, the papers by Schwaighofer [98], Coull and Choudhury [31], Coull and Puri [32], Capuani *et al.* [20-22] can be mentioned. In the same way, for the evaluation of the stiffening

effect due to out-of-plane rigid slabs, the first approach, based on the finite difference method, was proposed in the paper by Qadeer and Stafford Smith [90].

Then, experimental studies focused on the determination of the effective bending stiffness of floor slabs coupling shear walls followed, as shown in the papers by Coull and Hag [36], Schwaighofer and Collins [99]. Finally, other works, proposed by Coull and Chee [38-40], exploited Finite Element analysis to evaluate the stresses arisen in slabs as effect of the rigid connection with planar shear walls. In this way they provided a design procedure for checking against punching shear failure in slabs.

A complete mathematical analogy exists between laterally loaded coupled planar shear walls and shafts constituted by open section shear walls subjected to torsional actions. In effect, the same hypotheses can be considered valid in this case. Rosman [96] himself proposed a synthetic method for the analysis of concrete shafts constituted by three-dimensional thin-walled elements and Michael [81] obtained a synthetic differential equation for the torsional coupling of core walls connected by floor beams between the tips of the flanges, whose general solution was confirmed by published test values.

The extension of the theory to a complete three-dimensional continuous method, focusing on prismatic and non-prismatic elements arranged asymmetrically in the floor plan, was later performed by Gluck [53], whereas Heidebrecht and Swift [57] based their analysis on the matrix stiffness method.

Only later, Tso and Biswas [117] added to the previous formulations the possibility of taking into account also the axial deformations of the walls, whereas, through the application of the transfer matrix method, Liauw and Leung [74] formulated an approach able to consider the possible changes, at different storeys, of wall thickness, storey height, loading and depth of the connecting beams.

After the seventies, from an analytical point of view, this issue was totally abandoned, because of the developments of Finite Element methods, which, supported by advanced technology, became popular for structural analyses. Very few works appeared: among all, the last ones, implementing the continuous connection method, were proposed by Wdowicki and Wdowicka [123, 124] for the evaluation of the stress state in non-planar asymmetric shear wall structures having stepwise changes in cross-section.

Most of the mentioned papers offer simplified and convenient methods for hand calculations; nevertheless, even though able to consider several details of the possible structural configuration, they prove to be unsuitable to be inserted in a global formulation for the analysis of complex tall buildings whose horizontal resistant system is composed by various vertical bracings.

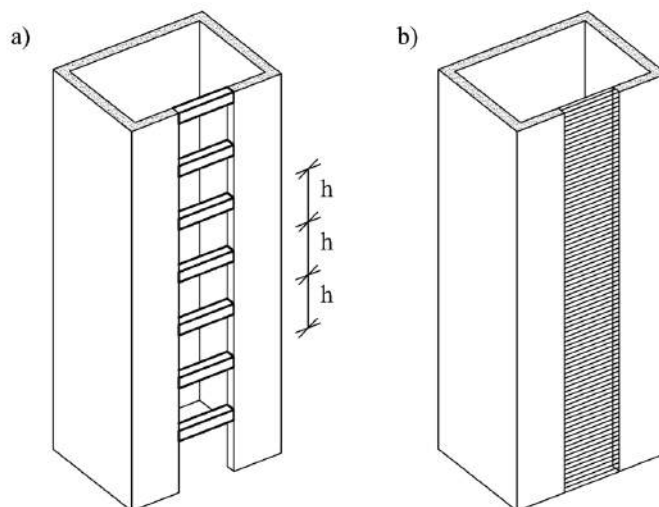


Figure 3.28 – Shear wall stiffened by uniformly spaced lintel beams (a); the discrete system of lintel beams reduced to a continuum of equivalent mechanical properties (b).

A simplified approach which can be easily considered for the definition of the stiffness matrix of core walls stiffened by lintel beams or out-of-plane rigid slabs is hereinafter proposed.

For the sake of simplicity, a single thin-walled open section shear wall is taken into account for the analysis. Along the cut edge some lintel beams of rectangular section are arranged as horizontal elements connecting the extremities of the open section (Fig. 3.28).

The main effect due to the horizontal braces is the increase of the rigidity of the shear wall when subjected to torsion. From this point of view, this configuration moves away from the theory of open sections and gets closed to the one related to hollow sections.

Also for these elements, the hypotheses proposed by Vlasov and Rosman are supposed to be valid. In addition, the horizontal braces are considered deformable in their plane and their structural behaviour depends on their flexural deformations.

If the shear wall is stiffened by n discrete lintel beams, it is necessary to solve a system of n compatibility equations in which the unknowns are defined by n transversal forces developed in the beams. Unfortunately, this procedure turns out to be not suitable for the proposed aim.

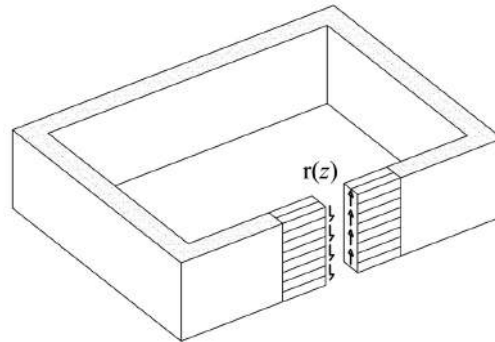


Figure 3.29 - Longitudinal distributed shear loads $r(z)$ absorbed by the equivalent continuum.

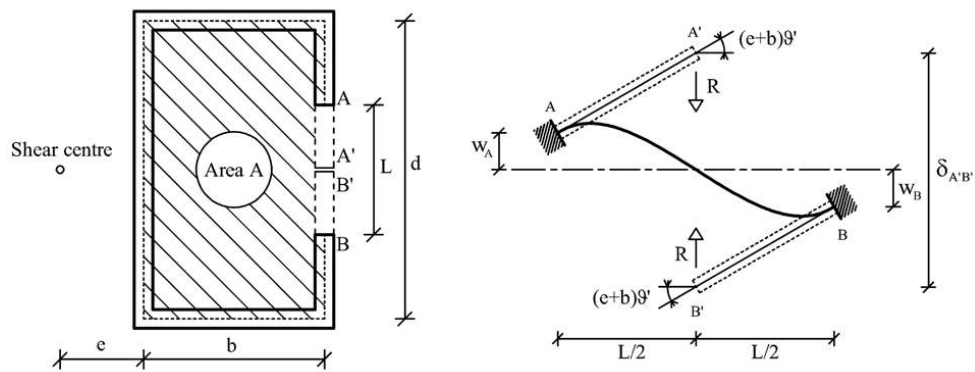


Figure 3.30 – Effect of a single lintel beam on a thin-walled open section beam.

In the case of tall buildings, the storey height is such that the lintel beams corresponding to the floors are closely spaced along the shear wall. Therefore, the resultant system can be reduced to a composite spatial system constituted by the thin-walled shear wall and a plate equivalent in its mechanical properties to the transversal connections and able to sustain only shear stresses.

The stiffening effect of the plate can easily envisaged by cutting it longitudinally where the flexural moment is supposed to vanish and simulating the presence of longitudinal distributed shear loads $r(z)$ applied to the sides of the cut with opposite direction. These actions do not produce any bending moment on the

vertical cantilever and the resultant axial force is equal to zero. On the contrary, only bimoment action is produced, since the two equal and opposite forces cause the warping of the cross-section of the shear wall (Fig. 3.29).

With the aim of identifying this stiffening contribution, let us consider the structural resistance of a single lintel beam defined by a rectangular section. Due to the warping of the section, the extremities of the horizontal beam undergo the same deformations, but with opposite sign: a transversal displacement and a plane rotation (Fig. 3.30). If we consider the extreme points A and B of the section, their vertical displacements due to the warping can be computed taking into account Eqn (3.13).

$$w_A = -\omega_A \vartheta' \quad (3.101)$$

$$w_B = -\omega_B \vartheta' \quad (3.102)$$

The rotations can be obtained after the computation of the same vertical displacements related to the points A' and B', which correspond to the sides of the imaginary cut.

$$\varphi_A = \frac{(w_{A'} - w_A)}{(L/2)} = (b + e) \vartheta' \quad (3.103)$$

$$\varphi_B = \frac{(w_{B'} - w_B)}{(L/2)} = (b + e) \vartheta' \quad (3.104)$$

being L the length of the lintel beam, b and e the characteristic dimensions of the open section.

Because of these displacements, the lintel beam is subjected to an internal shear force of constant value R, which is given by:

$$R = \frac{12EI_b}{L^3} [\omega_B - \omega_A + L(b + e)] \vartheta' \quad (3.105)$$

For the case shown in Fig. 3.30, the term included in the square brackets can be simplified according to the following relationship, which takes into account the area A enclosed by the profile line of the channel:

$$[\omega_B - \omega_A + L(b + e)] = 2A \quad (3.106)$$

If the beam is considered cut in mid-span, a relative displacement between A' and B' occurs. Therefore, this implies that, in order to restore the continuity of the beam, a couple of forces R has to be applied to both sides of the cut.

According to the theory of sectorial areas, the bimoment action produced by any axial force applied to the section is the negative product of the force and the

sectorial coordinate ω of the point to which the force itself is applied. This means that, due to the couple of forces R , a resultant bimoment action is produced:

$$B = -R(\omega_{B'} - \omega_{A'}) \quad (3.107)$$

in which

$$\omega_{A'} = \omega_A - \frac{(b+e)L}{2} \quad (3.108)$$

$$\omega_{B'} = \omega_B + \frac{(b+e)L}{2} \quad (3.109)$$

Consequently, a relationship between the bimoment action and the first derivative of the twist angle is acquired and a stiffness coefficient which takes into account the presence of the lintel beam can be highlighted:

$$B = -\frac{48EI_b}{L^3} A^2 \vartheta' = -k\vartheta' \quad (3.110)$$

$$k = \frac{48EI_b}{L^3} A^2 \quad (3.111)$$

These findings can be used to consider the global system of lintel beams connected to the open section shear wall.

According to the hypothesis of a plate having equivalent mechanical properties, if the spacing of the lintel beams is uniform, the concentrated forces R related to the single beam and applied to the sides of the cut can be transformed into two loads $r(z)$ uniformly distributed along the sides of the longitudinal continuum cut (Fig. 3.29).

$$r(z) = R/h = \frac{24EI_b}{hL^3} A\vartheta' = \frac{k}{2Ah} \vartheta' \quad (3.112)$$

The infinitesimal loads $r(z)dz$ produce a resultant infinitesimal bimoment action, which is given by:

$$dB = -rdz(\omega_{B'} - \omega_{A'}) \quad (3.113)$$

from which we obtain:

$$-r(\omega_{B'} - \omega_{A'}) = dB/dz \quad (3.114)$$

Exploiting Eqn (3.67c) and differentiating Eqn (3.113) with respect to z , a distributed torsional action is computed.

$$m^* = r'(\omega_{B'} - \omega_{A'}) = \frac{48EI_b}{hL^3} A^2 \vartheta'' \quad (3.115)$$

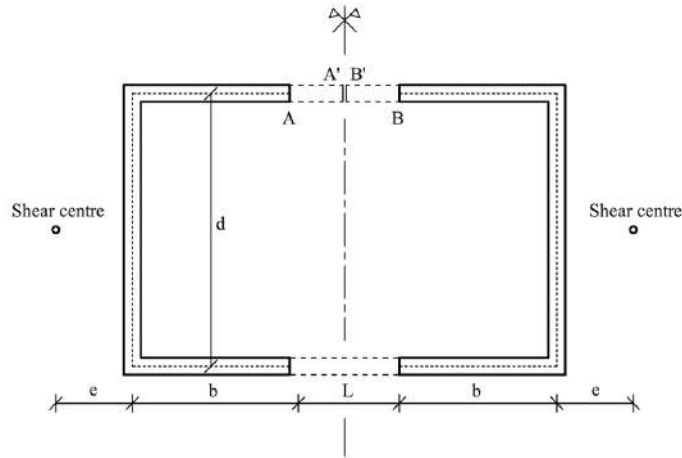


Figure 3.31 – Coupled shear walls constituting a symmetrical shaft.

This contribution can directly inserted in the differential equilibrium equation related to the angle of rotation ϑ (Eqn 3.60d):

$$EI_{\omega}\vartheta^{IV} - GJ_t\vartheta'' = m + m^* \quad (3.116)$$

Substituting Eqn (3.115) in (3.116) and gathering the coefficients of the second derivative of ϑ , a new differential equilibrium equation is obtained, in which the inertia J_t is increased because of the presence of lintel beams closely spaced along the cut edge of the open section shear wall.

$$EI_{\omega}\vartheta^{IV} - GJ_t^*\vartheta'' = m \quad (3.117)$$

$$J_t^* = J_t + \frac{96I_b(1+\nu)}{hL^3}A^2 \quad (3.118)$$

The expression (3.118) proves to be very convenient for practical use. In effect, regardless of the approach considered for the structural analysis of the shear wall, the stiffening effect caused by rigid lintel beams can be taken into account simply computing the increased inertia J_t^* instead of the original one J_t . In addition, the same approach can be implemented for the analysis of coupled open section shear walls constituting a symmetrical shaft. According to this configuration, the flanges of the walls are connected each other by means of rigid beams. Referring to Fig. 3.31, the previous expressions can be used taking into account that the simplification (3.106) is no more valid.

Finally, if the stiffening effect is caused by out-of-plane rigid slabs, the proposed formulation remains valid, since their contribution is reduced to the definition of the corresponding stiffness term k of Eqn (3.111). The latter can be found in literature, most of times acquired through experimental tests. Otherwise, it can be obtained analytically, as the case of Vlasov, who considered slabs acting as flat plates in torsion. In this way he defined the following expression:

$$k = \frac{bdEt^3}{6(1+\nu)} \quad (3.119)$$

where b and d are the slab dimensions, whereas t is the corresponding thickness.

Another convenient approach, based on experimental analyses, is to consider an equivalent lintel beam and determine its corresponding geometrical dimensions in order to simulate the stiffening effect of the real slab.

3.5.1 Numerical Example

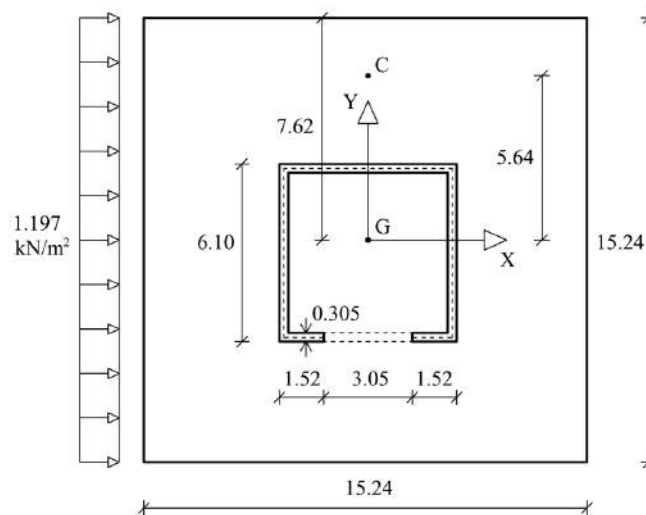


Figure 3.32 – Floor plan of a 15-storey building stiffened by an internal core tube. Dimensions in metres.

Table 3.4 - Geometrical properties of the core tube. Within brackets the properties changed due to the stiffening effect of the lintel beams.

I_x [m ⁴]	I_y [m ⁴]	I_ω [m ⁶]	J_t [m ⁴]	x_C [m]	y_C [m]
30.5	38.8	302.7	0.189 (2.75)	0	5.64

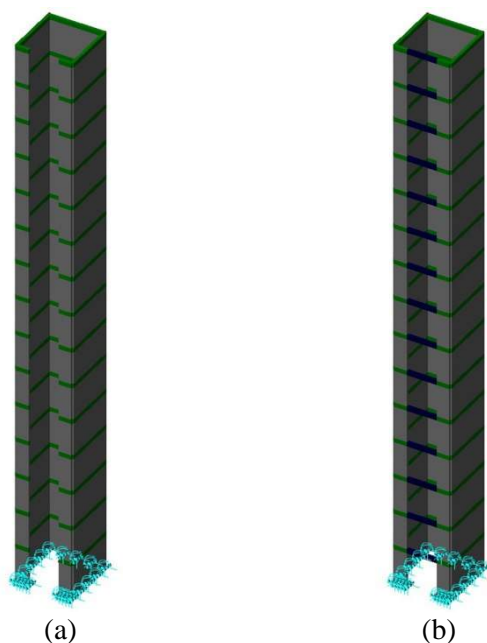


Figure 3.33 – Core tube system modelled in the FE program without (a) and with (b) rigid lintel beams.

To highlight the effectiveness of the proposed method, a well-known example proposed in the paper by Taranath and Stafford Smith [110] and, then, resumed by Pekau *et al.* [87] is here modelled. It is the case of a core tube, constituted by a thin-walled open section beam, subjected to an horizontal action which causes, at the same time, bending and torsion of the building, since the shear centre does not coincide with the centroid of the structural system.

The analysis is performed through the formulation described in the previous section and by means of a computer software implementing the Finite Element method.

The scheme of the 15-storey building having a square plan is shown in Fig. 3.32. The structural material is defined by the following mechanical properties: Young's modulus equal to $E = 2.76 \times 10^4$ MPa and Poisson's ratio $\nu = 0.15$. The storey height is $h = 3.81$ m, corresponding to a total height $H = 57.15$ m. The geometrical parameters of the resistant cantilever are given in Table 3.4.

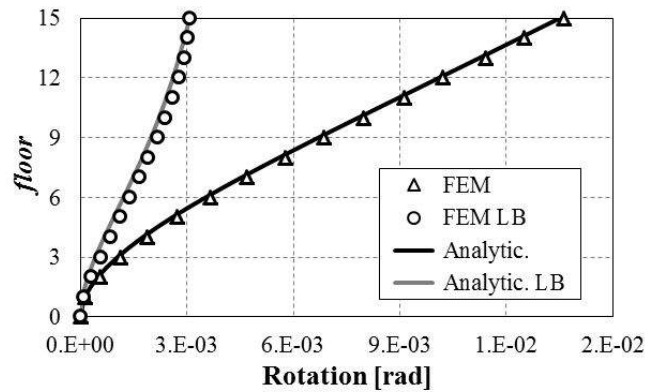


Figure 3.34 – Comparison in terms of torsional rotations between the present method and FE method, with (LB) or without the stiffening effect due to rigid lintel beams.

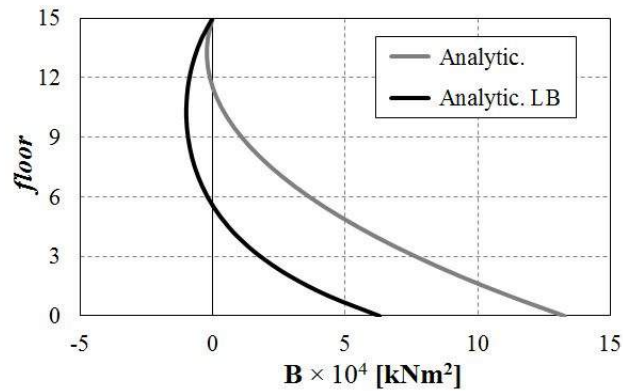


Figure 3.35 – Trend of the bimoment action with (LB) or without the stiffening effect due to rigid lintel beams.

In the analysis the effect of rigid lintel beam connecting the free ends of the cut edge of the open section is taken into account. From a geometrical point of view, these beams are characterised by a depth of 0.457 m and a width equal to the thickness of the shear wall.

The structure is subjected to a distributed horizontal load in X direction whose intensity is 1.197 kN/m²; it corresponds to a resultant action, passing through the

geometrical centroid of the core tube, equal to 69.5 kN for each floor, with the exception of the top floor, where the value is halved.

In Fig. 3.34 the results in terms of torsional rotations are highlighted. As it can be seen, the analytical method is very closed to FE approach for both examined configurations.

The change in the structural behaviour of the building due to the stiffening effect of rigid lintel beams is self-evident. The curve related to the stiffer case proves to be very different in shape from the other case and, moreover, we can assume that it gets closer to the case of a thin-walled cantilever defined by an hollow section.

In the same way, as a consequence of the reinforcement, also the bimoment action, which is not clearly obtainable from the FE program, is strongly affected, as shown in Fig. 3.35. The presence of the lintel beams determines the appearance of concentrated resistant bimoment actions which oppose to the one generated by the external load.

The achieved results, consistent with those indicated by Taranath and Pekau, underline that, in the design process, the presence of stiffening elements, such as lintel beams or slabs, has to be taken into consideration for a correct analysis even if approximate, since the structural behaviour of the entire building can be totally different from the case where no reinforcement is contemplated.

Chapter 4

Conceptual Design of Unconventionally Shaped Structures

4.1 Introduction

The constructions of the last years showed an evolution of the architectural shape of tall buildings. At the beginning, the parameter which classified the exceptional nature of these constructions was the height. Therefore, for many decades, a race for greater structures arose, inevitably conditioning the appearance of the buildings. In this phase, designers often preferred to model the external casing in order to exhibit innovative structural skeletons; in other cases the external shell was conceived to cover them. In any case, the structural component always represented one of the main factors able to lead the design of high-rise constructions.

Only recently, aesthetics has acquired a prime role, undermining the previous which has been adapted to it. The evolution caused by the emerging architectural trends in design and the developments in structural analysis techniques, due to the advent of high-speed digital computers, has led to the current state, in which the structural component has to be in the service of non-conventional forms.

The scale of skyscrapers is such that their architectural expression turns out to be very significant for the urban context in which they are located. Therefore, a deep study on the aesthetic adequacy of the external form with respect to the existing constructions is compulsory from the point of view of public opinion and municipal regulations. The impact on the building aesthetics can often depend on the structural solution employed to stiffen the construction, primarily against horizontal loads: in effect, some systems show an environmental impact more decisive than others.

In braced frames, if the diagonal bracings are inserted within local systems, such as inner cores, their effect on the aesthetics is absent and the external casing can be modelled according to the requirements of the district.

On the contrary, outrigger systems, which exploit the perimeter columns in combination with huge belt trusses to reach the stiffness required by the legislation, are visually cumbersome since they cause a structural domination in the expression of the buildings; in effect, in these cases, very intimate cooperation between architects and engineers is required for the final solution.



Figure 4.1 – Shanghai World Financial Centre (492 m).

It is possible to conclude that, when the height is a dominant design factor, the construction geometry imposes the external shape of the building. Outrigger and tube systems are included in this field, since most of the horizontal resistant contribution is located along the perimeter of the structure and, therefore, it is almost impossible to hide their aesthetic effect.

Often architects exploit these configurations to model futuristic forms, such as the case of bundled tubes, which give the idea that the structure grows up to the sky.

On the contrary, when the structural solutions are adapted to architectural projects, the aesthetics prevails, as the case of diagrid structures, and curved forms replace prismatic ones.

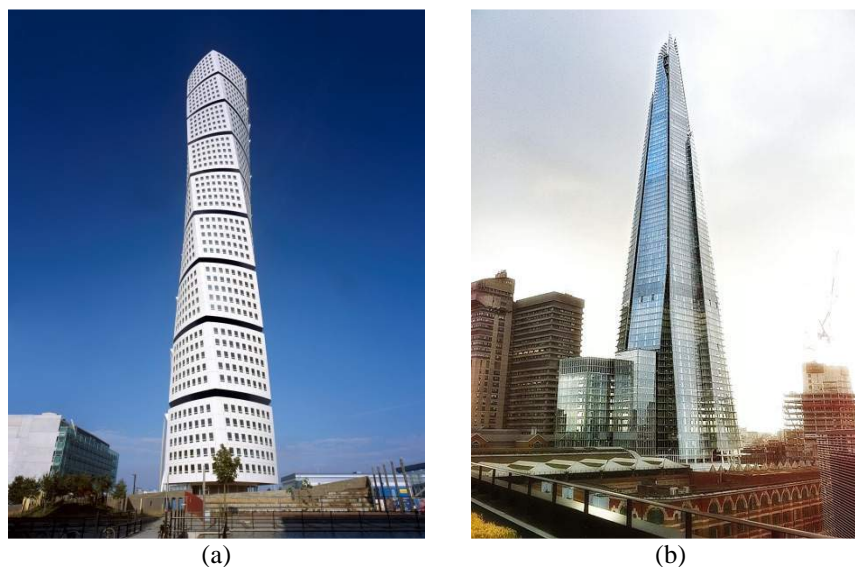


Figure 4.2 – HSB Turning Torso (a) and London Bridge Tower (b).

Another factor which, recently, has influenced the external casing of the structure is the aerodynamics. This trend develops from the need of reducing the horizontal wind forces in super-tall buildings. Therefore, chamfered and rounded corners are designed as well as streamlined and tapered forms, with openings through the building and notches: an example of this idea is the Shanghai World Financial Centre, being a tapered building which employs a large through-building opening in its top part (Fig. 4.1). Further advantages of this choice are the reduction of the along-wing response as well as the across-wind vibration of the building caused by vortex shedding.

This logic has determined the appearance of twisting and tilting shapes with discontinuities and multi-planar facades that are characterising the urban skylines all over the world. In particular, twisting forms, developed in these last years as a reaction to boxed ones of the modern architecture, provide an improvement in the dynamic response of the building, since the vortex shedding is still reduced, although, from the structural point of view, they represent a disadvantageous solution. In effect, if we consider a square solid section, its moment of inertia is the same for any angle of twist considered, but, if a twisting building constituted by frames is taken into account, its lateral stiffness is quite reduced if compared to the corresponding related to the straight form.

The last evolution of curved shapes is represented by free form building, for which a geometrical law along the height is missing. For these cases, however, it is clear that the conception is possible only thanks to the developments of sophisticated computer software which enhance the capabilities of the structural analyses.

Nowadays, all over the world, some bizarre shapes have been commissioned and, in some cases, already built. Glaring examples are the HSB Turning Torso, a twisted skyscraper of 54 storeys (190 m) in Malmo (Sweden), and the 66-storey (308 m) London Bridge Tower, also known as Shard of Glass, which is a pyramidal shaped building, now the tallest structure in Europe (Fig. 4.2).

The emerging complexity of the forms can be balanced by powerful computers and innovative Finite Element (FE) software; nevertheless, in the phase of preliminary design, in which several resistant configurations are examined, the use of approximate methods can support the engineers and address their judgement on the choice of the better structural solution. In effect, they would allow to clearly identify the key parameters governing the response of the structure as well as the force flow acting within the stiffening members of the resistant skeleton.

For this purpose, in this chapter numerical procedures for the computation of the stiffness matrix of vertical bracings employed in tall buildings, whose geometry varies along the height, are proposed. Unusually shaped structures, such as tapered or twisted buildings, are considered in the analyses. In order to evaluate the effectiveness and the suppleness of the method, comparisons with other approaches derived from the literature and numerical examples regarding new architectural trends are carried out.

4.2 Stiffness Matrix for Bracings with Variable Cross-Section

The computation of the stiffness matrix of vertical bracings having prismatic shapes is well-known in literature. The corresponding analytical method can be easily implemented in a computer program to evaluate the contribution of the main resistant elements to the horizontal strengthening of high-rise buildings.

If new architectural trends are taken into account, which require, in some cases, bracings with variable cross-section, the evaluation of their stiffening effect becomes more complex. This situation can be met when the structural component contributes to the external shape of the building casing: in particular, it is the case of tube systems which allow to freely model a three-dimensional body, still remaining the main load bearing system.

To this aim, appropriate methods able to analyse stiffeners having innovative geometry are proposed below, focusing the attention on tapered and twisted bracings, having closed or open sections.

4.2.1 Tapered and Twisted Bracings (Warping Negligible)

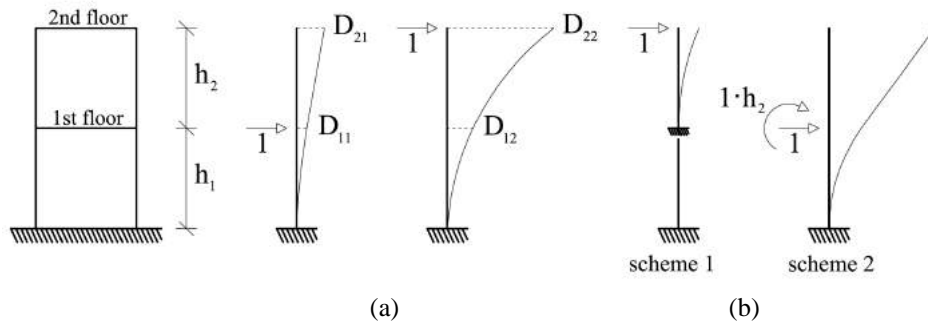


Figure 4.3 – Evaluation of the terms belonging to the compliance matrix of the shear wall (a); schemes for the computation of the displacement D_{22} (b).

Because of the nature of the problem and the type of structure involved which can be easily assimilated to a planar shear wall for each principal direction of inertia, it's advantageous, for a practical point of view, to consider its plane behaviour and compute the floor displacements starting from the applied loads.

It's well-known that a unitary force applied to the i -th level gives rise to displacements of all the levels: these values constitute the i -th column of the compliance matrix of the stiffener.

In the case of 2-storey shear wall, the coefficients of the compliance matrix \mathbf{D} are:

$$\begin{aligned} D_{11} &= \frac{h_1^3}{3EJ_1} & D_{21} &= D_{11} + \frac{h_1^2 h_2}{2EJ_1} \\ D_{12} &= D_{21} & D_{22} &= \frac{h_1^3}{3EJ_1} + \frac{h_2 h_1^2}{2EJ_1} + \frac{h_1^2 h_2}{2EJ_1} + \frac{h_2^2 h_1}{EJ_1} + \frac{h_2^3}{3EJ_2} \end{aligned} \quad (4.1)$$

being h_i and J_i the storey height and the moment of inertia of the i -th level (from bottom to top) respectively (Fig. 4.3a).

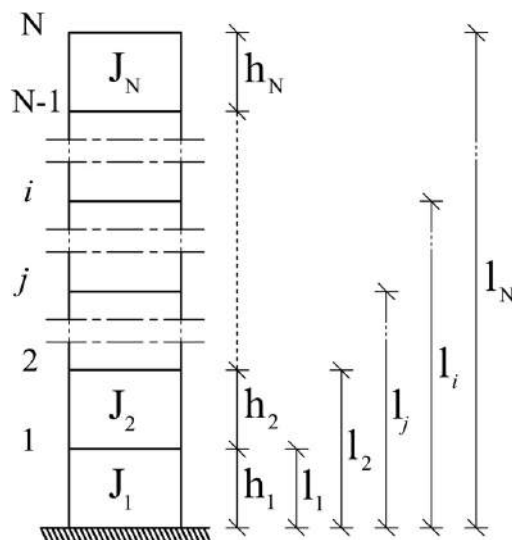


Figure 4.4 – Multi-storey shear wall having different geometrical characteristics for each floor.

Since some geometrical characteristics related to the two levels of the shear wall have been considered different each other, for the definition of the term D_{22} it's more convenient to take into consideration two structural schemes: scheme 1 shows, for the specific load condition, the first floor constrained; scheme 2, free from additional constraints, shows at the first level the resultant system of forces due to the initial loading case (Fig. 4.3b). The first four components of the term D_{22} concern the scheme 2: the first two describe the displacement of the first level, while the third and fourth are the consequent rigid displacements of the second level. The last term of D_{22} is related to the scheme 1 and represents the displacement of the second level being the first one constrained.

This procedure can be easily extended to consider N floors, each having its own storey height h_i and its own moment of inertia J_i (Fig. 4.4).

The generalised term D_{ij} (with $j \leq i$), representing the displacement of the i -th level due to the application of a unitary force to the j -th level, can be evaluated through a recursive process.

For a given load condition applied to the j -th level, the resultant system of forces at the first level is estimated. Then, the displacement of the i -th level for this load case is deduced:

$$\frac{h_1^3}{3EJ_1} + \frac{(l_j-l_1)h_1^2}{2EJ_1} + \left(\frac{h_1^2}{2EJ_1} + \frac{(l_j-l_1)h_1}{EJ_1} \right) (l_i - l_1) \quad (4.2)$$

The same computation is repeated considering the resultant system of forces at the k -th level ($k = 2, 3, \dots, j$). A complete expression of D_{ij} is given by the sum of all contributions.

$$D_{ij} = \sum_{j=1}^i \sum_{k=1}^j \left[\frac{h_k^3}{3EJ_k} + \frac{(l_j-l_k)h_k^2}{2EJ_k} + \left(\frac{h_k^2}{2EJ_k} + \frac{(l_j-l_k)h_k}{EJ_k} \right) (l_i - l_k) \right] \quad (4.3)$$

By means of the Eqn (4.3) the computation of the lower triangular part of the $N \times N$ matrix \mathbf{D} is executed. Exploiting its symmetry, as proved by Betti's theorem, the upper triangular part is completed.

The same method can be extended to assess its torsional behaviour. In this case, neglecting the warping of the section, the generic term of the $N \times N$ torsional compliance matrix \mathbf{D}_θ is expressed by means of the torsional moment of inertia J_t and the shear modulus G .

$$D_{\theta,ij} = \sum_{j=1}^i \sum_{k=1}^j \frac{h_k}{GJ_{tk}} \quad (4.4)$$

The last step is the evaluation of the $3N \times 3N$ stiffness matrix \mathbf{k}^* of the generic bracing, in its own coordinate system. Its structure is block diagonal, constituted by the $2N \times 2N$ stiffness matrix related to the local displacements u and v , \mathbf{k}_d^* , and the $N \times N$ stiffness matrix related to the rotation, \mathbf{k}_θ^* . Each of them is obtained by inverting the corresponding compliance matrix.

$$\mathbf{k}_d^* = \begin{bmatrix} \mathbf{k}_u^* & \mathbf{0} \\ \mathbf{0} & \mathbf{k}_v^* \end{bmatrix} \quad (4.5)$$

$$\mathbf{k}^* = \begin{bmatrix} \mathbf{k}_d^* & \mathbf{0} \\ \mathbf{0} & \mathbf{k}_\theta^* \end{bmatrix} \quad (4.6)$$

In the case of twisted bracings, the structure of the stiffness matrix is no longer block diagonal, since the sub-matrix \mathbf{k}_d^* becomes full.

The computation of its components follows the same approach used for tapered structures, taking into account the increasing rotation of the sections from the ground to the top.

Referring to the case of a 2-storey shear wall, a principal coordinate system for each floor is defined, so that the system XY is related to the ground level while the system $(X^*Y^*)_i$ is related to the i -th level.

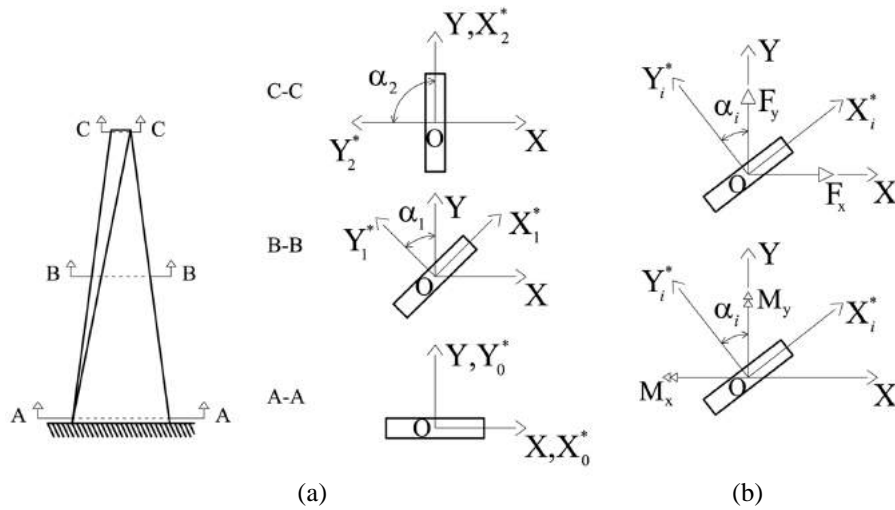


Figure 4.5 – Model of a twisted bracing, each level showing its own local coordinate system $(X^*Y^*)_i$ (a); scheme for the definition of the local components of the external forces and flexural moments (b).

According to this arrangement, all the coordinate systems show the same origin (Fig. 4.5). With regards to the first level, let F_1^* be the 2-vector representing the shear-loading along the principal axes of the local coordinate system $(X^*Y^*)_1$ and F_1 the 2-vector representing the shear-loading along the axes of the coordinate system XY , so that:

$$F_1^* = \begin{Bmatrix} F_{u,1} \\ F_{v,1} \end{Bmatrix} = \begin{bmatrix} \cos \alpha_1 & \sin \alpha_1 \\ -\sin \alpha_1 & \cos \alpha_1 \end{bmatrix} \begin{Bmatrix} F_{x,1} \\ F_{y,1} \end{Bmatrix} = \mathbf{N}_1 F_1 \quad (4.7)$$

where \mathbf{N}_1 represents the orthogonal matrix from the system XY to the local system $(X^*Y^*)_1$ and α_1 is the rotation angle between the Y axis of the ground level and Y_1^* axis of the first level. Likewise, the displacement vector δ_1^* related to the local coordinate system $(X^*Y^*)_1$ is connected with the displacement vector δ_1 related to the coordinate system XY through the same matrix \mathbf{N}_1 . The local displacements of the first floor due to forces placed at the same level along the local axes are expressed by means of the principal moments of inertia, as follows:

$$\delta_{u,11} = \frac{h^3}{3EJ_v} F_{u,1} \quad \delta_{v,11} = \frac{h^3}{3EJ_u} F_{v,1} \quad (4.8)$$

Taking into account the expression (4.7) for the actions and that corresponding to the displacements, the Eqns (4.8), referred to the coordinate system XY, are given by:

$$\begin{aligned}\delta_{x,11} &= \left(\frac{h^3}{3EJ_v} \cos \alpha_1^2 + \frac{h^3}{3EJ_u} \sin \alpha_1^2 \right) F_{x,1} + \\ &\quad + \left[\left(\frac{h^3}{3EJ_v} - \frac{h^3}{3EJ_u} \right) \cos \alpha_1 \sin \alpha_1 \right] F_{y,1} \\ \delta_{y,11} &= \left[\left(\frac{h^3}{3EJ_v} - \frac{h^3}{3EJ_u} \right) \cos \alpha_1 \sin \alpha_1 \right] F_{x,1} + \\ &\quad + \left(\frac{h^3}{3EJ_v} \sin \alpha_1^2 + \frac{h^3}{3EJ_u} \cos \alpha_1^2 \right) F_{y,1}\end{aligned}\quad (4.9)$$

which, in a concise form, become:

$$\begin{aligned}\delta_{x,11} &= D_{x,11} F_{x,1} + D_{xy,11} F_{y,1} \\ \delta_{y,11} &= D_{xy,11} F_{x,1} + D_{y,11} F_{y,1}\end{aligned}\quad (4.10)$$

In the same manner, the rigid displacements of the second floor due to the same load condition, in the coordinate system $(X^*Y^*)_1$, are defined as:

$$\begin{aligned}\delta_{u,21} &= \delta_{u,11} + \frac{h^3}{2EJ_v} F_{u,1} = \left(\frac{h^3}{3EJ_v} + \frac{h^3}{2EJ_v} \right) F_{u,1} \\ \delta_{v,21} &= \delta_{v,11} + \frac{h^3}{2EJ_u} F_{v,1} = \left(\frac{h^3}{3EJ_u} + \frac{h^3}{2EJ_u} \right) F_{v,1}\end{aligned}\quad (4.11)$$

and, with regards to the coordinate system of the ground level, as:

$$\begin{aligned}\delta_{x,21} &= \left[\left(\frac{h^3}{3EJ_v} + \frac{h^3}{2EJ_v} \right) \cos \alpha_1^2 + \left(\frac{h^3}{3EJ_u} + \frac{h^3}{2EJ_u} \right) \sin \alpha_1^2 \right] F_{x,1} + \\ &\quad + \left[\left(\frac{h^3}{3EJ_v} + \frac{h^3}{2EJ_v} \right) \cos \alpha_1 \sin \alpha_1 - \left(\frac{h^3}{3EJ_u} + \frac{h^3}{2EJ_u} \right) \cos \alpha_1 \sin \alpha_1 \right] F_{y,1} \\ \delta_{y,21} &= \left[\left(\frac{h^3}{3EJ_v} + \frac{h^3}{2EJ_v} \right) \cos \alpha_1 \sin \alpha_1 - \left(\frac{h^3}{3EJ_u} + \frac{h^3}{2EJ_u} \right) \cos \alpha_1 \sin \alpha_1 \right] F_{x,1} + \\ &\quad + \left[\left(\frac{h^3}{3EJ_v} + \frac{h^3}{2EJ_v} \right) \sin \alpha_1^2 + \left(\frac{h^3}{3EJ_u} + \frac{h^3}{2EJ_u} \right) \cos \alpha_1^2 \right] F_{y,1}\end{aligned}\quad (4.12)$$

Their synthetic form is expressed as follows:

$$\delta_{x,21} = D_{x,21} F_{x,1} + D_{xy,21} F_{y,1}$$

$$\delta_{y,21} = D_{xy,21}F_{x,1} + D_{y,21}F_{y,1} \quad (4.13)$$

As regards the displacements δ_2 due to the loading F_2 , it's convenient to consider three different contributions. The first two, related to the coordinate system $(X^*Y^*)_1$, depend on the resultant system of forces at the first level: a shear-loading $F_2^{(1)}$ equal in modulus to F_2 and a 2-vector $M^{(1)}$, representing the flexural moments, equal to F_2h . The last contribution refers to the coordinate system $(X^*Y^*)_2$ and describes the displacement of the second floor due to F_2 having considered the first level constrained. It should be noted that the aforementioned actions are referred to the coordinate system of the ground level.

The terms related to the shear-loading $F_2^{(1)}$ are defined by the Eqns (4.11), by means of the components $F_{x,2}$ and $F_{y,2}$ applied to the first floor.

$$\begin{aligned} \delta_{u,21}(F_2^{(1)}) &= \left(\frac{h^3}{3EJ_v} + \frac{h^3}{2EJ_v}\right)(F_{x,2} \cos \alpha_1 + F_{y,2} \sin \alpha_1) \\ \delta_{v,21}(F_2^{(1)}) &= \left(\frac{h^3}{3EJ_u} + \frac{h^3}{2EJ_u}\right)(-F_{x,2} \sin \alpha_1 + F_{y,2} \cos \alpha_1) \end{aligned} \quad (4.14)$$

The bending contribution of the force F_2 at the first level is expressed by the components M_y and M_x , from which the local flexural moments M_v and M_u can be defined.

$$\begin{aligned} M_v &= M_y \cos \alpha_1 + M_x \sin \alpha_1 = h(F_{x,2} \cos \alpha_1 + F_{y,2} \sin \alpha_1) \\ M_u &= -M_y \sin \alpha_1 + M_x \cos \alpha_1 = h(-F_{x,2} \sin \alpha_1 + F_{y,2} \cos \alpha_1) \end{aligned} \quad (4.15)$$

Therefore, with respect to the system $(X^*Y^*)_1$, the local displacements of the second level due to applied moments M_v and M_u at the first level are easily computed:

$$\begin{aligned} \delta_{u,21}(M^{(1)}) &= \left(\frac{h^2}{2EJ_v} + \frac{h^2}{EJ_v}\right)M_v = \left(\frac{h^3}{2EJ_v} + \frac{h^3}{EJ_v}\right)(F_{x,2} \cos \alpha_1 + F_{y,2} \sin \alpha_1) \\ \delta_{v,21}(M^{(1)}) &= \left(\frac{h^2}{2EJ_u} + \frac{h^2}{EJ_u}\right)M_u = \left(\frac{h^3}{2EJ_u} + \frac{h^3}{EJ_u}\right)(-F_{x,2} \sin \alpha_1 + F_{y,2} \cos \alpha_1) \end{aligned} \quad (4.16)$$

The last contribution, which considers the first floor constrained, is given by the Eqns (4.8) through the rotation angle α_2 between the Y axis of the ground level and the Y_2^* axis of the second level.

$$\begin{aligned}\delta_{u,22}(F_2) &= \frac{h^3}{3EJ_v} F_{u,2} = \frac{h^3}{3EJ_v} (F_{x,2} \cos \alpha_2 + F_{y,2} \sin \alpha_2) \\ \delta_{v,22}(F_2) &= \frac{h^3}{3EJ_u} F_{v,2} = \frac{h^3}{3EJ_u} (-F_{x,2} \sin \alpha_2 + F_{y,2} \cos \alpha_2)\end{aligned}\quad (4.17)$$

Thus, the components of the displacement vector δ_2 in the coordinate system XY are defined by means of the coefficients $D_{x,22}$, $D_{y,22}$ and $D_{xy,22}$:

$$\begin{aligned}\delta_{x,22} &= D_{x,22} F_{x,2} + D_{xy,22} F_{y,2} \\ \delta_{y,22} &= D_{xy,22} F_{x,2} + D_{y,22} F_{y,2}\end{aligned}\quad (4.18)$$

where

$$\begin{aligned}D_{x,22} &= \left(\frac{h^3}{3EJ_v} + 2\frac{h^3}{EJ_v}\right) \cos^2 \alpha_1 + \left(\frac{h^3}{3EJ_v}\right) \cos^2 \alpha_2 + \left(\frac{h^3}{3EJ_u} + 2\frac{h^3}{EJ_u}\right) \sin^2 \alpha_1 + \\ &\quad + \left(\frac{h^3}{3EJ_u}\right) \sin^2 \alpha_2 \\ D_{y,22} &= \left(\frac{h^3}{3EJ_v} + 2\frac{h^3}{EJ_v}\right) \sin^2 \alpha_1 + \left(\frac{h^3}{3EJ_v}\right) \sin^2 \alpha_2 + \left(\frac{h^3}{3EJ_u} + 2\frac{h^3}{EJ_u}\right) \cos^2 \alpha_1 + \\ &\quad + \left(\frac{h^3}{3EJ_u}\right) \cos^2 \alpha_2 \\ D_{xy,22} &= \left[\left(\frac{h^3}{3EJ_v} + 2\frac{h^3}{EJ_v}\right) - \left(\frac{h^3}{3EJ_u} + 2\frac{h^3}{EJ_u}\right)\right] \cos \alpha_1 \sin \alpha_1 + \\ &\quad + \left[\left(\frac{h^3}{3EJ_v}\right) - \left(\frac{h^3}{3EJ_u}\right)\right] \cos \alpha_2 \sin \alpha_2\end{aligned}\quad (4.19)$$

As a result, the compliance matrix related to the displacements can be assembled and, by inversion, gives rise to the stiffness matrix, whose coefficients are referred to the coordinate system of the ground level. In this case, the full stiffness matrix is composed by four 2×2 sub-matrices.

Considering N floors, the same matrix is hence composed by four N×N sub-matrices:

$$\mathbf{k}_d^* = \begin{bmatrix} \mathbf{k}_x^* & \mathbf{k}_{xy}^* \\ \mathbf{k}_{xy}^* & \mathbf{k}_y^* \end{bmatrix}\quad (4.20)$$

A general procedure for a N-storey structure assimilated to a three-dimensional shear wall that tapers and twists at the same time along the height can be developed. Therefore, the displacement of the i -th level, in X direction, due to the

loading vector $F_j = \{F_{x,j} \ F_{y,j}\}$ applied to the j -th level, is defined by two contributions $D_{x,ij}$ and $D_{xy,ij}$:

$$D_{x,ij} = \sum_{j=1}^i \sum_{k=1}^j \left\{ \left[\frac{h_k^3}{3EJ_{v,k}} + \frac{(1_j-1_k)h_k^2}{2EJ_{v,k}} + \left(\frac{h_k^2}{2EJ_{v,k}} + \frac{(1_j-1_k)h_k}{EJ_{v,k}} \right) (l_i - l_k) \right] \cos \alpha_k^2 + \right. \\ \left. + \left[\frac{h_k^3}{3EJ_{u,k}} + \frac{(1_j-1_k)h_k^2}{2EJ_{u,k}} + \left(\frac{h_k^2}{2EJ_{u,k}} + \frac{(1_j-1_k)h_k}{EJ_{u,k}} \right) (l_i - l_k) \right] \sin \alpha_k^2 \right\} \\ D_{xy,ij} = \sum_{j=1}^i \sum_{k=1}^j \left\{ \left[\frac{h_k^3}{3EJ_{v,k}} + \frac{(1_j-1_k)h_k^2}{2EJ_{v,k}} + \left(\frac{h_k^2}{2EJ_{v,k}} + \frac{(1_j-1_k)h_k}{EJ_{v,k}} \right) (l_i - l_k) \right] + \right. \\ \left. - \left[\frac{h_k^3}{3EJ_{u,k}} + \frac{(1_j-1_k)h_k^2}{2EJ_{u,k}} + \left(\frac{h_k^2}{2EJ_{u,k}} + \frac{(1_j-1_k)h_k}{EJ_{u,k}} \right) (l_i - l_k) \right] \right\} \cos \alpha_k \sin \alpha_k$$

In the same way, the generic term $D_{y,ij}$ is given by the following expression:

$$D_{y,ij} = \sum_{j=1}^i \sum_{k=1}^j \left\{ \left[\frac{h_k^3}{3EJ_{v,k}} + \frac{(1_j-1_k)h_k^2}{2EJ_{v,k}} + \left(\frac{h_k^2}{2EJ_{v,k}} + \frac{(1_j-1_k)h_k}{EJ_{v,k}} \right) (l_i - l_k) \right] \sin \alpha_k^2 + \right. \\ \left. + \left[\frac{h_k^3}{3EJ_{u,k}} + \frac{(1_j-1_k)h_k^2}{2EJ_{u,k}} + \left(\frac{h_k^2}{2EJ_{u,k}} + \frac{(1_j-1_k)h_k}{EJ_{u,k}} \right) (l_i - l_k) \right] \cos \alpha_k^2 \right\} \quad (4.21)$$

By means of the Eqns (4.21), the computation of the lower triangular part of the $2N \times 2N$ matrix \mathbf{D} of the displacements is executed. Due to the symmetry, the upper triangular part is completed. Once defined, by inversion, the $2N \times 2N$ sub-matrix \mathbf{k}_d^* , according to the Eqn (4.6), the complete $3N \times 3N$ stiffness matrix \mathbf{k}^* is obtained.

In order to evaluate the effectiveness of the Eqns (4.3) and (4.21), two comparisons regarding tapered and twisted beams are performed.

In the first case, a thin-walled hollow section cantilever is analysed through a Finite Element program, in which the structure is modelled by means of thin shell elements. Information concerning the geometrical dimensions and the mechanical properties are shown in Fig. 4.6a, whereas the results in terms of transversal displacements are highlighted in Table 4.1.

In the second case, the transversal displacements of a twisted beam are acquired from the paper by Zupan and Saje [129]. The scheme of the model as well as the geometrical and mechanical properties are indicated in Fig. 4.6b; Table 4.2 reports the comparison of the acquired results.

In both cases, subdividing the beams in 40-50 sub-elements, Eqns (4.3) and (4.21) lead to solutions with an adequate degree of accuracy. Besides, such

segmentation proves to be plausible in high-rise buildings, being the number of floors equal or, at most, greater.

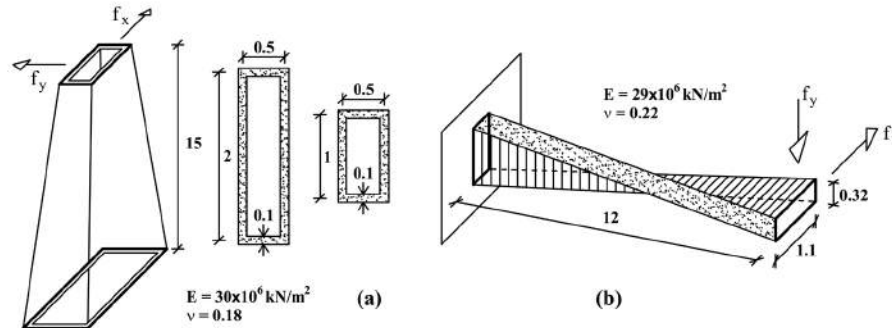


Figure 4.6 – Tapered hollow (a) and twisted double symmetrical (b) section cantilever.

Table 4.1 – Free end displacement of a tapered cantilever.

N. of levels	Centroidal force $f_x = 10$ kN		Centroidal force $f_y = 10$ kN	
	x disp. [m]	Err. [%]	y disp. [m]	Err. [%]
5	2.840E-03	1.626E+01	1.662E-02	5.090E+00
10	2.572E-03	5.302E+00	1.614E-02	2.097E+00
20	2.482E-03	1.611E+00	1.597E-02	1.015E+00
30	2.457E-03	5.628E-01	1.592E-02	7.009E-01
40	2.444E-03	6.836E-02	1.590E-02	5.520E-01
FEM	2.443E-03		1.581E-02	
Error [%] = (Present model - FEM)/FEM $\times 100$				

Table 4.2 – Free end displacement of a twisted cantilever.

N. of levels	Unitary force f_x				Unitary force f_y			
	x disp. [m]	Err. [%]	y disp. [m]	Err. [%]	x disp. [m]	Err. [%]	y disp. [m]	Err. [%]
10	5.5001E-03	1.43E+00	1.4805E-03	-1.39E+01	1.4805E-03	-1.39E+01	1.6720E-03	-4.06E+00
50	5.4426E-03	3.72E-01	1.6730E-03	-2.66E+00	1.6730E-03	-2.66E+00	1.7295E-03	-7.62E-01
100	5.4344E-03	2.20E-01	1.6960E-03	-1.32E+00	1.6960E-03	-1.32E+00	1.7377E-03	-2.89E-01
150	5.4316E-03	1.68E-01	1.7036E-03	-8.82E-01	1.7036E-03	-8.82E-01	1.7405E-03	-1.28E-01
200	5.4302E-03	1.42E-01	1.7074E-03	-6.61E-01	1.7074E-03	-6.60E-01	1.7419E-03	-4.75E-02
Zupan et al.	5.4224E-03		1.7187E-03		1.7187E-03		1.7427E-03	
Error [%] = (Present model - Zupan et al.)/(Zupan et al.) $\times 100$								

4.2.2 Tapered Bracings (Warping Prevalent)

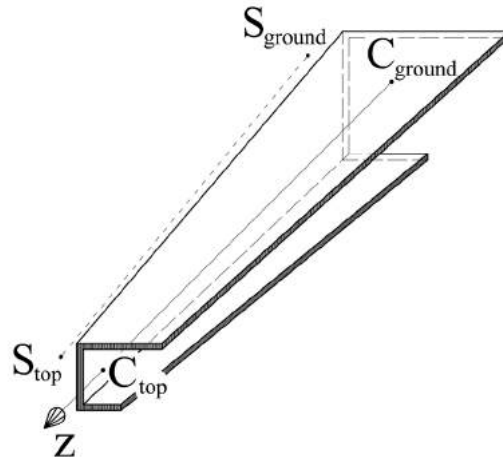


Figure 4.7 – Thin-walled open section bracing, which tapers with respect to the centroidal axis.

A numerical procedure for the definition of the stiffness matrix of tapered thin-walled open section bracings in their local coordinate system is now derived. For these structures, the process of tapering refers to a vertical axis passing through the barycentre of the section. Since the centroid and the shear centre do not coincide, the location of the latter varies section by section (Fig. 4.7).

As in the previous cases, the expression of the stiffness matrix \mathbf{k}^* is obtained by the inversion of the $3N \times 3N$ compliance matrix \mathbf{D} .

For this purpose, the computation of the coefficients of the above matrix is executed by means of the Principle of Virtual Work, in which the contribution of the bimoment action is considered:

$$1^{(f)} \cdot \eta^{(r)} = \int_z \left(M^{(f)} \frac{M^{(r)}}{EI} + B^{(f)} \frac{B^{(r)}}{EI_\omega} \right) dz \quad (4.22)$$

where the apex f stands for the fictional system of internal forces and r for the real system of displacements.

The proposed method is based on the assumptions that the shear effects on very slender structures are negligible and the bimoment action is evaluated supposing the torsional rigidity GJ_t equal to zero.

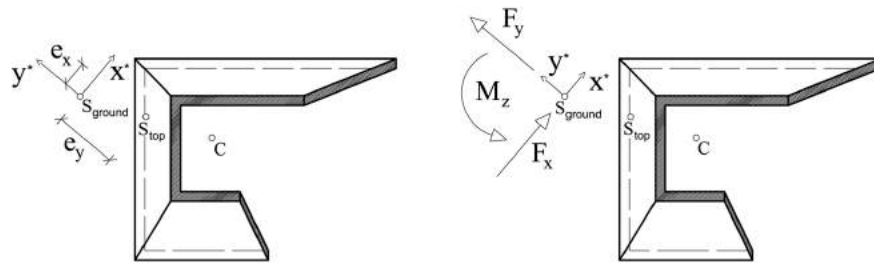


Figure 4.8 – Local coordinate system for a tapered thin-walled open section bracing.

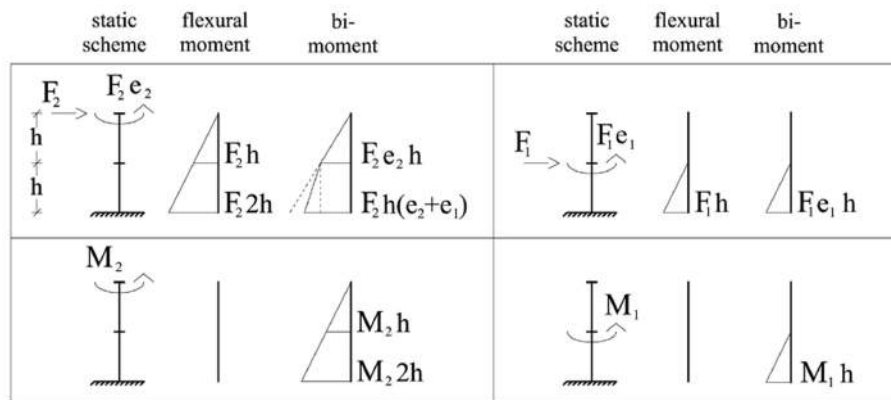


Figure 4.9 – Main diagrams for the computation of the compliance matrix of a 2-storey bracing.

By means of the Eqn (4.22), further coefficients arise, so that **D** becomes a full matrix. This means that the torsional behaviour is connected to the flexural one, as well as the forces acting along a principal direction give rise also to displacements in the other direction. This behaviour is due to the variation of location of the shear centre along the longitudinal axis, which consequently affects the definition of the resultant actions on the generic level.

For the analysis, we suppose to apply the local coordinate system to the shear centre of the ground level. The actions, applied to the generic floor according to this coordinate system, show an eccentricity compared to the shear centre of the same level. This scheme involves further torsional actions on the generic section, which have to be taken into account in the study (Fig. 4.8). In this way, each local

force, at the same time, causes displacements in its principal direction, according to the flexural behaviour, rotations, due to the additional torsional component, and displacements in the other principal direction, derived from the contribution of the bimoment action.

For the case of a 2-storey shear wall, the diagrams of flexural moment and bimoment which are taken into account as the contribution of the real system of displacements in Eqn (4.22) are reported in Fig. 4.9. The same diagrams, in which the generic action is substituted by a unitary load, allow to identify the contribution of the fictional system of forces. Thus, after performing the calculations, the generic expression for the compliance matrix is

$$\mathbf{D} = \begin{bmatrix} \mathbf{D}_x & \mathbf{D}_{xy} & \mathbf{D}_{x\theta} \\ \mathbf{D}_{xy}^T & \mathbf{D}_y & \mathbf{D}_{y\theta} \\ \mathbf{D}_{x\theta}^T & \mathbf{D}_{y\theta}^T & \mathbf{D}_\theta \end{bmatrix} \quad (4.23)$$

in which only \mathbf{D}_x , \mathbf{D}_y and \mathbf{D}_θ are symmetrical sub-matrices. In addition, it should be noted that the sub-matrices belonging to the lower triangular part of \mathbf{D} are related to those of the upper part by means of the transpose operation.

Once obtained the stiffness matrix by the inversion of (4.23), the last step focuses on the addition of the component related to the torsional rigidity GJ_t , previously neglected. It can be easily computed through the Eqn (4.4), which defines the corresponding compliance matrix. Then it is inverted and added to the $N \times N$ sub-matrix related to the rotations. In this way the expression of the matrix \mathbf{k}^* for tapered thin-walled open section bracings is completed.

Table 4.3 – Geometrical and mechanical properties of the U-shaped profile.

L [cm]	E [kg/cm ²]	G [kg/cm ²]	I ₀ [m ⁶]	J _t [m ⁴]	M _z [kgcm]
40	2100000	805000	314 (min) 11059.2 (max)	5.48 (min) 11.14 (max)	300

In order to evaluate the capabilities of the method, the practical example computed by Eisenberger [47] for the analysis of tapered thin-walled open section profiles is performed.

In Fig. 4.10 the scheme of the beam as well as the dimensions of the extreme sections are reported. The geometrical and mechanical properties are indicated in Table 4.3.

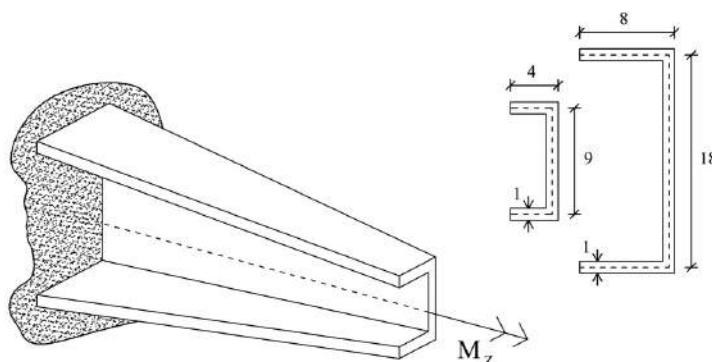


Figure 4.10 – Tapered open section cantilever subjected to torque [47].

Table 4.4 – Free end rotation [rad] of a tapered thin-walled open section cantilever.

N. of levels	Present model	Err. [%]	N. of equations	Analytical solution	Err. [%]
10	5.081E-04	1.83E+01	10	5.073E-04	1.82E+01
30	4.671E-04	8.79E+00	30	4.670E-04	8.78E+00
50	4.604E-04	7.24E+00	50	4.604E-04	7.24E+00
100	4.557E-04	6.14E+00	100	4.557E-04	6.14E+00
150	4.542E-04	5.79E+00	150	4.542E-04	5.79E+00
200	4.534E-04	5.62E+00	200	4.534E-04	5.61E+00
Eisenberger	4.293E-04		FEM	4.296E-04	
Error [%] = (Computed - Eisenberger)/Eisenberger × 100					

The loading case considered by the author was very simple, being defined by a torque applied to the free end of the cantilever beam. The comparison of the results in terms of rotation of the free end of the cantilever are highlighted in Table 4.4. In particular, in addition to the solutions acquired through the present method, the table includes the results obtained subdividing the beam in sub-elements of equal length, each having constant geometrical properties. In this case, for each element, the equation of torsional equilibrium related to thin-walled open section beams [119] is solved analytically, employing the following boundary conditions: rotation and its derivative equal to zero at the clamped end; bimoment action equal to zero at the free end; continuity conditions for the rotation, its derivative and the bimoment action at the intermediate sections. As it can be seen observing the table

of results, the degree of accuracy of the proposed approach is good, if the procedure is applied to the case of high-rise buildings, being the per cent error lower than 7%.

4.3 Numerical Examples

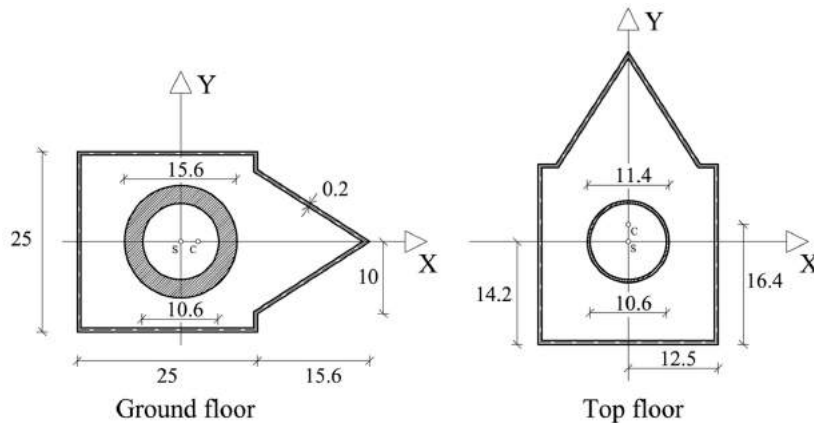


Figure 4.11 – Presumed floor plan of the HSB Turning Torso (dimensions in metres).

The developed numerical procedures can be easily adapted to the analytical method proposed in Chapter 2 which allows to analyse the load distribution of external actions in tall buildings, stiffened by different types of vertical bracings.

In order to highlight the adaptability of the Eqns (4.21) and (4.22), two numerical examples which take into account high-rise buildings stiffened by twisted or tapered bracings are performed. Both of them are theoretical since any structural details have not been provided by the project managers.

The first model concerns the 54-storey HSB Turning Torso, design by Calatrava in Malmo (Sweden). It is a twisted skyscraper reaching 190 m of height with a rotation from the base to the top of 90 degrees (Fig. 4.2a).

It is assumed that the lateral stiffening relies on two concentric bracings: the innermost element exhibits a circular hollow section which tapers upwards by reducing its thickness from 2.5 to 0.4 m; the outermost has a mono symmetrical section which twists anticlockwise around its shear centre. Since the latter does not coincide with the barycentre, further torsional actions are expected in the computation.

Table 4.5 – Cross-section properties of the bracings constituting the HSB Turning Torso.

	Circular hollow section		Mono symmetrical section
Second moment J_{xx} [m ⁴]	2229.89 (B)	209.35 (T)	2070.00 (B)
Second moment J_{yy} [m ⁴]	2229.89 (B)	209.35 (T)	4007.09 (B)
Torsional rigidity J_t [m ⁴]	4459.79 (B)	418.70 (T)	3940.03
Global coordinate x_s of the shear centre [m]	0.00		0.00
Global coordinate y_s of the shear centre [m]	0.00		0.00
Angle φ [°] *	0.00		0.00

(B) At the base of the building. (T) At the top of the building.

* Rotation of the local coordinate system with respect to the global coordinate one.

It is assumed that both the cantilevers are made of concrete, whose Young's modulus is 4.5×10^4 and 2.5×10^4 MPa for the circular and mono symmetrical section respectively, whereas Poisson's ratio is 0.18 for both. The influence of creep and shrinkage is not taken into account in the analysis. The member cross-section properties are given in Fig. 4.11 and Table 4.5.

Concerning the load, only wind actions are considered according to the formulas indicated by the Italian Technical Regulations [82], which follow the same method contained in Eurocode 1 [48]. Therefore, the wind action can be reduced to a system of concentrated static loads, applied to the barycentre of the pressure distribution. The size, shape and dynamic properties of the building as well as the region and the altitude of the location affect the computation of the intensity of the action. For the sake of simplicity, none of the mentioned properties has been considered. Therefore, a wind pressure equal to 390.62 N/m^2 has been adopted. The resultant system of forces acting along the principal directions is reported in Fig. 4.12.

The results of the analysis are presented in Fig. 4.13 and 4.14. As regards Fig. 4.13a and 4.13b, the displacements along the principal directions of the coordinate system are reported, whereas Fig. 4.13c shows the rotations at the floor levels.

Similarly, in Fig. 4.14 the load distribution of the external actions between the stiffeners highlights the resistant contribution of the twisted element compared to the tapered one. In particular, the former plays a predominant role in the top part of the building, whereas, in the bottom part, the latter constitutes the main horizontal stiffening.

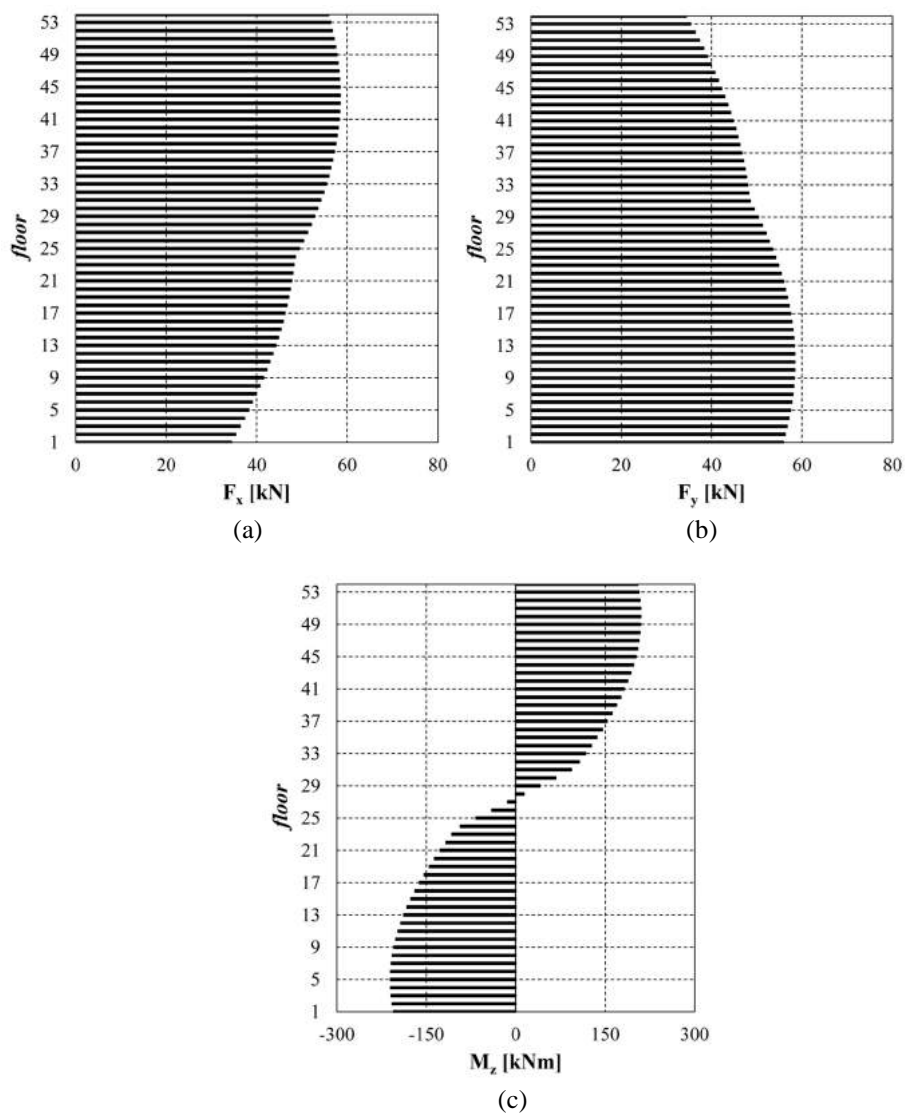


Figure 4.12 – Wind actions applied to the floors: shear forces along the X (a) and Y (b) direction and torque (c).

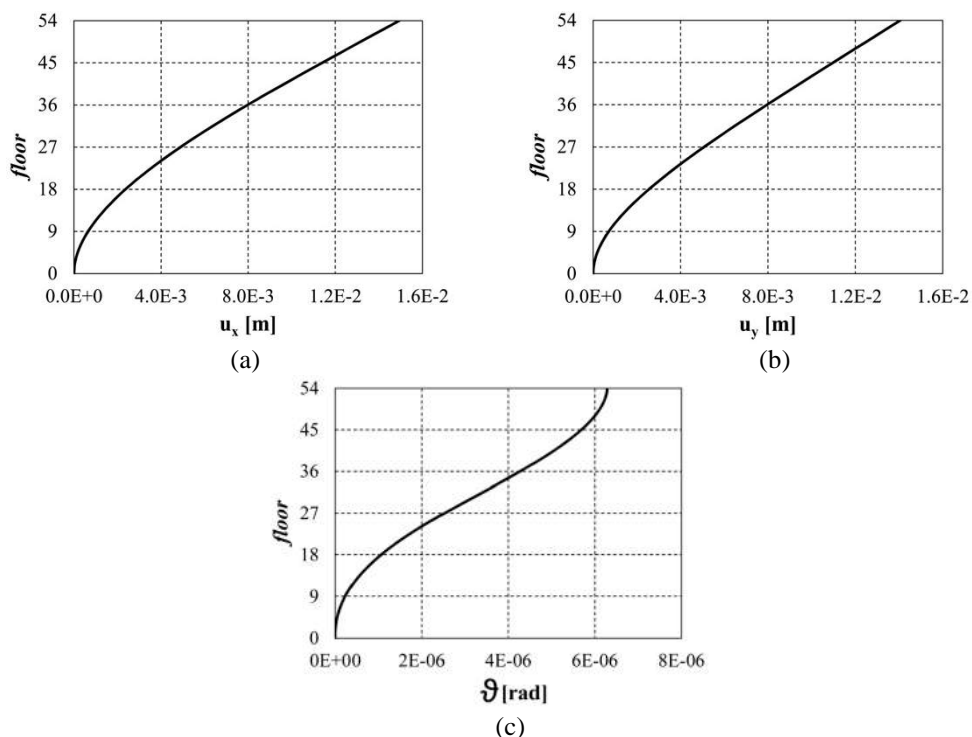


Figure 4.13 – Displacements of the floors in the global coordinate system: translation in X (a) and Y (b) direction and rotation (c).

It should be noted a discontinuity next to the constraint due to the different law of variation which characterises the bracings. Such difference leads to an exchange of high interaction forces in the bottom part of the building, which modifies the trend of the shear.

The second numerical example is focused on the analysis of a conical structure conceived by Norman Foster in 1989 for the city of Tokyo (Japan). The Millennium Tower is an high-rise building composed by 170 storeys, which correspond to a total height of 840 metres (Fig. 4.15).

The present model is imaginary, because only a preliminary design has been performed until now. Therefore no details on the floor layout or on the horizontal stiffening has been found. Consequently the following structural choices as well as geometrical properties can represent a valid proposal for its practical construction.

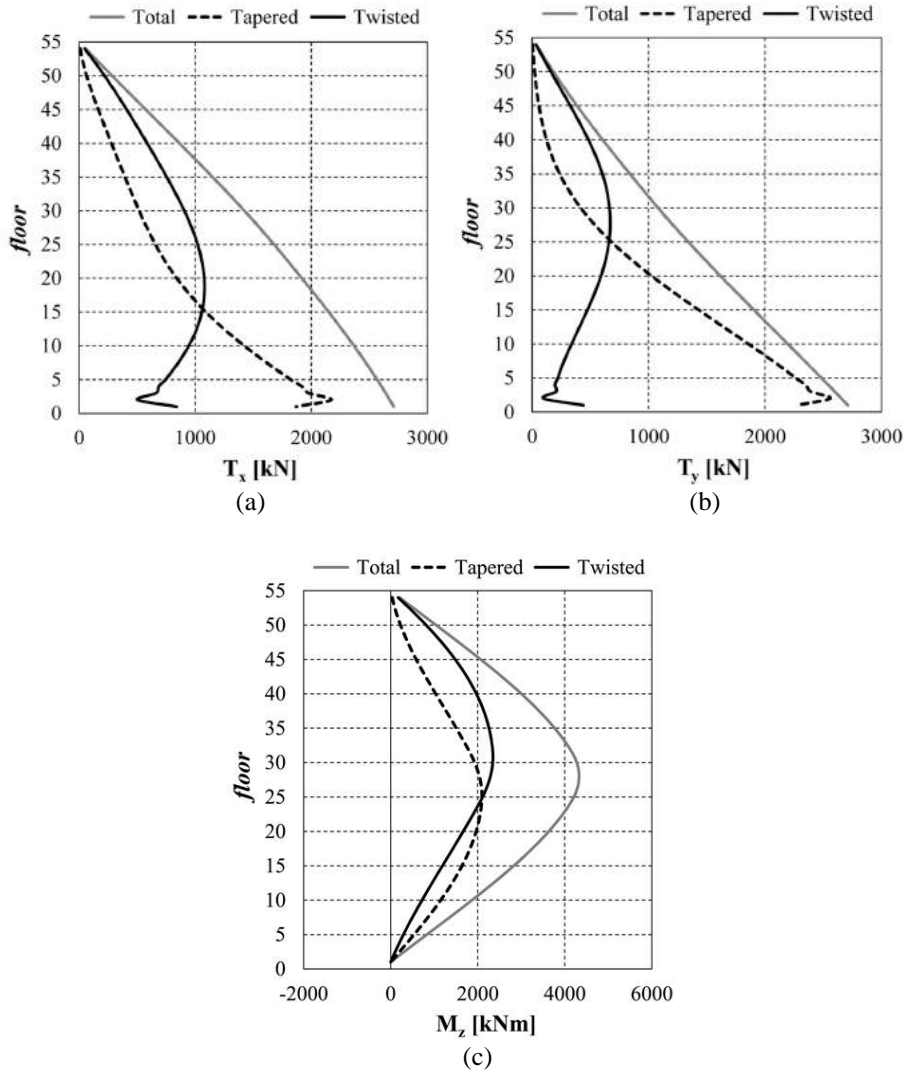


Figure 4.14 – Loading distribution between the tapered and twisted element: shear in X (a) and Y (b) direction and torsional moment (c).

The proposed horizontal stiffening is composed by seven thin-walled open section shear walls which taper upwards, until the 170th floor (Fig. 4.16).



Figure 4.15 – Millennium Tower by Sir Norman Foster (www.fosterandpartners.com).

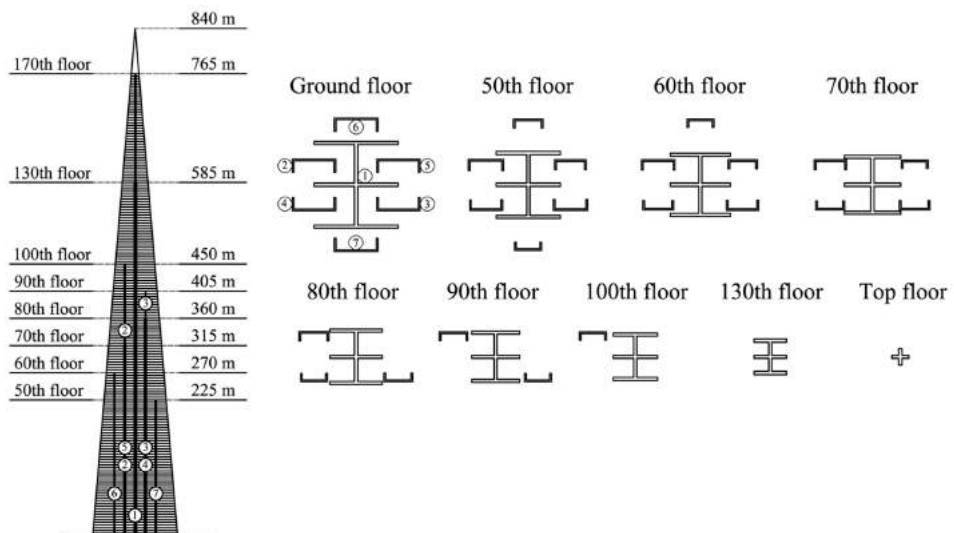


Figure 4.16 – Hypothetical scheme of the horizontal stiffening for the Millennium Tower: the structural members taper upwards, each having its own tapering law, and reach different heights.

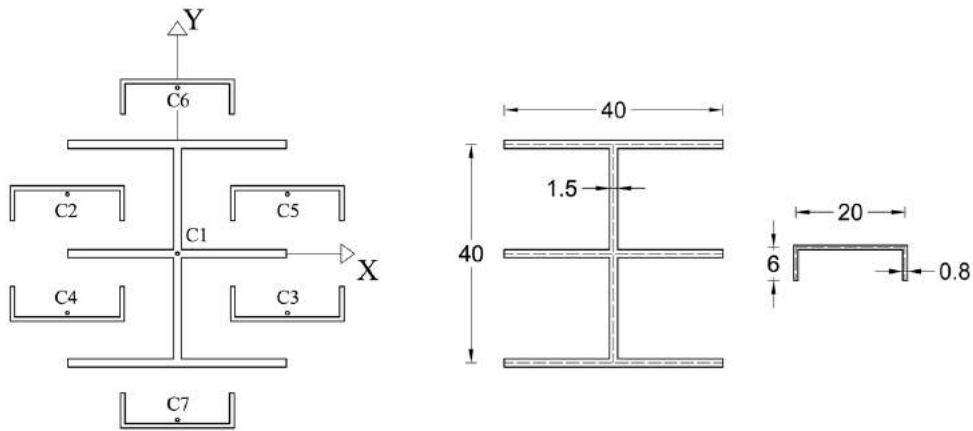


Figure 4.17 – Hypothetical scheme of the horizontal stiffening for the Millennium Tower: global coordinate system XY (a) and geometrical dimensions of the cross-sections at the ground floor (in metres) (b).

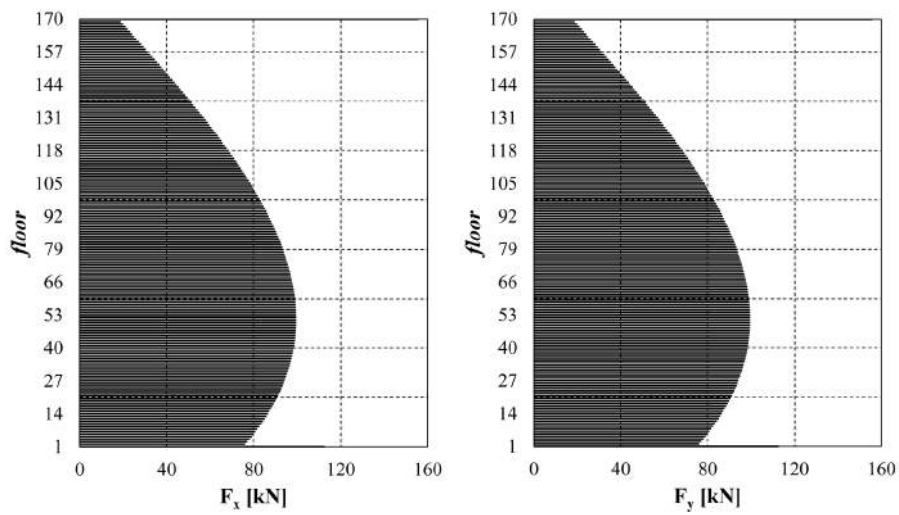


Figure 4.18 – External load condition for the Millennium Tower: shear actions in X and Y direction.

Table 4.6 – Cross-section properties of the thin-walled open section bracings related to the Millennium Tower.

Open section shear wall N.	1		2, ..., 5		6, 7	
	Ground floor	Top floor	Ground floor	Top level	Ground floor	Top level
Second moment J_{xx} [m^4]	55605.64	66.29	82.30	18.06	82.30	18.06
Second moment J_{yy} [m^4]	23830.99	66.29	1484.39	325.80	1484.39	325.80
Warping constant J_{ω} [m^6]	6325059.37	-	5906.30	471.68	5906.30	471.68
Torsional rigidity J_t [m^4]	179.58	18.21	5.45	3.29	5.45	3.29
Global coordinate x_c of the barycentre [m]	0.00	0.00	-20.15 (2)	-20.15 (2)	0.00	0.00
Global coordinate y_c of the barycentre [m]	0.00	0.00	10.88 (2)	10.88 (2)	30.38 (6)	30.38 (6)
Angle φ [$^\circ$] *	0.00	0.00	0.00	0.00	0.00	0.00

(2) Open section shear wall N. 2; (6) Open section shear wall N. 6.

* Rotation of the local coordinate system with respect to the global coordinate one.

In particular, the inner section reaches the top level with a dimensional reduction of 80 per cent, whereas the others, defined by different heights corresponding to the 50th, 60th, 70th, 80th, 90th and 100th floor, show a reduction of 40 per cent. Nevertheless, in all cases the thickness of the walls remains constant.

Further details characterise the model: for the case of ‘C’-shaped bracings, the same top section has been considered; for the inner bracing, between the 130th and 170th floor, the initial section has been reduced to a cross-shaped one.

The levels, which correspond to a structural discontinuity, are shown in Fig. 4.16; the geometrical dimensions of the cross-sections are reported in Table 4.6 and Fig. 4.17. In this case, the material properties are described by Young’s modulus equal to 5.0×10^4 MPa for the ‘C’-shaped bracings and 7.0×10^4 MPa for the inner element; Poisson’s ratio for the entire structural skeleton is 0.18. The creep and shrinkage effects are excluded from the analysis. The same load condition is taken into account for this numerical example, with a wind pressure of 390.62 N/m^2 applied to the lateral surface of the building. The resultant system of concentrated horizontal loads, acting along the principal directions of the global coordinate system, is shown in Fig. 4.18. The results concerning the displacements along the principal directions of the global coordinate system are highlighted in Fig. 4.19, whereas Fig. 4.20 reports the load distribution between the main horizontal members.

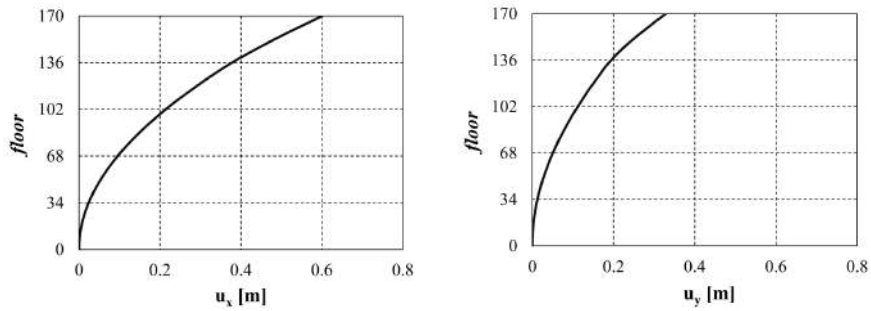


Figure 4.19 – Displacements of the Millennium Tower in X and Y direction.

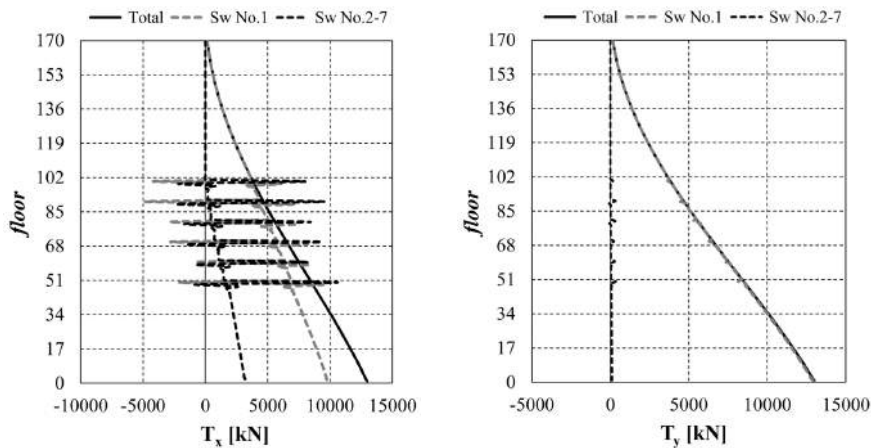


Figure 4.20 – Loading distribution between the inner (Sw N.1) and the ‘C’-shaped bracings (Sw N.2-7): shear trend in X and Y direction.

A clear difference between the two principal directions is observed with respect to the shear distribution: on the one hand, the flexural stiffness of the inner section along the Y axis is so large that the contribution of the ‘C’-shaped bracings is almost negligible; on the other hand, with regard to the X axis, remarkable discontinuities are evident due to the different heights of the ‘C’-shaped elements. In effect, along this direction, since the latter exhibit a flexural stiffness quite comparable to that of the inner member, high interaction forces arise allowing the ‘C’-shaped sections to absorb, in the bottom part of the building, about 25 per cent of the total shear.

These findings may suggest to the designer the possibility of considering further structural arrangements or different solutions, such as outrigger systems or tubular elements, in order to avoid to concentrate most of the load on a single huge bracing.

In summary, the previous figures demonstrate the capabilities of the analytical method in the evaluation of the gross displacements as well as in the detection of the distribution of the external forces between the main horizontal bracings which concur to stiffen high-rise buildings.

The method can be used to find out the optimal configuration of the structural members, which allow to achieve the best performance in presence of static wind loads. As a matter of fact, the choice of different heights with respect to the ‘C’-shaped elements has been driven by the need of reducing the displacements, without compromising the living space of the floors.

Thus, analytical methods prove to be adequate in the early stage of the conceptual design of so complex constructions. With the qualities of a quick data preparation and a more transparent evaluation of the results, they can play a prime role in support of the designer’s judgment.

Chapter 5

Dynamic Analysis: Evaluation of Free Vibrations and Mode Shapes

5.1 Introduction

Tall buildings differ from short buildings in terms of the actions which are predominant for the global resistance of the construction. In the case of short buildings, the geometrical dimensions of the structural components are determined evaluating the intensity of the vertical actions; on the contrary, the higher the building, the more sensitive it becomes to lateral actions coming from wind and earthquakes [111].

As described in Chapter 1, when the total height exceeds 30-40 storeys, tubular systems are usually employed, but, within 70 storeys, core wall structures are also designed to participate to the horizontal resistance, since they provide the adequate lateral stiffness with a relatively low amount of construction material. Such elements are present in tall buildings in the form of stairwells or shafts or in addition to other shear wall systems, as a service ducts. The corresponding geometrical dimensions as well as the location in the floor plan are designed, at the same time, to absorb part of the vertical actions and transfer the horizontal actions from the superstructure to the foundation.

Usually these resistant systems are constituted by thin-walled open section bracings, isolated in different position of the floor plan or connected together, with

rigid lintel beams, to realise a single element more resistant than the sum of its single components.

In the design process, particular attention is focused on the determination of the principal axes of the resistant skeleton. In effect, if the central axes of the whole building coincides with the ones related to the resistant skeleton, lateral loads can be assumed to act through these axes and the building is supposed to behave as a cantilever structure, exclusively subjected to flexure along its principal directions and torsion. On the contrary, when the axes of the building do not coincide with those of the horizontal resistant system, combined bending and torsion occur. Indeed, this is the effect that arises in presence of asymmetrical core wall structure if its shear centre is far from the centroid of the building floor. In these circumstances, the response of the building to lateral actions becomes torsionally coupled and three-dimensional analyses are needed.

Even if, nowadays, most of the structural investigations are conducted by means of Finite Element (FE) methods, with the aim of obtaining a preliminary assessment of the dynamic behaviour of such structures, simplified analytical procedures can represent a valid tool for the evaluation of the main parameters which govern the dynamic response of the building.

In addition, being based on some chosen hypotheses, they guarantee reduced times of modelling and analysis as well as a good accuracy of the results, if compared to the ones obtained using FE programs.

The investigation can be directed considering two different configurations: the dynamic analysis of a single core wall, which depends on its own mass, or the total resistant skeleton of the building, where the contribution of mass is just due to the presence of the floors. In both cases, the coupling between flexural and torsional behaviour must be taken into account. In the first case, in effect, the centre of mass, which coincides - by definition - with the centroid of the section, is far from the shear centre and, therefore, since the resultant inertial forces are eccentric with respect to the shear centre, torsional actions are combined with flexural ones. In the second case, thin-walled open section bracings are coupled with other structural reinforcements to constitute a single resistant skeleton.

The mass considered in the dynamic analysis is concentrated in the building floors, whereas the one related to the vertical bracings is assumed negligible.

For the examination of these two configurations simplified procedures are reported below. The unknown variables are expressed in terms of transversal displacements of the section, in the case of a single core wall, or related to the building floors, in the case of a system of vertical bracings.

5.2 Coupling and Uncoupling Behaviour

From the analytical point of view, the evaluation of the dynamic response of thin-walled open section profiles caught the attention of many researchers of the last century. In the early 1970s, Timoshenko [115] synthetically resumed the last findings about the coupled flexural and torsional vibrations of beams defined by sections in which the centroid did not coincide with the shear centre. He reported the exact analytical solution in the case of simply supported beams, highlighting that, in the case of different end conditions, the solution of the differential equations became more complicated and, therefore, it was necessary to refer to approximate values by using energy methods. This was confirmed by Garland [49], who analysed in 1940 the case of a cantilever beam exploiting the Rayleigh-Ritz method. In his paper he reported a diagram showing the variation of the natural frequencies of the beam with respect to some geometrical properties of the section. Nevertheless, he himself recognised that the analytical solutions indicated in the paper were approximate and did not allow to obtain the frequencies for modes of high order, whereas the ones related to the modes of lower order exhibited a reduced accuracy.

The drawback could be overtaken if additional terms in the expressions of the displacement unknowns were considered. But this meant an extra labour of computation, that was implausible for that time.

In the same direction, the papers by Gere [51, 52] extended the analysis to consider thin-walled profiles without any symmetry, with various end conditions. In this case, in the equilibrium equations the warping rigidity was inserted. Design curves were again proposed for each end condition analysed.

Further simplified approaches based on Vlasov's theory and Wagner-Kappus's theory were proposed by Bishop *et al.* [10, 11]. The first attempts for the exact determination of coupled bending and torsion vibration characteristics were conducted by Dokumaci [44], who undoubtedly filled a significant gap in understanding of the structural dynamics of thin-walled open section profiles.

The method, later extended by Bishop [12] taking into account also the warping of the section, was focused on the analysis of the typology of the roots of the characteristic equation, to which the problem could be reduced. Once defined the typology of the roots, the displacement unknowns could be represented by real functions with which any end condition could be associated.

Later, Yaman [126] extended this formulation to analyse the forced vibrations of these beams through the application of the wave propagation approach.

Approaches based on FE methods dealt with the shape functions which included the effect of cross-sectional warping: Zhang [128], Chen [29] and Hu *et al.* [62] derived mass and stiffness matrices, considering also the contribution of the rotary inertia.

The effects caused by the shear flexibility, neglected in Vlasov's theory, the rotatory inertia as well as the presence of variable cross-sectional properties were examined in depth by Ambrosini *et al.* [3] by means of the state variable approach. This method was later employed for the dynamic analysis of a thin-walled reinforced concrete core, designed to resist to lateral loads [4].

Finally, Tanaka and Bercin [109] resumed the exact formulation proposed by Dokumaci and Bishop and devised, using the computer algebra system Mathematica, a compact program able to implement and solve the governing differential equations describing the coupled bending and torsional vibrations of uniform beams having no cross sectional symmetry.

In order to highlight the clearness and the effectiveness of the analytical method proposed by Dokumaci, a brief summary of the main passages is reported below. Furthermore, some practical examples are proposed to evaluate the correctness of the results obtained by a compact program, which implements the aforementioned analytical procedure and to verify the degree of accuracy through the comparison of the results with a FE program.

5.2.1 Analytical Procedure

In Fig. 5.1 typical thin-walled open sections, defined by double, single and no symmetry, are shown. In the last two cases, due to their geometrical properties, the centroid G and the shear centre C do not coincide and, therefore, the corresponding relative distance, in the dynamic phase, causes coupling between bending and torsion. When bending vibrations in two perpendicular directions are coupled with the torsional ones, that is in presence of no symmetry, we refer to the case of triple coupling; on the contrary, if the section shows an axis of symmetry, the bending in this direction remains independent from the other vibrations, which are coupled instead. This is the case of double coupling. Finally, in the case of a doubly symmetrical section, each vibration is independent from the others and, thereby, the corresponding differential equations can be treated separately.

Considering a section free from axis of symmetry (Fig. 5.2), as described in Chapter 3, opportune choices of the coordinate systems can conduct to the following system of equilibrium equations for a beam subjected to distributed transversal actions:

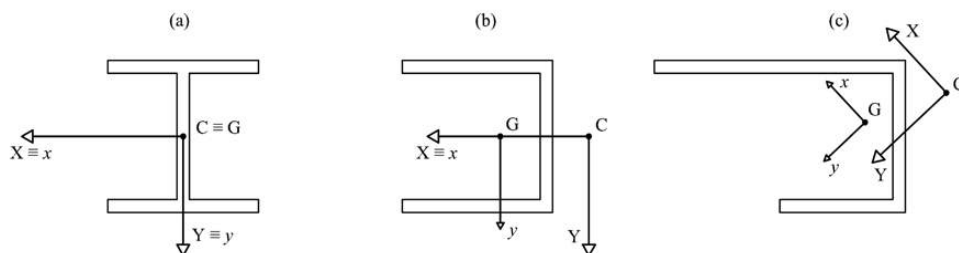


Figure 5.1 – Thin-walled open sections: double symmetry (a), single symmetry (b), no symmetry (c).

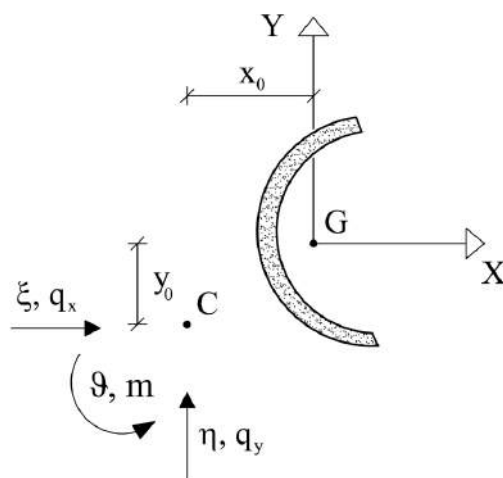


Figure 5.2 – Thin-walled open section beam subjected to distributed transversal actions.

$$\begin{aligned}
 EI_y \xi^{IV} &= q_x \\
 EI_x \eta^{IV} &= q_y \\
 EI_\omega \vartheta^{IV} - GJ_t \vartheta'' &= m
 \end{aligned}
 \tag{5.1}$$

Let's suppose that the beam, free from external actions, begins to vibrate. Due to its own mass, some inertial forces arise and oppose the transversal movements of the sections (Fig. 5.3).

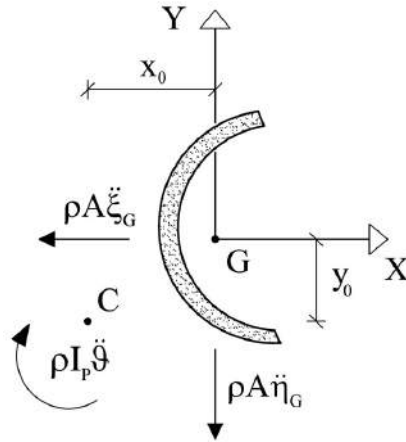


Figure 5.3 – Inertial forces arising as a consequence of the vibration of the beam.

Defining the displacements of the centroid in terms of those related to the shear centre and differentiating twice with respect to the time t , the accelerations of the sections are computed:

$$\begin{aligned} \xi_G &= \xi - y_0\vartheta \\ \eta_G &= \eta + x_0\vartheta \end{aligned} \quad (5.2)$$

$$\begin{aligned} \ddot{\xi}_G &= \frac{d^2}{dt^2}(\xi - y_0\vartheta) \\ \ddot{\eta}_G &= \frac{d^2}{dt^2}(\eta + x_0\vartheta) \end{aligned} \quad (5.3)$$

The inertial forces in X and Y direction can be obtained exploiting the expressions of the accelerations of the centroid and considering the area A and the mass density ρ [kg/m^3]:

$$f_x = -\rho A \frac{d^2}{dt^2}(\xi - y_0\vartheta) \quad (5.4)$$

$$f_y = -\rho A \frac{d^2}{dt^2}(\eta + x_0\vartheta) \quad (5.5)$$

The whole rotational inertial force is expressed taking into account the polar moment of inertia I_p about the barycentre and the eccentricities of the force f_x and f_y with respect to the shear centre:

$$f_z = -\rho I_P \frac{d^2}{dt^2}(\vartheta) + \left[\rho A \frac{d^2}{dt^2}(\xi - y_0 \vartheta) \right] y_0 - \left[\rho A \frac{d^2}{dt^2}(\eta + x_0 \vartheta) \right] x_0 \quad (5.6)$$

Due to D'Alembert's Principle, the inertial forces can be considered as static forces and, therefore, they can be added to the expressions (5.1):

$$\begin{aligned} EI_y \xi^{IV} + \rho A \frac{d^2}{dt^2}(\xi - y_0 \vartheta) &= 0 \\ EI_x \eta^{IV} + \rho A \frac{d^2}{dt^2}(\eta + x_0 \vartheta) &= 0 \\ EI_\omega \vartheta^{IV} - GJ_t \vartheta'' + \rho I_0 \frac{d^2}{dt^2}(\vartheta) - \rho A y_0 \frac{d^2}{dt^2}(\xi) + \rho A x_0 \frac{d^2}{dt^2}(\eta) &= 0 \end{aligned} \quad (5.7)$$

where I_0 is the polar moment of inertia about the shear centre.

As it can be seen, the equilibrium equations are coupled each other due to the presence of the eccentricities x_0 and y_0 . If the section is defined by an horizontal axis of symmetry, the term y_0 is null and the first equation becomes independent. In the same way, if the section is doubly symmetrical, both the eccentricities are null and the vibrations develop separately.

A hypothesis of solution of the system (5.7) requires to write the displacement unknowns ξ , η , ϑ as a product of a function of the spatial coordinate z and a function of the temporal one t : the former represents the deformation shape of the beam, whereas the latter the angular frequency of its free vibration.

$$\begin{aligned} \xi &= Z(z)T(t) \\ \eta &= H(z)T(t) \\ \vartheta &= \Theta(z)T(t) \end{aligned} \quad (5.8)$$

Replacing the previous expressions in the system (5.7), it is possible to adopt the method of separation of the variables. Therefore, an identity between the variables dependent on t and those dependent on z is acquired. Since the values of t and z are arbitrary, the identity is always made possible if and only if both the members are equal to a constant, here represented by the term $(-p_n^2)$.

$$\begin{aligned} \frac{EI_y Z^{IV}}{\rho A(-Z+y_0\Theta)} &= \frac{\ddot{T}}{T} = -p_n^2 \\ \frac{EI_x H^{IV}}{\rho A(H+x_0\Theta)} &= \frac{\ddot{T}}{T} = -p_n^2 \\ \frac{EI_\omega \Theta^{IV} - GJ_t \Theta''}{\rho(-I_0\Theta + Ay_0Z - Ax_0H)} &= \frac{\ddot{T}}{T} = -p_n^2 \end{aligned} \quad (5.9)$$

From the system (5.9) a differential equation related to the variable t is obtained, whose solution is well-known and depends on the initial conditions of the problem:

$$\ddot{T} + p_n^2 T = 0 \quad (5.10)$$

$$T_n(t) = A_n \cos(p_n t) + B_n \sin(p_n t) \quad (5.11)$$

where the argument p_n of the trigonometric functions represents the angular frequency of the free vibration of the beam.

If we refer to the equations related to the variable z , the system (5.7) becomes:

$$\begin{aligned} EI_y Z^{IV} + \rho A p_n^2 (-Z + y_0 \Theta) &= 0 \\ EI_x H^{IV} + \rho A p_n^2 (H + x_0 \Theta) &= 0 \\ EI_\omega \Theta^{IV} - GJ_t \Theta'' - \rho I_0 p_n^2 \Theta + \rho A p_n^2 (y_0 Z - x_0 H) &= 0 \end{aligned} \quad (5.12)$$

Exploiting the following expressions, the system (5.12) can be re-written in a synthetic form.

$$\begin{aligned} D &= d/dz & \lambda_\omega &= \frac{GJ_t}{EI_\omega} & \lambda_0 &= \frac{\rho I_0 p_n^2}{EI_\omega} \\ \alpha_y &= \frac{\rho A p_n^2}{EI_y} & \alpha_x &= \frac{\rho A p_n^2}{EI_x} & \alpha_\omega &= \frac{\rho A x_0 p_n^2}{EI_\omega} \\ \beta_y &= \frac{\rho A y_0 p_n^2}{EI_y} & \beta_x &= \frac{\rho A x_0 p_n^2}{EI_x} & \beta_\omega &= \frac{\rho A y_0 p_n^2}{EI_\omega} \\ (D^4 - \alpha_y)Z + \beta_y \Theta &= 0 \\ (D^4 - \alpha_x)H - \beta_x \Theta &= 0 \\ (D^4 - \lambda_\omega D^2 - \lambda_0)\Theta + \beta_\omega Z - \alpha_\omega H &= 0 \end{aligned} \quad (5.13)$$

Setting the determinant of the above system equal to zero conducts to an ordinary differential equation of 12th order for each spatial function Z , H or Θ , which is given by:

$$\det \begin{bmatrix} D^4 - \alpha_y & 0 & \beta_y \\ 0 & D^4 - \alpha_x & -\beta_x \\ \beta_\omega & -\alpha_\omega & D^4 - \lambda_\omega D^2 - \lambda_0 \end{bmatrix} = 0$$

$$(D^{12} + a_1 D^{10} + a_2 D^8 + a_3 D^6 + a_4 D^4 + a_5 D^2 + a_6)F = 0 \quad (5.14)$$

in which:

$$\begin{aligned}
 a_1 &= -\lambda_\omega & a_2 &= -\lambda_0 - \alpha_x - \alpha_y \\
 a_3 &= \lambda_\omega(\alpha_x + \alpha_y) & a_4 &= -\beta_y\beta_\omega + \lambda_0(\alpha_x + \alpha_y) + \alpha_x\alpha_y - \alpha_\omega\beta_x \\
 a_5 &= -\alpha_x\alpha_y\lambda_\omega & a_6 &= \alpha_x\beta_y\beta_\omega - \alpha_x\alpha_y\lambda_0 + \alpha_\omega\alpha_y\beta_x
 \end{aligned}$$

and F denotes Z, H or Θ .

Taking for the spatial unknowns a solution similar to Ce^{rz} and introducing a new variable $s = r^2$, Eqn (5.14) becomes

$$s^6 + a_1s^5 + a_2s^4 + a_3s^3 + a_4s^2 + a_5s + a_6 = 0 \quad (5.15)$$

Dokumaci and Bishop demonstrated that the six roots of the variable s are real, not null, different each other, three positive and three negative, all depending on the value of the angular frequency p_n , which is still unknown.

As a consequence of s , the roots of the variable r are acquired, together with twelve integration constants for each transversal displacement.

Since the nature of the roots of s are known, the spatial variables Z, H and Θ can be written in the flowing form:

$$\begin{aligned}
 Z(z) &= X_1 \cos(s_1z) + X_2 \sin(s_1z) + X_3 \cos(s_2z) + X_4 \sin(s_2z) + \\
 &X_5 \cos(s_3z) + X_6 \sin(s_3z) + X_7 \cosh(s_4z) + X_8 \sinh(s_4z) + \\
 &X_9 \cosh(s_5z) + X_{10} \sinh(s_5z) + X_{11} \cosh(s_6z) + X_{12} \sinh(s_6z)
 \end{aligned}$$

$$\begin{aligned}
 H(z) &= Y_1 \cos(s_1z) + Y_2 \sin(s_1z) + Y_3 \cos(s_2z) + Y_4 \sin(s_2z) + \\
 &Y_5 \cos(s_3z) + Y_6 \sin(s_3z) + Y_7 \cosh(s_4z) + Y_8 \sinh(s_4z) + \\
 &Y_9 \cosh(s_5z) + Y_{10} \sinh(s_5z) + Y_{11} \cosh(s_6z) + Y_{12} \sinh(s_6z)
 \end{aligned}$$

$$\begin{aligned}
 \Theta(z) &= R_1 \cos(s_1z) + R_2 \sin(s_1z) + R_3 \cos(s_2z) + R_4 \sin(s_2z) + \\
 &R_5 \cos(s_3z) + R_6 \sin(s_3z) + R_7 \cosh(s_4z) + R_8 \sinh(s_4z) + \\
 &R_9 \cosh(s_5z) + R_{10} \sinh(s_5z) + R_{11} \cosh(s_6z) + R_{12} \sinh(s_6z) \quad (5.16)
 \end{aligned}$$

The substitution of $Z(z)$ and $\Theta(z)$ in Eqn (5.12a) allows to identify a relationship between the integration constants X_i and R_i :

$$X_i = \left(\frac{-\beta_y}{r_i^4 - \alpha_y} \right) R_i \quad (5.17)$$

In the same way, if $H(z)$ and $\Theta(z)$ are inserted in Eqn (5.12b) a similar relation is found between Y_i and R_i :

$$Y_i = \left(\frac{\beta_x}{r_i^4 - \alpha_x} \right) R_i \quad (5.18)$$

The expressions (5.17) and (5.18) involves that the remaining unknowns related to the integration constants are the terms R_i . The latter can be easily computed taking into account the boundary conditions of the beam.

For each end and for each transversal displacement, two boundary conditions can be identified. Therefore, twelve boundary conditions referred to the spatial variables Z , H and Θ allow to write twelve linear homogeneous equations, which may be gathered in the following matrix form:

$$\mathbf{M}\mathbf{R} = 0 \quad (5.19)$$

being \mathbf{R} the vector of the unknowns R_i .

Nevertheless, since the coefficients of \mathbf{M} depends on the unknown p_n and the trivial solution $\mathbf{R} = 0$ has to be avoided, the annulment of the determinant of the matrix \mathbf{M} , that is the identification of specific values of p_n which make the determinant singular, is imposed.

Once a value of p_n is found, the six roots of s as well as the twelve roots of r are obtained and, exploiting the boundary conditions, by means of Eqns (5.17) and (5.18) the spatial functions Z , H and Θ are clearly derived.

Finally, the complete expressions of the transversal displacements ξ , η and ϑ can be written in terms of the infinite values of p_n :

$$\begin{aligned} \xi &= \sum_{n=1}^{\infty} Z_n(z) [A_n \cos(p_n t) + B_n \sin(p_n t)] \\ \eta &= \sum_{n=1}^{\infty} H_n(z) [A_n \cos(p_n t) + B_n \sin(p_n t)] \\ \vartheta &= \sum_{n=1}^{\infty} \Theta_n(z) [A_n \cos(p_n t) + B_n \sin(p_n t)] \end{aligned} \quad (5.20)$$

The characteristics of the method permit to consider any boundary condition. The latter can be static or kinematic. In general we can refer to clamped, hinged and free end conditions:

- *clamped end*: displacements and rotations are constrained; in particular also the warping of the section, which is proportional to the first derivative of ϑ , is impeded;

$$Z = 0 \qquad Z' = 0$$

$$H = 0 \qquad H' = 0$$

$$\Theta = 0 \qquad \Theta' = 0$$

- *hinged end*: as kinematic conditions, the translations and the torsional rotation are prevented, whereas, as static conditions, the flexural moments and the bimoment, proportional to the second derivative of ϑ , are considered equal to zero;

$$Z = 0 \qquad Z'' = 0$$

$$H = 0 \qquad H'' = 0$$

$$\Theta = 0 \qquad \Theta'' = 0$$

- *free end*: only static conditions are employed, since the flexural moments, the total torsional moment, the bimoment and the shears are null.

$$Z'' = 0 \qquad Z''' = 0$$

$$H'' = 0 \qquad H''' = 0$$

$$\Theta'' = 0 \qquad GJ_t \Theta' - EI_\omega \Theta''' = 0$$

5.2.2 Numerical Examples

The analytical procedure is evaluated performing some examples regarding thin-walled open section profiles defined by different end conditions.

The method is implemented with a program in Matlab environment and three cases, coming from the existing literature, are analysed. For each case, a comparison of results in terms of natural frequencies is carried out and a high accuracy is found. The practical examples are also modelled in a FE program in order to verify the effectiveness of the approach.

Three typologies of sections are examined in order to put the method on probation: the first case is defined by a double symmetry, the second one by a single symmetry and the last without symmetry.

- *Doubly symmetrical section.*

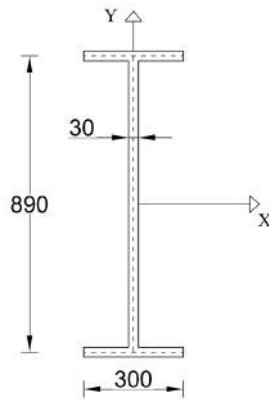


Figure 5.4 – Doubly symmetrical I-section beam.

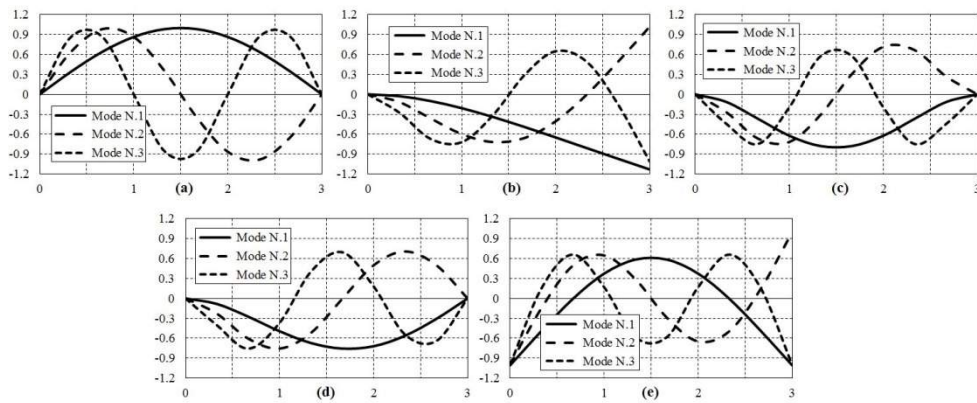


Figure 5.5 – Mode shapes of the I-section beam with various end conditions: simply supported (a), cantilever (b), doubly constrained (c), constrained-hinged (d) and free ends (e).

The first case is represented by a I-section beam shown in Fig. 5.4, whose geometrical and mechanical properties are reported in Table 5.1. Various end conditions are taken into account and the results, reported in Table 5.2, are compared to the ones obtained through the exact solution proposed by Timoshenko [115]. In Fig. 5.5 the first three mode shapes of the beam for each end condition are highlighted.

Table 5.1 – Geometrical and mechanical properties of the I-section beam.

E [N/m ²]	2.1×10 ¹⁰	I _x [m ⁴]	5.33×10 ⁻³	I _o [m ⁶]	2.67×10 ⁻⁵
ν [-]	0.3	I _y [m ⁴]	1.35×10 ⁻⁴	ρ [kg/m ³]	2700
L [m]	3	J _t [m ⁴]	1.34×10 ⁻⁵	I _o [m ⁴]	5.46×10 ⁻³

Table 5.2 – Natural frequencies [Hz] of the beam according to various end conditions.

Mode N.	Simply supported			Cantilever			Doubly constrained		
	X Dir.	Y Dir.	Rot.	X Dir.	Y Dir.	Rot.	X Dir.	Y Dir.	Rot.
1	26.75	168.03	36.93	9.53	59.86	15.47	60.64	380.91	78.82
2	107.00	672.12	139.18	59.72	375.14	80.30	167.15	1049.98	215.02
3	240.75	1512.27	309.46	167.22	1050.40	216.60	327.69	2058.38	419.60

Mode N.	Constrained - Hinged			Free ends		
	X Dir.	Y Dir.	Rot.	X Dir.	Y Dir.	Rot.
1	41.79	262.50	55.39	60.64	380.91	15.69
2	135.42	850.65	174.95	167.15	1049.98	83.53
3	282.54	1774.82	362.38	327.69	2058.38	218.01

- *U-shaped section beam with one axis of symmetry.*

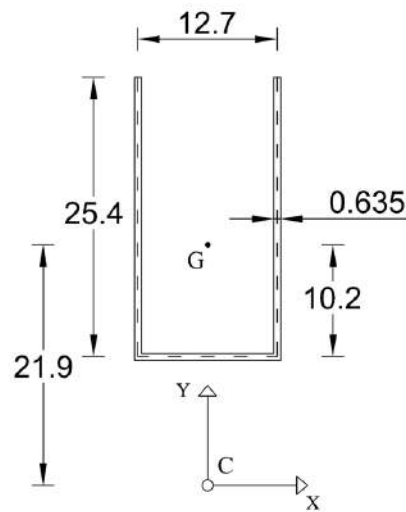


Figure 5.6 – U-shaped section beam having the Y axis as axis of symmetry.

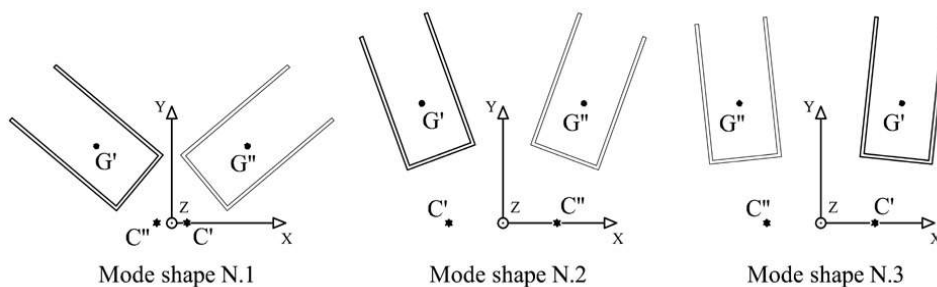


Figure 5.7 – Schemes related to the first three mode shapes of the U-shaped section beam, in the case of simply supported end conditions.

Table 5.3 – Geometrical and mechanical properties of the U-shaped section beam.

E [N/m ²]	6.89×10^{10}	I _x [m ⁴]	2.77×10^{-9}	I _ω [m ⁶]	8.61×10^{-14}
v [-]	0.316	I _y [m ⁴]	1.41×10^{-9}	ρ [kg/m ³]	2597
L [m]	1.016	J _t [m ⁴]	5.42×10^{-12}	I ₀ [m ⁴]	2.35×10^{-8}

Table 5.4 – Comparison in terms of natural frequencies [Hz] between the proposed method and a FE program.

Mode N.	Simply supported		Cantilever		Doubly constrained		Constrained - Hinged		Free ends		Max Err. [%]
	FEM	An.	FEM	An.	FEM	An.	FEM	An.	FEM	An.	
1	25.5	24.5	11.9	11.4	41.3	40.2	32.7	31.6	56.2	54.4	-4.2
2	65.8	65.0	24.0	23.2	102.7	101.2	87.1	85.4	57.5	59.3	-3.5
3	73.4	71.5	43.6	42.7	147.7	147.4	102.1	101.6	116.2	114.8	-2.6
4	123.3	126.0	57.5	58.3	188.7	189.0	166.7	165.8	148.6	147.4	2.2
5	146.3	144.7	109.1	107.4	254.7	266.0	181.8	187.6	198.4	198.4	4.5
Err. [%] = (Analytical-FEM)/FEM×100											
Uncoupled (Y direction)											

The geometry of the section of Fig. 5.6 is derived from the paper by Bishop *et al.* [10, 11]. Since an axis of symmetry is present, coupling between bending in X direction and torsion appears and, therefore, the corresponding natural frequencies coincide; on the contrary, the bending behaviour in Y direction is independent from the others.

The geometrical and mechanical properties of the beam are described in Table 5.3, whereas Table 5.4 reports the results in terms of the first three natural frequencies of the system. As regard the case of free ends, the results obtained by the implementation of the method in Matlab are perfectly comparable with those indicated first by Bishop [12] and, then, confirmed by Yaman [126].

Furthermore, in order to evaluate the effectiveness of the method, a comparison with a FE program is proposed. As it can be seen in Table 5.4, the per cent error remains less than 5% for all the considered schemes.

In Fig. 5.7 a scheme of the transversal displacements related to the case of simply supported beam is shown for the first three natural frequencies.

- *Generic thin-walled open section beam without any axis of symmetry.*

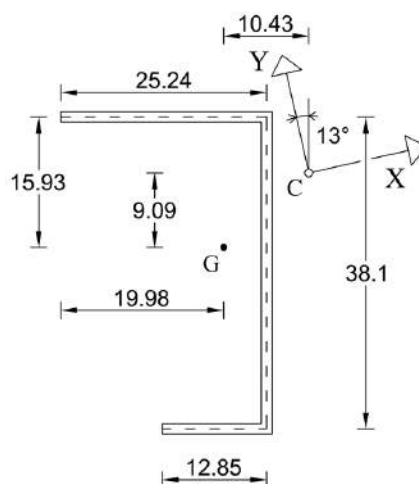


Figure 5.8 – Generic section beam having no axis of symmetry.

Table 5.5 – Geometrical and mechanical properties of the generic section beam.

E [N/m ²]	7×10^{10}	I_x [m ⁴]	2.34×10^{-8}	I_{ω} [m ⁶]	5.82×10^{-13}
ν [-]	0.35	I_y [m ⁴]	4.1×10^{-9}	ρ [kg/m ³]	2700
L [m]	1	J_t [m ⁴]	5.21×10^{-11}	I_0 [m ⁴]	4.6×10^{-8}

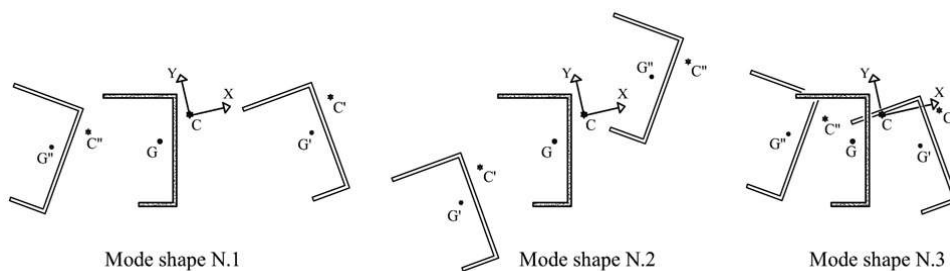


Figure 5.9 - Schemes related to the first three mode shapes of the generic section beam, in the case of simply supported end conditions.

Table 5.6 – Comparison in terms of natural frequencies [Hz] between the proposed method and a FE program.

Mode N.	Simply supported		Cantilever		Doubly constrained		Constrained - Hinged		Free ends		Max Err. [%]
	FEM	An.	FEM	An.	FEM	An.	FEM	An.	FEM	An.	
1	51.53	47.78	19.21	18.13	87.37	82.03	69.50	65.06	70.04	71.26	-7.28
2	66.41	64.38	30.56	30.26	130.27	127.54	93.21	90.49	114.81	107.19	-6.64
3	155.55	146.07	59.98	61.20	211.18	202.31	181.87	172.45	147.29	143.44	-6.10
4	160.53	161.69	102.59	99.49	342.37	347.70	242.23	247.34	244.21	232.95	-4.61
5	229.56	225.33	133.49	132.20	347.71	355.25	285.56	282.91	356.25	352.91	2.17

Error [%] = (Analytical-FEM)/FEM×100

Information regarding the geometry and the mechanical characteristics of the generic section beam can be found in the paper by Yaman [126] and Arpaci [7].

The comparison with the results obtained by Yaman and Arpaci concerns the case of simply supported beam. All the other end conditions are verified through the definition of the model in a FE program. The results are reported in Table 5.6.

It is necessary to notice that the results indicated by Yaman and Arpaci are less accurate than those acquired by the present formulation. In effect, as the previous example, the per cent error related to the FE method proves to be very small, being not more than 8%. In Fig. 5.9 the scheme of the displacements of the section for the first three natural frequencies, in the case of simply supported beam, is highlighted. It is evident that the beam is subjected, at the same time, to bending in both principal directions and torsion.

5.3 Three-Dimensional Formulation for the Dynamics of Tall Buildings

In this section, a semi-analytical formulation for the evaluation of the free vibrations of a three-dimensional tall building is proposed. The need of a preliminary assessment of the free vibrations of such constructions in the phase of conceptual design is essential, being these structures usually subjected to dynamic actions. It is well-known that vibrations are of interest for the structural design, but, especially, for the living comfort of the occupants. Therefore, as demonstrated by Stafford Smith and Crowe [100], Wang *et al.* [122] and Zalka [127], an evaluation, even if approximate, of the predominant modes of vibration is compulsory.

Several papers dealt with this kind of subject, relying on different formulations and considering various vertical elements as horizontal bracing. Among all, the papers by Pekau *et al.* [86, 87] are noteworthy. By means of this approach, called Finite Storey Method (FSM), the global behaviour of the building depends on the nodal displacements of two-storey substructures into which the whole construction is split. As a result, a reduced number of nodes are considered so that the computational time turns out to be very short. Furthermore, the formulation allows to consider both frames and shear walls, in a single scheme or composed to represent a tube-in-tube configuration.

For the dynamic analysis of coupled shear walls, the continuum medium technique is commonly used, because it permits to replace the discrete system of connecting beams with an homogeneous medium of equivalent properties. The application to high-rise structures can be found in Tso and Chan [116], Capuani *et al.* [22] and Swaddiwudhipong *et al.* [105]. The analysis of coupled open section shear walls connected each other by means of rigid lintel beams is treated in the papers by Mendelson and Baruch [78, 79], who examined in depth the response of non-symmetrical multi-storey structures with or without damping effect. The same subject was also studied by Meftah *et al.* [76] who applied the Galerkin technique to formulate an approximate handy method for the evaluation of the free vibrations of buildings braced by shear walls and open section elements.

In line with the mentioned formulations, the proposed method allows to consider as components of the building resistant core several types of bracings, such as frames, braced frames and shear walls, having doubly symmetrical or asymmetrical, hollow or open sections. It is directly derived from the papers by Carpinteri *et al.* [24-28], in which only static analyses are computed.

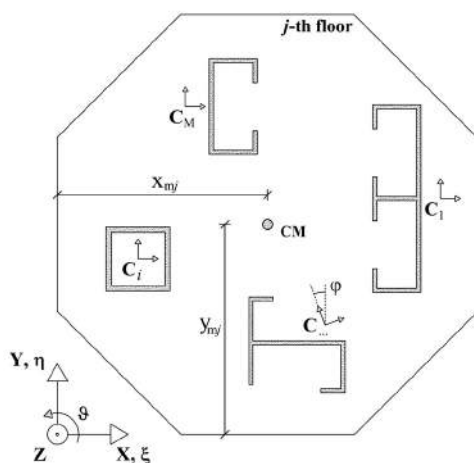


Figure 5.10 - Scheme of the j -th floor of a tall building stiffened by M vertical bracings in the global coordinate system XYZ .

The present approach shows some advantages if compared to other methodologies: first of all, the formulation is extremely clear and concise, limiting in this way the risk of unexpected errors; furthermore, it allows to model the resistant core as a three-dimensional body, avoiding to reduce it to a mere plane problem; finally, the number of nodes is reduced to only floor displacements, guaranteeing very short times of modelling and analysis, if compared to those of FE programs [18].

5.3.1 Semi-Analytical Approach

The dynamic analysis is directly derived from the formulation proposed in Chapter 2, since the mass of the building floors, along with the corresponding acceleration, appears in the global equilibrium equation (2.27).

Due to D'Alembert's Principle, the inertial forces of the structure can be considered as static forces and, therefore, they can be added to (2.27).

Since only free vibrations and mode shapes are evaluated, in this formulation no external actions are taken into account as well as no forced ground motion is included in the analysis.

The dynamic forces are expressed in terms of the mass and the rotational inertia of the floors; on the contrary, the mass corresponding to the structural core is considered negligible and, therefore, it is not inserted in the equilibrium

expression. As a consequence, the load vector is represented by the product of a mass matrix and a vector containing the global accelerations of the building storeys.

Let the point C_i be the origin of the local coordinate system and, at the same time, the shear centre of the section of the i -th bracing; its transversal displacements can be written in terms of the global floor displacements ξ , η and ϑ through the following expressions in a right-handed system (Fig. 5.10):

$$\xi_{Ci} = \xi - y_i\vartheta \quad \eta_{Ci} = \eta + x_i\vartheta \quad (5.21)$$

where (x_i, y_i) are the coordinates of C_i in the global coordinate system XYZ.

The equilibrium equation for the j -th floor in X direction is given by:

$$\sum_{i=1}^M [k_{x,ij}^T (u - y_i\Theta)] + m_j(\ddot{\xi}_j - y_{mj}\ddot{\vartheta}_j) = 0 \quad (5.22)$$

in which the following expressions are used:

- $k_{x,ij}^T$ represents, for the j -th floor, the row of the local stiffness matrix of the i -th bracing, conveniently rotated to be parallel to the global coordinate system;
- u is the vector including the floor displacements ξ_i in X direction;
- Θ is the vector including the N rotations ϑ_i of the floors;
- m_j is the mass of the j -th floor;
- y_{mj} is the coordinate, in Y direction, of the centre of mass of the j -th floor.

Eqn (5.22) can be extended to consider all the storeys of the building. The concise expression is reported below:

$$\sum_{i=1}^M [\mathbf{K}_{xi}(u - y_i\Theta)] + \mathbf{M}_{xx}\ddot{u} + \mathbf{M}_{x\vartheta}\ddot{\Theta} = 0 \quad (5.23a)$$

Similarly, in Y direction, the global equilibrium is given by:

$$\sum_{i=1}^M [\mathbf{K}_{yi}(v + x_i\Theta)] + \mathbf{M}_{yy}\ddot{v} + \mathbf{M}_{y\vartheta}\ddot{\Theta} = 0 \quad (5.23b)$$

whereas, for the rotational equilibrium, the following equation can be written:

$$\begin{aligned} & -\sum_{i=1}^M [\mathbf{K}_{xi}(u - y_i\Theta)y_i] + \sum_{i=1}^M [\mathbf{K}_{yi}(v + x_i\Theta)x_i] + \\ & + \mathbf{M}_{x\vartheta}\ddot{u} + \mathbf{M}_{y\vartheta}\ddot{v} + \mathbf{M}_{\vartheta\vartheta}\ddot{\Theta} = 0 \end{aligned} \quad (5.23c)$$

In Eqns (5.23) some stiffness and mass matrices are shown. In particular mass matrices include information regarding the mass, the coordinates of the centre of mass as well as the polar moment of inertia of the floors. The latter, referred to the global coordinate system, can be calculated by means of the mass density μ

[kg/m²], the geometrical polar moment of inertia I_G , the radial coordinate r of the floor barycentre in the XYZ system and the floor area A :

$$I_0 = \mu(I_G + Ar^2) \quad (5.24)$$

$$\begin{aligned} \mathbf{M}_{xx} = \mathbf{M}_{yy} &= \begin{bmatrix} m_1 & 0 & 0 \\ 0 & \dots & 0 \\ 0 & 0 & m_N \end{bmatrix} & \mathbf{M}_{\theta\theta} &= \begin{bmatrix} I_{01} & 0 & 0 \\ 0 & \dots & 0 \\ 0 & 0 & I_{0N} \end{bmatrix} \\ \mathbf{M}_{x\theta} &= \begin{bmatrix} -m_1 y_{m1} & 0 & 0 \\ 0 & \dots & 0 \\ 0 & 0 & -m_N y_{mN} \end{bmatrix} & \mathbf{M}_{y\theta} &= \begin{bmatrix} m_1 x_{m1} & 0 & 0 \\ 0 & \dots & 0 \\ 0 & 0 & m_N x_{mN} \end{bmatrix} \end{aligned} \quad (5.25)$$

Further simplifications can be adopted in the definition of Eqns (5.23), through the following relations:

$$\begin{aligned} \mathbf{K}_{xx} &= \sum_{i=1}^M \mathbf{K}_{xi} & \mathbf{K}_{yy} &= \sum_{i=1}^M \mathbf{K}_{yi} \\ \mathbf{K}_{x\theta} &= -\sum_{i=1}^M \mathbf{K}_{xi} y_i & \mathbf{K}_{y\theta} &= \sum_{i=1}^M \mathbf{K}_{yi} x_i \\ \mathbf{K}_{\theta\theta} &= \sum_{i=1}^M \mathbf{K}_{xi} y_i^2 + \sum_{i=1}^M \mathbf{K}_{yi} x_i^2 \end{aligned} \quad (5.26)$$

Therefore Eqns (5.23) become:

$$\begin{aligned} \mathbf{K}_{xx} \mathbf{u} + \mathbf{K}_{x\theta} \Theta + \mathbf{M}_{xx} \ddot{\mathbf{u}} + \mathbf{M}_{x\theta} \ddot{\Theta} &= 0 \\ \mathbf{K}_{yy} \mathbf{v} + \mathbf{K}_{y\theta} \Theta + \mathbf{M}_{yy} \ddot{\mathbf{v}} + \mathbf{M}_{y\theta} \ddot{\Theta} &= 0 \\ \mathbf{K}_{x\theta} \mathbf{u} + \mathbf{K}_{y\theta} \mathbf{v} + \mathbf{K}_{\theta\theta} \Theta + \mathbf{M}_{x\theta} \ddot{\mathbf{u}} + \mathbf{M}_{y\theta} \ddot{\mathbf{v}} + \mathbf{M}_{\theta\theta} \ddot{\Theta} &= 0 \end{aligned} \quad (5.27)$$

If the displacement vectors \mathbf{u} , \mathbf{v} and Θ are gathered together in the global displacement vector δ , Eqns (5.27) can be shown in a well-known and very synthetic form:

$$\bar{\mathbf{M}} \ddot{\delta} + \bar{\mathbf{K}} \delta = 0 \quad (5.28)$$

in which the global mass and stiffness matrices are highlighted.

$$\bar{\mathbf{M}} = \begin{bmatrix} \mathbf{M}_{xx} & \mathbf{0} & \mathbf{M}_{x\theta} \\ \mathbf{0} & \mathbf{M}_{yy} & \mathbf{M}_{y\theta} \\ \mathbf{M}_{x\theta} & \mathbf{M}_{y\theta} & \mathbf{M}_{\theta\theta} \end{bmatrix} \quad (5.29)$$

$$\bar{\mathbf{K}} = \begin{bmatrix} \mathbf{K}_{xx} & \mathbf{0} & \mathbf{K}_{x\theta} \\ \mathbf{0} & \mathbf{K}_{yy} & \mathbf{K}_{y\theta} \\ \mathbf{K}_{x\theta} & \mathbf{K}_{y\theta} & \mathbf{K}_{\theta\theta} \end{bmatrix} \quad (5.30)$$

Depending on the position of the origin of the global coordinate system XYZ, the term $\bar{\mathbf{K}}$, or $\bar{\mathbf{M}}$, can be reduced to a block diagonal matrix, since the mixed sub-matrices become null matrices. In particular, if the origin of the coordinate system coincides with the centre of rigidity of the building or the centre of mass of the floor, the expressions $\mathbf{K}_{x\theta}$ and $\mathbf{K}_{y\theta}$ or $\mathbf{M}_{x\theta}$ and $\mathbf{M}_{y\theta}$ vanish respectively. In the first case, the sum of the products $\mathbf{K}_{x_i y_i}$ and $\mathbf{K}_{y_i x_i}$ becomes equal to zero, whereas, in the second case, the coordinates $(x_{mj}; y_{mj})$ disappear.

The solution of Eqn (5.28) can be deduced supposing that the global displacement vector δ is given by the product of two terms: the first is a scalar depending on the time t ; the other is a vector depending on the spatial coordinate z . The latter represents the deformed configuration of the building or its mode shape.

$$\delta(z, t) = H(z)f(t) \quad (5.31)$$

Substituting the expression (5.31) in Eqn (5.28) and pre-multiplying the obtained relation with the transpose of the vector H, it is possible to adopt the method of separation of the variables. Therefore an identity between the variables depending on t and those depending on z is acquired. Since the values of t and z are arbitrary, the identity is always made possible if and only if both members are equal to a constant, here represented by the term (p^2) .

$$H^T \bar{\mathbf{M}} H \ddot{f} + H^T \bar{\mathbf{K}} H f = 0 \quad (5.32)$$

$$\frac{H^T \bar{\mathbf{K}} H}{H^T \bar{\mathbf{M}} H} = -\frac{\ddot{f}}{f} = p^2 \quad (5.33)$$

From Eqn (5.33) two independent equations can be deduced, one related to the angular frequency of the free vibration, the other to the mode shapes of the building.

$$\begin{cases} \ddot{f} + p^2 f = 0 \\ H^T (\bar{\mathbf{K}} - p^2 \bar{\mathbf{M}}) H = 0 \end{cases} \quad (5.34)$$

The solution of Eqn (5.34a) is well-known and can be written in the following form:

$$f(t) = A \cos(pt) + B \sin(pt) \quad (5.35)$$

where A and B are constants of integration, whose numerical value is found considering the initial conditions of the problem.

Eqn (5.34b) can be reduced to an eigenvalue problem, from which 3N eigenvalues p^2 are extracted in order to define the natural frequencies p of the structural system. This is developed imposing that the determinant of $(\bar{\mathbf{K}} - p^2\bar{\mathbf{M}})$ vanishes. Once a root p^2 is obtained, it is substituted back into the original set of equations, in order to acquire the corresponding eigenvector or mode shape \mathbf{H} of the system. At the end of the procedure, the displacement vector δ can be expressed in terms of all the roots p^2 ; consequently, a $3N \times 3N$ matrix containing the eigenvectors and a 3N vector composed by the functions $f(t)$ can be defined:

$$\mathbf{\Psi}(z) = [H_1 \quad \dots \quad H_{3N}] \quad \Phi^T(t) = [f_1 \quad \dots \quad f_{3N}] \quad (5.36)$$

$$\delta(z, t) = \mathbf{\Psi}(z)\Phi(t) \quad (5.37)$$

Eqn (5.37) represents the solution of Eqn (5.28). By means of it, together with Eqns (2.11) and (2.25), the displacements of the i -th bracing δ_i^* can be derived.

The proposed semi-analytical formulation proves to be clear and concise so that errors of interpretation as well as calculation are absolutely minimised. In addition, the method demonstrates to take into account a very small number of degrees of freedom, ensuring competitive times of modelling and analysis.

In the next section two numerical examples highlight the flexibility and effectiveness of the proposed approach.

5.3.2 Numerical Examples

The free vibrations of a high-rise building are evaluated performing two numerical examples in which the horizontal resistance is provided by different types of vertical bracings. Some of them are characterised by thin-walled open sections and, therefore, are analysed by means of Vlasov's theory of the sectorial areas [119]. The investigation is also performed through a computer program which implements the FE method. In this way, a comparison regarding the obtained results allows to appreciate the benefit provided by the semi-analytical formulation.

The model structure is a 60-storey building, defined by a square floor plan. The storey height is $h = 5$ m, corresponding to a total height $H = 300$ m. Each floor is 0.5 m thick, with a mass density equal to 2.548 ton/m^3 or 25 kN/m^3 , if the reference acceleration is 9.81 m/s^2 . The material constituting the resistant skeleton is concrete having Young's modulus $E = 3 \times 10^4 \text{ MPa}$ and Poisson's ratio $\nu = 0.18$.

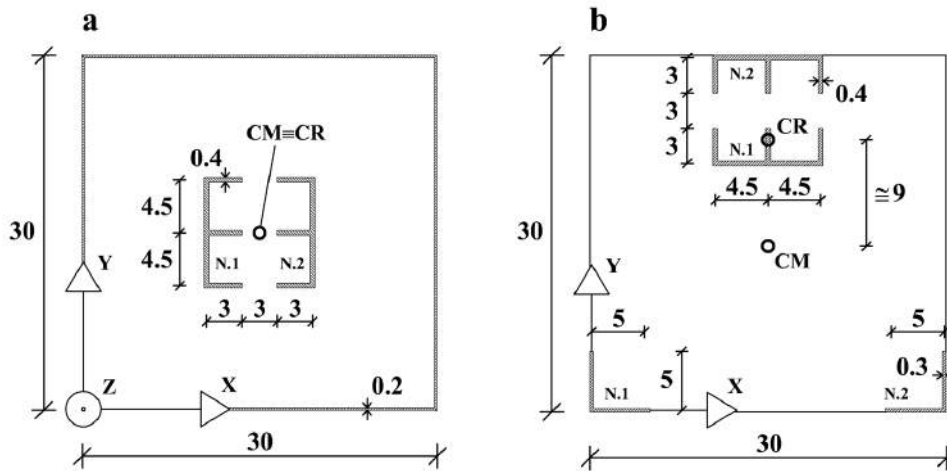


Figure 5.11 - Regular (a) and not regular (b) floor plan of the high-rise building.

Table 5.7 - Regular floor plan: geometrical properties of the stiffening elements.

Element type	External Tube	Internal Core	
		Open section N.1	Open section N.2
Description	Square hollow section	Open section N.1	Open section N.2
Second moment I_x [m^4]	3600	72.9	72.9
Second moment I_y [m^4]	3600	6.75	6.75
Warping constant I_ω [m^6]	-	72.9	72.9
Torsional rigidity J_t [m^4]	5400	0.38	0.38
Global coordinate x_c of the shear centre [m]	15	9.5	20.5
Global coordinate y_c of the shear centre [m]	15	15	15

The stiffening elements show a constant section along the height and their contribution to the inertial forces, in the dynamic analysis, is considered negligible, as supposed in the previous formulation.

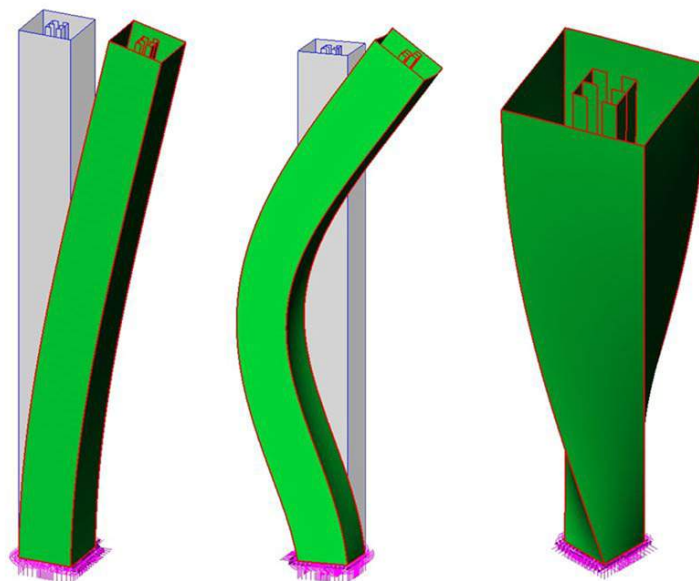


Figure 5.12 - Regular floor plan: mode shapes N. 1, 3 and 5.

Table 5.8 - Regular floor plan: comparison of the results in terms of natural frequencies [Hz].

Mode N.	Analytical	FEM	Error [%]	Description
1	0.1394	0.1372	1.56	Flexural in X direction
2	0.1419	0.1389	2.13	Flexural in Y direction
3	0.8736	0.7531	16.00	Flexural in X direction
4	0.8895	0.7692	15.64	Flexural in Y direction
5	1.2278	1.1583	6.00	Torsional
Error [%] = (Analytical-FEM)/FEM × 100				

Table 5.9 - Not regular floor plan: geometrical properties of the stiffening elements.

Element type	Shear walls		Internal core	
	L-shaped section N.1	L-shaped section N.2	Open section N.1	Open section N.2
Second moment I_x [m ⁴]	12.51	12.51	6.75	6.75
Second moment I_y [m ⁴]	3.14	3.14	72.9	72.9
Warping constant I_ω [m ⁶]	-	-	72.9	72.9
Torsional rigidity J_t [m ⁴]	0.09	0.09	0.38	0.38
Global coordinate x_c of the shear centre [m]	0	30	15	15
Global coordinate y_c of the shear centre [m]	0	0	20	31
Angle φ [°]	45	-45	0	0
*The term φ is the angle between the central axes of the section and the global XY axes.				

The floor plan of the first numerical example is shown in Fig. 5.11a. Its horizontal resistant system is composed by two devices: an external tube covering the perimeter of the building with an equivalent thickness of 0.2 m and an internal core, constituted by two profiles having thin-walled open sections.

For the specific structural configuration, the centre of mass coincides with the centre of rigidity, involving the uncoupling between flexural and torsional behaviour.

The geometrical characteristics of the shear walls are reported in Table 5.7 as well as the comparison in terms of natural frequencies between the proposed and the FE method are highlighted in Table 5.8 and Fig. 5.12.

As it can be seen, the per cent errors concerning the mode shapes N.1, 2, 5 just reach 6%, while, for the second order flexural mode shapes N.3 and N.4, they increase up to 16%. The latter is caused, in the FE program, by the shear lag which affects the tube systems, inducing a non-linear distribution of the stresses in the walls, as underlined in [111]. This corresponds to a lower global stiffness and a lower natural frequency.

Table 5.10 – Not regular floor plan: comparison of the results in terms of natural frequencies [Hz].

Mode N.	Analytical	FEM	Error [%]	Description
1	0.0125	0.0149	-15.96	Uncoupled flexural in Y direction
2	0.0239	0.0250	-4.62	Torsional and flexural in X direction
3	0.0447	0.0455	-1.56	Torsional and flexural in X direction
4	0.0785	0.0816	-3.90	Uncoupled flexural in Y direction
5	0.1360	0.1364	-0.29	Bending in X direction and torsion
Error [%] = (Analytical-FEM)/FEM × 100				

In the second case, the stiffening system is formed by an eccentric core, similar to the previous one, and two angular L-shaped section elements, which develop from the ground to the top of the building (Fig. 5.11b).

Due to this structural configuration, the centre of mass is about 9 m far from the centre of rigidity, determining the coupling of flexural and torsional deformations.

Tables 5.9 and 5.10 summarise the information regarding the geometrical properties of the shear walls and the natural frequencies acquired by the semi-analytical and the FE method.

Also in this case, only the first five frequencies are reported (Fig. 5.13). With the exception of the first frequency, corresponding to a flexural deformation in Y direction, the results show a high accuracy of the proposed approach, since the per cent errors are lower than 5%. On the contrary, the error related to the first natural frequency is clearly due to a local stiffening effect caused by the out-of-plane rigidity of the floors in the FE program (Fig. 5.14).

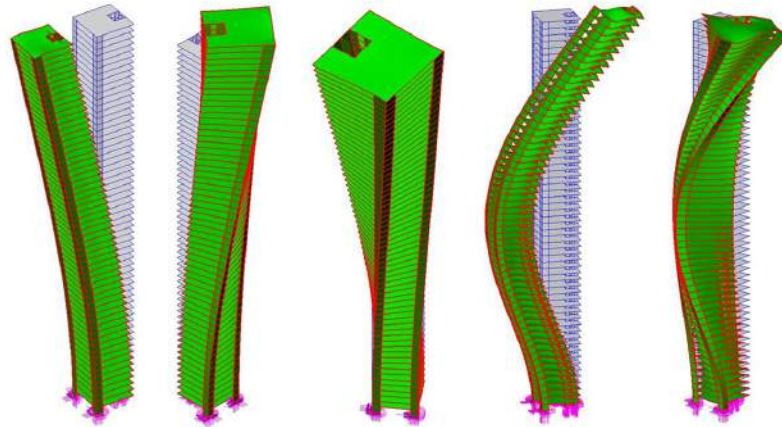


Figure 5.13 - Not regular floor plan: mode shapes N. 1-5.

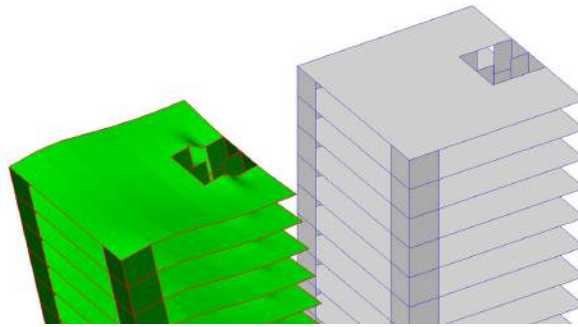


Figure 5.14 - Mode shape N. 1: detail of the local stiffening effect caused by the out-of-plane rigidity of the slabs.

In effect, as shown in [26], the latter reduces the relative vertical displacements of the open section shear walls, producing, at the same time, the increase of the global stiffness and, therefore, the growth of the corresponding natural frequency.

The proof is given by the second order flexural mode shape in Y direction, where a reduction of the local stiffening effect is observed and the corresponding per cent error between the approaches decreases.

Chapter 6

Conclusions

In the design of high-rise buildings, the role of the vertical bracings, devised to carry the horizontal actions coming from wind and earthquakes, is a crucial factor which usually governs the structural and architectural choices of the professionals.

In the preliminary phase of the process, sophisticated tools, such as Finite Element programs, are widely used because of their high level of accuracy as well as their usability, also in presence of very complex structures. Actually, they can also hide some drawbacks: as the complexity increases, they make the process more and more expensive and the displayed results demand a substantial degree of experience to be understood. On the contrary, a simplified analytical formulation can help the engineer find, under specific hypotheses, a clear solution from which more thorough computations can start.

In this thesis, a synthetic three-dimensional approach, adoptable for static and dynamic analyses and aimed for the evaluation of the structural behaviour of tall buildings stiffened by different types of vertical bracings, is proposed. The structural typologies, considered as independent components of the whole resistant skeleton, are represented by shear walls, frames, braced frames and thin-walled open section profiles, whose stiffening contribution is evaluated according to Vlasov's theory of sectorial areas. In this last case, an entire chapter is devoted to their particular behaviour, being one of the most employed bracings in tall constructions; their unusual deformation, called warping deformation, is carefully studied and even an experimental test is performed in order to measure, for the first time, its effect on slender beams subjected to torsion.

Due to the leading role acquired by the aesthetics in the design of the modern

high-rise buildings, such as the case of 30 St. Mary Axe (London) and Turning Torso (Malmo), special attention is paid to twisting and tapering structures and, in particular, synthetic expressions are proposed for the definition of their corresponding stiffness matrices. In this way, the original approach can be extended to consider also curved shapes apart from the traditional ones.

The characteristics of the approach allow the professional to devise a simple computer program aimed to perform preliminary analyses for the evaluation of the structural behaviour of a tall construction subjected to transversal loads and stiffened by various vertical bracings. Starting from basic information, such as the geometry of the building, the number and the typology of the horizontal reinforcements, the properties of the material and the intensity of the loads, substantial data can be acquired: the deformed shape of the entire system, the distribution of the loads between the components of the resistant skeleton, the free vibrations, the modal shapes and the internal actions described by Saint Venant and Vlasov's theories.

Ultimately, the semi-analytical method proves to be an adequate support to the designer's judgement as well as can be considered as a complementary tool for more advanced approaches during the preliminary phases: thanks to the reduced number of degrees of freedom, the data preparation and the modelling time are definitely faster and clearer and the corresponding analysis can evolve more transparently, thus making the process less liable to unexpected errors.

Therefore, the design community has to become aware of the possibility to rely on both advanced and simplified formulations, since they are aimed to two different levels of the structural investigation: in the early stages, approximate methods can help to quickly identify the key parameters of the project, whereas, during the final ones, Finite Element programs allow to perform detailed analyses by means of more thorough computations.

References

- [1] Aggarwal, H.R. and Cranch, E.T., A theory of torsional and coupled bending torsional waves in thin-walled open section beams, *Journal of Applied Mechanics*, **34**: 337-343, 1967.
- [2] Ali, M.M. and Moon, K.S., Structural developments in tall buildings: current trends and future prospects, *Architectural Science Review*, **50** (3): 205-223, 2007.
- [3] Ambrosini, D, Riera, J.D. and Danesi, R.F., Dynamic analysis of thin-walled and variable open section beams with shear flexibility, *International Journal for Numerical Methods in Engineering*, **38** (17): 2867-2885, 1995.
- [4] Ambrosini, D, Riera, J.D. and Danesi, R.F., A modified Vlasov theory for dynamic analysis of thin-walled and variable open section beams, *Engineering Structures*, **22**: 890-900, 2000.
- [5] Ambrosini, D., On free vibration of non-symmetrical thin-walled beams, *Thin-Walled Structures*, **47**: 629-636, 2009.
- [6] Ambrosini, D., Experimental validation of free vibrations from non-symmetrical thin walled beams, *Engineering Structures*, **32** (5): 1324-1332, 2010.
- [7] Arpacı, A. and Bozdağ, E., On free vibration analysis of thin-walled beams with nonsymmetrical open-cross sections, *Computers and Structures*, **80**: 691-695, 2002.
- [8] Barsoum, R. and Gallagher, R., Finite element analysis of torsional and torsional-flexural stability problems, *International Journal for Numerical Methods in Engineering*, **2** (3): 335-352, 1970.
- [9] Beck, H., Contribution to the analysis of coupled shear walls, *ACI Journal Proceedings*, **59** (8): 1055-1070, 1962.
- [10] Bishop, R.E.D., Price, W.G. and Cheng, Z.X., On the structural dynamics of a Vlasov beam, *Proceedings of the Royal Society*, **388**: 49-73, 1983.
- [11] Bishop, R.E.D., Price, W.G. and Cheng, Z.X., A note on the dynamical behaviour of uniform beams having open channel section, *Journal of Sound and Vibration*, **99** (2), 155-167, 1985.
- [12] Bishop, R.E.D., Cannon, S.M. and Miao, S., On coupled bending and torsional vibration of uniform beams, *Journal of Sound and Vibration*, **131** (3): 457-464, 1989.

- [13] Biswas, J.K. and Tso, W.K., Three-dimensional analysis of shear wall buildings to lateral load, *Journal of the Structural Division ASCE*, **100** (5): 1019-1036, 1974.
- [14] Boswell, L.F. and Li, Q., Consideration of the relationship between torsion, distortion and warping of thin-walled beams, *Thin-Walled Structures*, **21**: 147-161, 1995.
- [15] Bozdogan, K.B. and Ozturk, D., Vibration analysis of asymmetric shear wall structures using the transfer matrix method, *Iranian Journal of Science and Technology*, **34**: 1-14, 2010.
- [16] Cammarano, S., Lacidogna, G. and Carpinteri, A., L'effetto della deformazione di ingobbamento sul comportamento strutturale di edifici irrigiditi da mensole a sezione sottile aperta, *XXI Congresso Nazionale di Meccanica Teorica ed Applicata (AIMETA)*, Torino, Settembre 17-20, 2013, CD Rom, ISBN: 9788882391836.
- [17] Cammarano, S., Lacidogna, G. and Carpinteri, A., Formulazione analitica per la progettazione dei controventi verticali in edifici di grande altezza, *XXIV Giornate Italiane della Costruzione in Acciaio (CTA)*, Torino, 30 Settembre – 2 Ottobre, ISBN: 9788890587009, **2**: 983-990, 2013.
- [18] Cammarano, S. and Carpinteri, A., A Simplified Approach for the Dynamic Analysis of High-rise Structures, *Proceedings of the 32nd IMAC, A Conference and Exposition on Structural Dynamics* (Conference Proceedings of the Society for Experimental Mechanics Series), Orlando (USA), February 3-6, Dynamics of Civil Structures, **4**: 509-520, 2014.
- [19] Cammarano, S., Lacidogna, G., Montrucchio, B. and Carpinteri, A., Experimental Evaluation of the Warping Deformation in Thin-Walled Open Section Profiles, *Proceedings of the 2014 Annual Conference on Experimental and Applied Mechanics (SEM)*, Greenville (SC), June 2-6, Advancement of Optical Methods in Experimental Mechanics, **3**, 2015.
- [20] Capuani, D., Savoia, M. and Laudiero, F., Continuum model for analysis of multiply connected perforated cores, *Journal of Engineering Mechanics*, **120**: 1641-1660, 1994.
- [21] Capuani, D., Merli, M. and Savoia, M., An equivalent continuum approach for coupled shear walls, *Engineering Structures*, **16**: 63-73, 1994.
- [22] Capuani, D., Merli, M. and Savoia, M., Dynamic analysis of coupled shear wall-frame systems, *Journal of Sound and Vibration*, **192** (4): 867-883, 1996.
- [23] Capurso, M., Sul calcolo dei sistemi spaziali di controventamento. Estratto da "Giornale del Genio Civile", Fasc. I, II, III: 523-538, 1981.
- [24] Carpinteri, Al. and Carpinteri, An., Lateral loading distribution between the elements of a three-dimensional civil structure, *Computers and Structures*, **21**: 563-580, 1985.

- [25] Carpinteri, A., Lacidogna, G. and Puzzi, S., A global approach for three dimensional analysis of tall buildings, *The Structural Design of Tall and Special Buildings*, **19**: 518-536, 2010.
- [26] Carpinteri, A., Corrado, M., Lacidogna, G. and Cammarano, S. Lateral load effects on tall shear wall structures of different height, *Structural Engineering and Mechanics*, **41**: 313-337, 2012.
- [27] Carpinteri, A., Lacidogna, G. and Cammarano, S., Structural analysis of high-rise buildings under horizontal loads: A study on the Intesa Sanpaolo Tower in Turin, *Engineering Structures*, **56**: 1362-1371, 2013.
- [28] Carpinteri, A., Lacidogna, G. and Cammarano, S., Conceptual Design of Tall and Unconventionally Shaped Structures: A Handy Analytical Method, *Advances in Structural Engineering*, **17** (5): 757-773, 2014.
- [29] Chen, X. and Tamma, K.K., Dynamic response of elastic thin-walled structures influenced by coupling effects, *Computers and Structures*, **51** (1): 91-105, 1994.
- [30] Connor, J.J. and Pougare, C.C., Simple model for design of framed-tube structures, *Journal of the Structural Division ASCE*, **117**: 3623-3644, 1991.
- [31] Coull, A. and Choudhury, J.R., Stresses and deflections in coupled shear walls, *ACI Journal Proceedings*, **64** (2): 65-72, 1967.
- [32] Coull, A. and Puri R.D., Analysis of pierced shear walls, *Journal of the Structural Division ASCE*, **94** (1): 71-82, 1968.
- [33] Coull, A. and Subedi, N.K., Framed-tube structures for high-rise buildings, *Journal of the Structural Division ASCE*, **91**: 2097-2105, 1971.
- [34] Coull, A. and Irwin, A.W., Model investigation of shear wall structures, *Journal of the Structural Division ASCE*, **98**: 1233-1237, 1972.
- [35] Coull, A. and Irwin, A.W., Torsional analysis of multi-story shear-wall structures, *ACI Special Publication*, **35**: 211-238, 1973.
- [36] Coull, A. and Hag, A.A., Effective coupling of shear-walls by floor slabs, *ACI Journal Proceedings*, **72** (8): 429-431, 1975.
- [37] Coull, A. and Bose, B., Simplified analysis of framed-tube structures, *Journal of the Structural Division ASCE*, **101**: 2223-2240, 1977.
- [38] Coull, A. and Chee, W.Y., Design of floor slabs coupling shear walls, *Journal of Structural Engineering*, **109** (1): 109-125, 1983.
- [39] Coull, A. and Chee, W.Y., Stresses in slabs coupling flanged shear walls, *Journal of Structural Engineering*, **110** (1): 105-119, 1984.

- [40] Coull, A. and Chee, W.Y., Coupling action of slabs in hull-core structures, *Journal of Structural Engineering*, **110** (2): 213-227, 1984.
- [41] Di Egidio, A., Luongo, A. and Vestroni, F., A non-linear model for the dynamics of open cross-section thin-walled beams – Part I: formulation, *International Journal of Non-Linear Mechanics*, **38**: 1067-1081, 2003.
- [42] Di Egidio, A., Luongo, A. and Vestroni, F., A non-linear model for the dynamics of open cross-section thin-walled beams – Part II: forced motion, *International Journal of Non-Linear Mechanics*, **38**: 1083-1094, 2003.
- [43] Dickson, M. and Nilson, A., Analysis of cellular buildings for lateral loads, *ACI Journal Proceedings*, **67** (12): 963-966, 1970.
- [44] Dokumaci, E., An exact solution for coupled bending and torsion vibrations of uniform beams having single cross-sectional symmetry, *Journal of Sound and Vibration*, **119**: 443-449, 1987.
- [45] Dufort, L., Grédiac, M. and Surrel, Y., Experimental evidence of the cross-section warping in short composite beams under three point-bending, *Composite Structures*, **51**: 37-47, 2001.
- [46] Duncan, M., Torsion coupling of core walls in tall buildings, *The Structural Engineer*, **47** (2): 67-71, 1969.
- [47] Eisenberger, M., Nonuniform torsional analysis of variable and open cross-section bars, *Thin-Walled Structures*, **21**, 93-105, 1995.
- [48] European Committee for Standardization, Eurocode 1: Actions on structures. General actions. Densities, self-weight, imposed loads for buildings, *BS EN 1991-1-1:2002*, British Standard Institution, 2002.
- [49] Garland, C.F., The normal modes of vibrations of beams having noncollinear elastic and mass axes, *Journal of Applied Mechanics ASME*, **7**: 97-105, 1940.
- [50] Gendy, A.S., Saleeb, A.F. and Chang, T., Generalized thin-walled beam models for flexural-torsional analysis, *Computers and Structures*, **42**: 531-550, 1992.
- [51] Gere, J.M., Torsional vibrations of beams of thin-walled open section, *Applied Mechanics Division ASME*, **21**: 381-387, 1954.
- [52] Gere, J.M. and Lin, Y.K., Coupled vibrations of thin-walled beams of open cross section, *Applied Mechanics Division ASME*, **57**: 373-378, 1957.
- [53] Gluck, J., Lateral-load analysis of asymmetric multistory structures, *Journal of the Structural Division ASCE*, **96** (2): 317-333, 1970.
- [54] Gluck, J. and Krauss, M., Stress analysis of group of interconnected thin-walled

- cantilevers, *Journal of the Structural Division ASCE*, **99**: 2143-65, 1973.
- [55] Ha, K.H. and Desbois, M., Finite elements for tall buildings analysis, *Computers and Structures*, **33**: 249-255, 1989.
- [56] Haris, A.K., Approximate stiffness analysis of high-rise buildings, *Journal of the Structural Division ASCE*, **104** (4): 681-696, 1978.
- [57] Heidebrecht, A. C. and Swift, D., Analysis of asymmetrical coupled shear walls, *Journal of the Structural Division ASCE*, **97** (5): 1407-1422, 1971.
- [58] Heidebrecht, A. C. and Stafford Smith, B., Approximate analysis of tall wall-frame structures, *Journal of the Structural Division ASCE*, **99** (2): 199-221, 1973.
- [59] Heidebrecht, A. C. and Stafford Smith, B., Approximate analysis of open-section shear walls subjected to torsional loading, *Journal of the Structural Division ASCE*, **99** (12): 2355-2373, 1973.
- [60] Hoenderkamp, J.C.D. and Snijder, H., Approximate analysis of high-rise frames with flexible connections, *The Structural Design of Tall Buildings*, **9**: 233-248, 2000.
- [61] Howson, W.P., Global Analysis: Back to the Future, *The Structural Engineer*, **84**: 18-21, 2006.
- [62] Hu, Y., Jin, X. and Chen, B., A finite element model for static and dynamic analysis of thin-walled beams with asymmetric cross-sections, *Computers and Structures*, **61** (5): 897-908, 1996.
- [63] Humar, J.L., A computer program for three dimensional analysis of buildings, *Computers and Structures*, **11**: 369-387, 1980.
- [64] Khan, F.R. and Sbarounis, J.A., Interaction of shear walls and frames, *Journal of the Structural Division ASCE*, **90**: 285-335, 1964.
- [65] Khan, F.R., *Tubular structures for tall buildings. Handbook of concrete engineering*, Van Nostrand Reinhold Co., New York, USA, 1974.
- [66] Kim, H.S. and Lee, D.G., Analysis of shear wall with openings using super elements, *Engineering Structures*, **25**: 981-91, 2003.
- [67] Kim, N. and Kim, M., Exact dynamic-static stiffness matrices of non-symmetric thin-walled beams considering coupled shear deformation effects, *Thin-Walled Structures*, **43**: 701-734, 2005.
- [68] Kim, N., Fu, C. and Kim, M. Stiffness matrices for flexural-torsional/lateral buckling and vibration analysis of thin-walled beam, *Journal of Sound and Vibration*, **299**: 739-756, 2007.
- [69] Krajcinovic, D., Matrix force analysis of thin-walled structures, *Journal of the*

Structural Division ASCE, **96**: 107-121, 1970.

- [70] Lee, D., Kim, H. and Chun, M. Efficient seismic analysis of high-rise building structures with the effect of the floor slabs, *Engineering Structures*, **24**: 613-623, 2002.
- [71] Lee, J., Bang, M. and Kim, J.Y., An analytical model for high-rise wall-frame structures with outriggers, *The Structural Design of Tall and Special Buildings*, **17** (4): 839-851, 2008.
- [72] Leung, A., Micro-computer analysis of three-dimensional tall buildings, *Computers and Structures*, **21**: 639-661, 1985.
- [73] Leung, A. and Wong, S.C., Local-global distribution factors method for tall building frame, *Computers and Structures*, **29**: 497-502, 1988.
- [74] Liauw, T.C. and Leung, K.W., Torsion analysis of core wall structures by transfer matrix method, *The Structural Engineer*, **53** (4): 187-194, 1975.
- [75] Mallick, D.V. and Dungan, R., Dynamic characteristics of core wall structures subjected to torsion and bending, *The Structural Engineer*, **55**: 251-261, 1977.
- [76] Meftah, S.A., Tounsi, A. and Abbas, A.B. A simplified approach for seismic calculation of a tall buildings braced by shear walls and thin walled open section structures, *Engineering Structures*, **29**: 2576-2585, 2007.
- [77] Memon, M. and Narwani, T.D., Experimental investigations regarding behavior of tall buildings subjected to lateral loading, *Journal of Quality and Technology Management*, **4**: 39-50, 2008.
- [78] Mendelson, E. and Baruch, M., Earthquake response of non-symmetric multi-storey structures, *The Structural Engineer*, **51**: 61-70, 1973.
- [79] Mendelson, E. and Baruch, M., Damped earthquake response of non-symmetric multi-storey structures, *The Structural Engineer*, **53**: 165-171, 1975.
- [80] Mendis, P., Warping analysis of concrete cores, *The Structural Design of Tall Buildings*, **10** (1): 43-52, 2001.
- [81] Michael, D., Torsional coupling of core walls in tall buildings, *The Structural Engineer*, **47** (2): 67-72, 1969.
- [82] Ministero delle Infrastrutture DM 14/01/2008: Nuove norme tecniche per le costruzioni, *Gazzetta Ufficiale* 04.02.2008, 2008.
- [83] Moon, K.S., Stiffness-based design methodology for steel braced tube structures: A sustainable approach, *Engineering Structures*, **32**: 3163-3170, 2010.
- [84] Mortelmans, F., Roeck, G. and Gemert, D., Approximate method for lateral load analysis of high-rise buildings, *Journal of the Structural Division ASCE*, **107** (8): 1589-

- 1610, 1981.
- [85] Paulay, T. and Taylor, R.G., Slab coupling of earthquake-resisting shear walls, *ACI Journal Proceedings*, **78** (2): 130-140, 1981.
- [86] Pekau, O.A., Zielinski, Z.A. and Lin, L., Displacement and natural frequencies of tall building structures by finite story method, *Computers and Structures*, **54**: 1-13, 1995.
- [87] Pekau, O.A., Lin, L. and Zielinski, Z.A., Static and Dynamic analysis of tall tube-in-tube structures by finite story method, *Engineering Structures*, **18**: 515-527, 1996.
- [88] Pozzati, P. and Ceccoli, C., *Teoria e tecnica delle strutture*, UTET, Torino, Italy, 1977.
- [89] Prokic, A., Thin-walled beams with open and closed cross-sections, *Computers and Structures*, **47**: 1065-1070, 1993.
- [90] Qadeer, A. and Stafford Smith, B., The bending stiffness of slabs connecting shear walls, *ACI Journal Proceedings*, **66** (6): 464-473, 1969.
- [91] Qiusheng, L., Hong, C. and Guiqing, L., Analysis of free vibrations of tall buildings, *Journal of Engineering Mechanics*, **120**: 1861-1876, 1994.
- [92] Rajasekaran, S., Equation for tapered thin-walled beams of generic open section, *Journal of Engineering Mechanics*, **120**: 1607-1629, 1994.
- [93] Rendek, S. and Baláž, I., Distortion of thin-walled beams, *Thin-Walled Structures*, **42**: 255-277, 2004.
- [94] Resatoglu, R., Aksogan, O. and Emsen, E., Static analysis of laterally arbitrarily loaded non-planar non-symmetrical coupled shear walls, *Thin-Walled Structures*, **48**: 696-708, 2010.
- [95] Rosman, R., Approximate analysis of shear walls subjected to lateral loads, *ACI Journal Proceedings*, **61** (6): 717-733, 1964.
- [96] Rosman, R., Torsion of perforated concrete shafts, *Journal of the Structural Division ASCE*, **95** (5): 991-1010, 1969.
- [97] Rutenberg, A. and Heidebrecht, A.C., Approximate analysis of asymmetric wall-frame structures, *Building Science*, **10**: 27-35, 1975.
- [98] Schwaighofer, J., Door opening in shear walls, *ACI Journal Proceedings*, **64** (11): 730-734, 1967.
- [99] Schwaighofer, J. and Collins, M.P., Experimental study of the behaviour of reinforced concrete coupling slabs, *ACI Journal Proceedings*, **74** (3): 123-127, 1977.
- [100] Stafford Smith, B. and Crowe, E., Estimating periods of vibration of tall building, *Journal of Structural Engineering*, **112** (5): 1005-1019, 1986.

- [101] Stafford Smith, B. and Coull, A., *Tall building structures: analysis and design*, Wiley, New York, USA, 1991.
- [102] Stamato, M.C. and Mancini, E., Three-dimensional interaction of walls and frames, *Journal of the Structural Division ASCE*, **99**: 2375-90, 1973.
- [103] Steenbergen, R. and Blaauwendraad, J., Closed-form super element method for tall buildings of irregular geometry, *International Journal of Solids and Structures*, **44**: 5576-5597, 2007.
- [104] Swaddiwudhipong, S., Piriyaakontorn, S., Lim, YB. and Lee, SL., Analysis of tall buildings considering the effect of axial deformation by the Galerkin method, *Computers and Structures*, **32** (6): 1363-1369, 1989.
- [105] Swaddiwudhipong, S., Lee, S. and Zhou, Q., Effect of axial deformation on vibration of tall buildings, *The Structural Design of Tall Buildings*, **10** (2): 79-91, 2001.
- [106] Szymczak, C., Optimal design of thin-walled I beams for a given natural frequency of torsional vibrations, *Journal of Sound and Vibration*, **97**: 137-144, 1984.
- [107] Takabatake, H. and Matsuoka, O., The elastic theory of thin-walled open cross sections with local deformations, *International Journal of Solids and Structures*, **19** (12): 1065-1088, 1983.
- [108] Takabatake, H., Takesako, R. and Kobayashi, M., Simplified analysis of doubly symmetric tube structures, *The Structural Design of Tall Buildings*, **4**: 137-153, 1995.
- [109] Tanaka, M. and Bercin, A.N., Free vibration solution for uniform beams of non-symmetrical cross section using Mathematica, *Computers and Structures*, **71**: 1-8, 1998.
- [110] Taranath, B.S. and Stafford Smith, B., Torsion analysis of shear core structures, *ACI Special Publication*, **35**: 239-263, 1973.
- [111] Taranath, B.S., *Structural Analysis and Design of Tall Buildings*, McGraw-Hill, New York, USA, 1988.
- [112] Taranath, B.S., *Wind and Earthquake Resistant Buildings*, Marcel Dekker, New York, USA, 2005.
- [113] Timoshenko, S.P., *Theory of elastic stability* (1st Ed.), McGraw-Hill Book Company Inc., New York, USA, 1936.
- [114] Timoshenko, S.P., Theory of bending, torsion and buckling of thin-walled members of open cross section, *Journal of the Franklin Institute*, **239** (3, 4, 5): 201-361, 1945.
- [115] Timoshenko, S.P., Young, D.H. and Weaver, W., *Vibration problems in engineering*, Wiley, New York, USA, 1974.

- [116] Tso, W.K. and Chan, H.B., Dynamic analysis of plane coupled shear walls, *Journal of the Engineering Mechanics Division ASCE*, **97**: 38-48, 1971.
- [117] Tso, W.K. and Biswas, J.K., General analysis of non-planar coupled shear walls, *Journal of the Structural Division ASCE*, **99** (3): 365-380, 1973.
- [118] Vasquez, J. and Riddell, R., Thin-walled core element for multi-storey buildings, *Journal of Structural Engineering*, **110**: 1021-1034, 1984.
- [119] Vlasov, V., *Thin-Walled Elastic Beams* (2nd Ed.), (Jerusalem: Israeli Program for scientific translation) US Science Foundation, Washington, USA, 1961.
- [120] Waldron, P., Sectorial properties of straight thin-walled beams, *Computers and Structures*, **24**: 147-156, 1986.
- [121] Waldron, P., Equivalent beam analysis of thin-walled beam structures, *Computers and Structures*, **26**: 609-620, 1987.
- [122] Wang, Y., Arnaouti, C. and Guo, S., A simple approximate formulation for the first two frequencies of asymmetric wall-frame multi-storey building structures, *Journal of Sound and Vibration*, **236** (1): 141-160, 2000.
- [123] Wdowicki, J. and Wdowicka, E., System of programs for analysis of three-dimensional shear wall structures, *The Structural Design of Tall Buildings*, **2**: 295-305, 1993.
- [124] Wdowicki, J. and Wdowicka, E., Three-dimensional analysis of asymmetric shear wall structures with connecting and stiffening beams, *Engineering Structures*, **42**: 362-370, 2012.
- [125] Wong, C.W. and Lau, S.L., Simplified finite element analysis of three dimensional tall building structures, *Computers and Structures*, **33**: 821-830, 1989.
- [126] Yaman, Y., Vibration of open-section channels: a coupled flexural and torsional wave analysis, *Journal of Sound and Vibration*, **204** (1): 131-158, 1997.
- [127] Zalka, K.A., A simplified method for calculation of the natural frequencies of wall-frame buildings, *Engineering Structures*, **23**: 1544-1555, 2001.
- [128] Zhang, Z. and Chen, S., A new method for the vibration of thin-walled beams, *Computers and Structures*, **39** (6): 597-601, 1991.
- [129] Zupan, D. and Saje, M., The linearized three-dimensional beam theory of naturally curved and twisted beams: The strain vectors formulation, *Computer Methods in Applied Mechanics and Engineering*, **195**: 4557-4578, 2006.